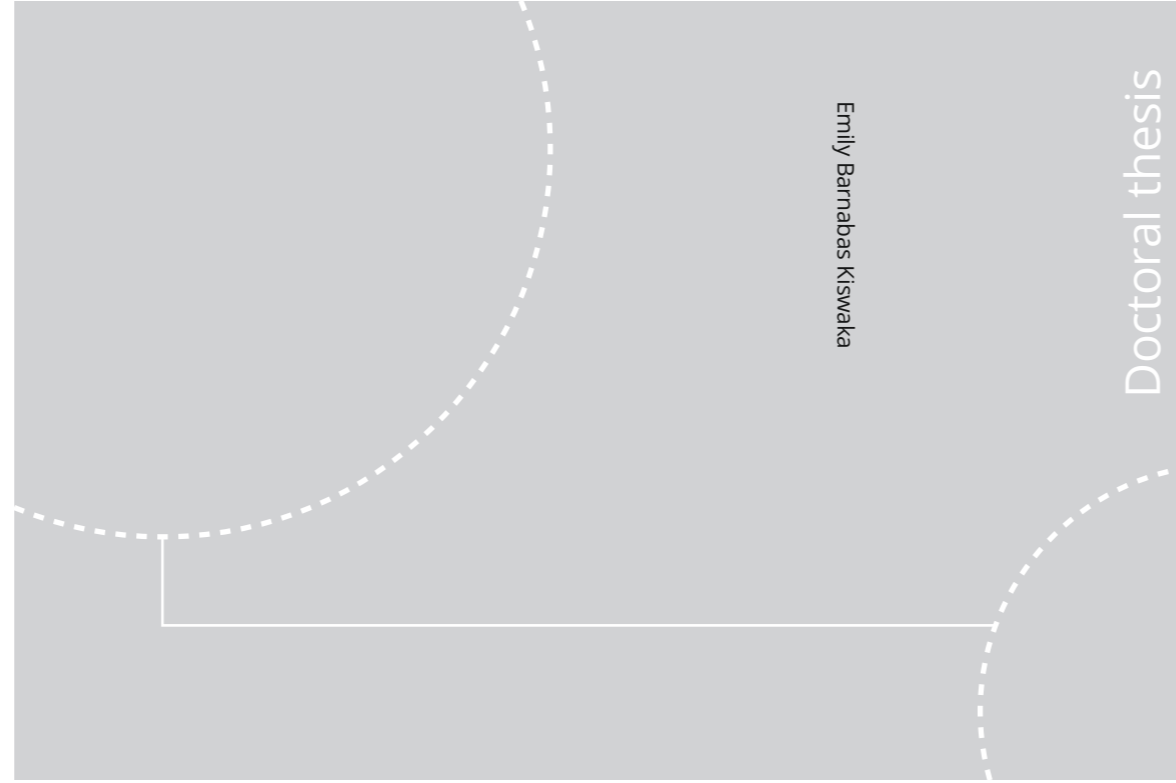


ISBN 978-82-326-4738-5 (printed ver.)
ISBN 978-82-326-4739-2 (electronic ver.)
ISSN 1503-8181



Emily Barnabas Kiswaka

Doctoral thesis

Doctoral theses at NTNU, 220:195

Emily Barnabas Kiswaka

Permian-Triassic Depositional Systems in the Norwegian Sea Area

Doctoral theses at NTNU, 220:195

NTNU
Norwegian University of Science and Technology
Thesis for the Degree of
Philosophiae Doctor
Faculty of Engineering
Department of Geoscience and Petroleum

 **NTNU**
Norwegian University of
Science and Technology

 **NTNU**
Norwegian University of
Science and Technology

 NTNU

Emily Barnabas Kiswaka

Permian-Triassic Depositional Systems in the Norwegian Sea Area

Thesis for the Degree of Philosophiae Doctor

Trondheim, June 2020

Norwegian University of Science and Technology
Faculty of Engineering
Department of Geoscience and Petroleum



Norwegian University of
Science and Technology

NTNU
Norwegian University of Science and Technology

Thesis for the Degree of Philosophiae Doctor

Faculty of Engineering
Department of Geoscience and Petroleum

© Emily Barnabas Kiswaka

ISBN 978-82-326-4738-5 (printed ver.)
ISBN 978-82-326-4739-2 (electronic ver.)
ISSN 1503-8181

Doctoral theses at NTNU, 2020:195

Printed by NTNU Grafisk senter

Permian-Triassic Depositional Systems in the Norwegian Sea Area

Emily Barnabas Kiswaka

Supervisor: Maarten Felix

Co-supervisor: Arve Næss

To Barnabas Edward Kiswaka and Ernest Maganza. Your thoughts have become a reality.

Acknowledgements

Completion of this PhD work has been possible through the support I received from many people.

I need to thank my supervisor, Maarten Felix, for his great support. He did a great job to make this work achievable. He worked tirelessly to give relevant feedback on time. I spent most of my time with Maarten at NTNU, discussing things while he provided his knowledge and expertise throughout my stay in Norway. His constant assistance will never be forgotten.

My co-supervisor, Arve Næss, arranged everything in making sure I gained access to Equinor facilities, both in Stjørdal-Norway and Dar es Salaam-Tanzania. Arve was always there to provide his expertise but also connecting me to relevant experts, including Olav Kvamme Leirfall and Halvor Bunkholt.

My stay in Norway was sponsored by EnPe under ANTHEI (Angola Tanzania Higher Education Initiative) scholarship scheme. ANTHEI coordinators are valued for their efforts in making sure that everything was settled for my scholarship to become reality. Jon Kleppe, Ambrose Itika and Richard Rwechungura were key contacts as far as ANTHEI issues were concerned. Oras Joseph Mkinga, my fellow ANTHEI PhD student, was good company in all conditions.

Seismic interpretation is an integral component of the findings reported in this thesis. I would like to extend my gratitude to TGS Spectrum and PGS for allowing me to use their 2D and 3D seismic lines respectively.

My MSc supervisor, Stephen John Lippard, who linked me with Maarten when I first asked him to supervise my PhD study, remained connected to me. I must admit that Stephen was the first person that I was comfortable talking to before I got used to Maarten and Arve. I relied on Stephen for some references that were not easily accessed from my end and he was always there to assist.

This PhD work allowed me to work with the best team of my life to this point. I am indebted to Equinor Exploration, Norway and UK, Norwegian sea South, Frøya project team. Everyone I met there always wanted to know if there is anything they can help. I remember Niclas Fredman would come to my desk and ask if I had any problem he could assist. Morten Krogh, Janine Zweigel, Bjørn Terje Oftedal, Bjørn Arve Moen, Ingunn Helgemo Sundt, Koen van den

Bril, and Erlend Eldholm have all assisted me in one way or another. Special thanks go to Halvor Bunkholt and Olav Kvamme Leirfall for their untiring support and discussions, which improved the quality of the manuscripts.

I am thankful to all Equinor employees at the Dar es Salaam office. They received me well when I stayed there for about five months. My stay in Dar es Salaam would have been difficult without access to Equinor facilities. I appreciate the positive reception I got from everyone, including Bernard David Lema who could not hide his thirst of seeing me making it on time. He was always concerned about my whereabouts and he would even make calls and emails to follow-up whenever I was missing for some time.

My family has always encouraged me to move on despite staying far away from home for a long time. Their love and support are priceless. I have nothing to repay but rather to always remain committed to them.

Mama Kiswaka should not be forgotten. She fought many battles to raise me when the world was upside down to her. I still remember her tears when we faced difficult moments together, and told me that I should concentrate on my studies for my own future. I thank her for everything.

Margareth Mlaguzi and Sabita L. Mtui are highly appreciated for their participation in creating a platform for my academic endeavour. If I remember quite well, Margareth was the first teacher I spoke with when I started my formal education at Majengo primary school, Muheza. A parental smile and friendly talk, and advice, from Sabita are things that strengthened me during my early struggles.

Abstract

Upper Permian deposits from the eastern margin of the Helgeland Basin, offshore Norway, are known to contain two organic-carbon-rich (OCR) intervals within the Lower Turbidite Unit. These intervals were so far not proven in the deeper basinal areas and their depositional conditions in the margin areas were not fully understood. In order to understand the general depositional conditions and lateral extents of the two organic rich intervals, Upper Devonian-Triassic successions have been investigated. Core logging, analysis of element proxies, qualitative and quantitative seismic interpretation and intercept and gradient (IG) crossplotting were used to investigate these successions in the Trøndelag Platform, specifically the Helgeland and Froan basins and partly the Nordland Ridge. Seismic interpretation, both qualitative and quantitative, and IG crossplotting were used to investigate possible geophysical manifestations of these upper Permian OCR sediments in the deeper basinal areas. Qualitative seismic interpretation, which focused on the analysis of the Upper Devonian-Triassic sedimentary fill geometries and fault-strata relationships, and a combination of core logging and element proxies were used to assess conditions that controlled deposition and preservation of the OCR sediments. These conditions include local tectonic developments, which are not as well understood as the regional development, and variation in oxygen levels in the deep basinal areas. A portable X-Ray Fluorescence (PXRF) scanner was used to determine major, minor, and trace element concentrations. The measurements of these element concentrations on core started below the lower organic-carbon-rich interval and continued above the upper organic-carbon-rich interval to track changes over time that might indicate what caused deposition to change. Changes in element values were then correlated to grain size, deposit types and organic content to understand the sedimentological influence on element distributions.

Results show that the Trøndelag Platform has a long history of rifting with several tectonic pulses from the Carboniferous to the late Triassic. These tectonic pulses include two local late Permian and two Early Triassic tectonic events. Thus, the upper Permian organic carbon rich intervals were deposited during a period of active tectonics. The seismic analysis showed that organic-carbon-rich rocks are present in the deep basin areas, and not just on the margins where previous work has shown their existence. These organic rich rocks are present in most of the Helgeland Basin, and present but spatially restricted in the Froan Basin since the Froan

Basin was highly compartmentalized by the late Permian tectonic events. Depositional processes, oxygen concentration and fluvial and terrestrial influx varied significantly during deposition, as indicated by the element concentrations. The lower organic-carbon-rich interval was deposited in the deep basinal areas under anoxic conditions that may have resulted from restricted oxygen circulation caused by tectonically induced isolation of the sub-basins from the main ocean. Sediment input into the basin changed between the deposition of the lower and upper organic-carbon-rich intervals with a more constant input of fine silt and sand. If this sediment influx was from fluvial input, this could potentially have caused stratification of the water column and subsequently anoxia. Another feature which is found in this work is the possible presence of upper Permian carbonate build-ups in the Helgeland Basin. These carbonates were deposited on the structural highs showing that anoxia was not developed there, in contrast to the deeper basinal areas where organic-rich rocks were laid down. This may explain the patchy occurrence of the upper Permian organic-carbon-rich layers.

Table of Contents

Acknowledgements.....	i
Abstract	iii
CHAPTER 1: INTRODUCTION.....	1
1.1. Tectono-sedimentary evolution	4
1.2. Stratigraphy	6
CHAPTER 2: METHODS USED	10
2.1. Data Sources.....	10
2.2. Core logging.....	10
2.3. Seismic interpretation.....	10
2.3.1. Qualitative seismic interpretation	10
2.3.2. Quantitative seismic interpretation	11
2.4. Element proxies	17
2.4.1. Concentration of Mo, Ni, Cu, Zn, Al, Fe, K, Ti, Zr, Si and T.....	18
2.4.2. Barium (Ba) and Phosphorus (P) versus productivity	19
2.4.3. Elements analysed.....	20
CHAPTER 3: RESULTS AND DISCUSSION	24
3.1. Upper Permian-organic-carbon rich layers	24
3.2. Number of tectonic phases	25
3.3. Influence of tectonics on organic rocks distribution	26
3.4. Alternation of organic rich rocks and carbonates	26
CHAPTER 4: RESEARCH PAPERS	27
4.1. Paper I	27
4.1.1. Author contributions	27
4.2. Paper II	66
4.2.1. Author contributions	66

4.3. Paper III	115
4.3.1. Author contributions	115
CHAPTER 5: SUMMARY AND CONCLUSIONS.....	160
CHAPTER 6: RECOMMENDATIONS AND FUTURE RESEARCH	161
REFERENCES.....	162
APPENDICES.....	169
Appendix 1. Matlab scripts used to analyse the recorded elements.....	169
Appendix 2. Crossplots of selected elements	184
Appendix 3. Plots of element distributions across the studied core interval.	186
Appendix 4. Presentation of results in conferences	190
<i>Poster presentations</i>	190
<i>Oral presentation</i>	191

CHAPTER 1: INTRODUCTION

Bugge et al. (2002) found upper Permian organic-carbon-rich (OCR) rocks in shallow cores (6611/09-U-01 and 6611/09-U-02) from the eastern margin of the Helgeland Basin (see Figure 1 for location), and suggested such rocks may also exist in the deeper parts of the Trøndelag Platform. The existence of the upper Permian OCR rocks in the deeper parts of the Trøndelag Platform was assumed based on the understanding that mid Norway and East Greenland formed a common basin during the Permo-Triassic (Bugge et al., 2002; Müller et al., 2005) and the fact that these rocks are found onshore East Greenland (Surlyk et al., 1984; Surlyk et al., 1986; Piasecki & Stemmerik, 1991; Christiansen et al., 1992; Christiansen et al., 1993; Stemmerik et al., 1993; Stemmerik et al., 1998; Kreiner-Møller & Stemmerik, 2001). Nonetheless, the presence of organic-carbon-rich (OCR) rocks in the deeper basinal areas was merely a suggestion and has remained an unanswered question. The aim of this thesis work was therefore to continue investigations of potential OCR deposits in the deeper parts of the Trøndelag platform, finding out where they are and what influenced their deposition. The focus of this thesis has been to improve the understanding of the lateral distribution and depositional conditions of the upper Permian organic-carbon-rich sediments, but a longer interval has been investigated on seismic data and in core in order to get a broader picture of what may have controlled deposition and preservation of organic matter in the area. A combination of seismic interpretation and core logging and analysis of element proxies has been used to study tectonic development, change in provenance characteristics, influence of fluvial inputs and change in oxygen conditions during deposition. In general, organic carbon rich deposits form as a result of the interplay between basin fill (sedimentation)/ basin history, and productivity and preservation of the organic matter (Demaison and Moore, 1980; Arthur et al., 1984; Tyson, 2005). These different aspects are addressed in this work, with the basin fill and basin history part addressed in chapters 4.1 and 4.2, and the productivity and preservation aspects addressed in chapter 4.3. It was found that it is critical to understand the tectonic history to understand both the spatial and temporal distribution of the organic carbon rich deposits.

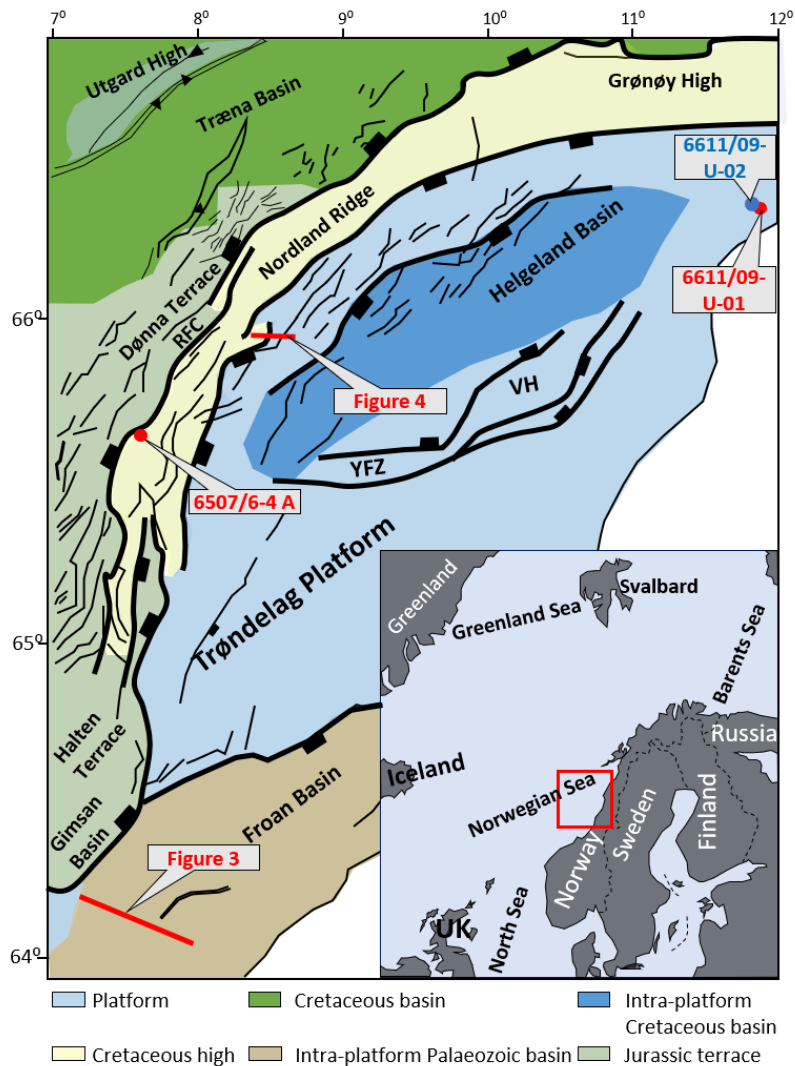


Figure 1. Location map for the Trøndelag Platform off central Norway. The Trøndelag Platform constitutes the Helgeland Basin, Froan Basin, Ylvingen Fault Zone, Vega High, Nordland Ridge and Frøya High (Blystad et al., 1995). RFC - Revfallet Fault Complex, VH - Vega High and YFZ - Ylvingen Fault Zone.

The Trøndelag Platform (Blystad et al., 1995) has characteristic features of a proximal margin (Peron-Pinvidic et al., 2013; Peron-Pinvidic & Osmundsen, 2016, 2018). These features include a number of normal faults which bound sub-basins accommodating syn-rift sedimentary wedges and sole out at shallow stratigraphic levels (Peron-Pinvidic & Osmundsen, 2018). In the Trøndelag platform, these features can be seen especially in the Froan Basin (Müller et

al., 2005; Redfern et al., 2010). As shown in this thesis, it was in the deeper parts of these sub-basins that the organic-rich rocks were deposited. From regional studies it is known that the basins within the Trøndelag platform formed during the opening of the Norway-Greenland seaway (Surlyk, 1990; Blystad et al., 1995). This opening occurred in several extension phases (Blystad et al., 1995). Some of these tectonic phases were regional and have been found throughout the Norway-Greenland basin, but it is known that some tectonic events only affected individual basins (Müller et al., 2005). The basin development of the Trøndelag Platform was partly different than the regional development, but this has not been described properly anywhere, so in the first part of this work the geological development during the Permo-Triassic is addressed. The study is based on qualitative interpretation of seismic surveys. Results from this work are presented in chapter 4.1 where the tectonostratigraphic developments of the Trøndelag Platform, including its subsidiary elements the Froan and Helgeland basins, are described.

Seismic methods are also used to investigate the spatial and temporal distribution of OCR deposits. The reason for using seismic data is that cores are available only from the basin margins and not from the basin centre. Both qualitative (seismic interpretation of deformation structures) and quantitative (AVO and IG crossplotting) methods are used to determine the distribution of organic carbon rich deposits. The results are presented in chapter 4.2, where it is shown that organic carbon rich rocks are present in the deep basin areas, but they are not distributed equally over the area, nor over time. The results also show that the distribution of the OCR deposits was affected by the basin shapes and formation style. The basin shape resulted in elongated deposits where the deposition in the deepest parts followed the basin orientation. The formation style of the basin, where numerous normal faults bound sub-basins especially in the Froan Basin (e.g. Figure 3 and Müller et al., 2005; Redfern et al., 2010), resulted in small deposits, while the less compartmentalised Helgeland Basin contains a larger deposit.

The final part of the work focusses on the preservation part of the organic carbon rich deposits: why were they preserved during some time periods and not others? In this part the data are obtained from a core taken on the margin of the Helgeland Basin. Bugge et al. (2002) have described two main intervals in this core with high total organic carbon (TOC) values. It

was these two intervals that led to their suggestion of wide-spread organic carbon deposits in the area. These intervals are the focus of the work presented in chapter 4.3. A portable X-Ray Fluorescence scanner was used to measure concentrations of elements in the core. The distribution of these elements has been linked to sedimentological processes, grain size distribution and organic-richness. The deposits in the core show multiple fining upward cycles containing gravity flow deposits, which are related to tectonic pulses. The measured core interval includes one cycle before and two cycles after the one which contains the organic carbon rich intervals. The depositional conditions were described using a combination of sedimentological logging for flow process understanding, and geochemical measurements of element concentrations that were used as proxies for palaeoenvironmental conditions. The results show that the two intervals both formed during anoxic conditions, but anoxia during deposition of the lower interval is interpreted to have been caused by restricted circulation due to blocked basins while anoxia during deposition of the upper interval may have been caused by fluvial stratification.

1.1. Tectono-sedimentary evolution

The tectonic history of the Norwegian Sea area is divided into three major episodes (Blystad et al., 1995). These episodes are:

- closing of the Iapetus Ocean during the Caledonian Orogeny (late Silurian/Early Devonian),
- dominance of an extensional regime that created a series of sub-basins (e.g. Müller et al., 2005) in the Norwegian Sea area (Late Devonian to Palaeocene) leading to separation of Norway from Greenland in the late Palaeocene – early Eocene (Surlyk, 1990; Doré et al., 1999; Tsikalas et al., 2005; Peron-Pinvidic et al., 2013), and
- active seafloor spreading in the North Atlantic between Eurasia and Greenland from the earliest Eocene to present (Blystad et al., 1995).

The second episode, the extension, is the time period of interest for the work presented here. Several major tectonic phases are reported to have occurred during the extensional regime of the Carboniferous-late Palaeocene between mid Norway and East Greenland (Brekke, 2000). These tectonic events took place during the Devonian-early Carboniferous, late Carboniferous-early Permian, middle Permian and late Permian-Early Triassic (Surlyk et al.,

1984; Surlyk, 1990; Doré, 1992; Blystad et al., 1995; Doré et al., 1999; Seidler, 2000; Stemmerik, 2000; Seidler et al., 2004; Müller et al., 2005; Oftedal et al., 2005; Bøe et al., 2010; Guarnieri et al., 2017). The late Carboniferous-early Permian tectonic event may have resulted in the early Permian unconformity of Brekke (2000). Brekke (2000) did neither describe nor give details of this early Permian unconformity other than mentioning that it can be found in the platform areas. In this thesis, a basement related unconformity is described which may be the early Permian unconformity of Brekke (2000). The unconformity has been mapped in the Nordland Ridge, Helgeland Basin and in the area between the Helgeland and Froan basins. The mid Permian rifting led to a regional unconformity that is widespread in eastern Greenland and the western Barents Sea (Surlyk et al., 1984; Surlyk, 1990; Seidler, 2000; Oftedal et al., 2005; Guarnieri et al., 2017; Stoker et al., 2017). This unconformity had not been mapped offshore mid Norway but it has been mapped in the current work. The mid Permian unconformity offshore mid Norway has been found to overlie various sedimentary basin fill geometries, as discussed in Section 4.1.

Late Palaeozoic sedimentary basins were formed during early extension regimes that lead to the initial opening of the Atlantic Ocean (Surlyk et al., 1984). These tectonics episodes are regional tectonic phases since they are recorded on both sides of the Norway-Greenland basin. Several other intervening local, episodic tectonic pulses may have influenced basin and sedimentological development of the Trøndelag Platform offshore mid Norway. This thesis presents a number of such local, episodic tectonic pulses that caused basin geometry modification and influenced sedimentation in the area. These episodes include two late Permian and two Early Triassic tectonic events. The late Permian tectonic events influenced the spatial distribution of the upper Permian organic-rich rocks in the deeper parts of the Trøndelag Platform. The upper Permian organic rich deposits are more extensive in the Helgeland Basin, which was less compartmentalized by the late Permian tectonic events, than in the Froan Basin. These tectonic events influenced not only the spatial distribution of the organic-carbon-rich rocks, but also their temporal distribution in that they resulted in development of anoxia which was a key condition for preservation of the lower organic-carbon-rich interval. The late Permian tectonic events were followed by the early Triassic tectonic pulses. In this thesis, two Early Triassic rift phases are found in the Froan Basin, in

contrast to the one which was reported by Müller et al. (2005). The Early Triassic rift phases are associated with two Early Triassic unconformities which have been mapped in the Froan Basin. Two Early Triassic rift phases have also been recognized in eastern Greenland where they are associated with erosive surfaces (Seidler, 2000). The erosive surfaces are also documented in the western Barents Shelf where they are due to the Early Triassic tectonic event which uplifted the shelf (Bøe et al., 2010). One key sedimentary feature for the late Permian and Early Triassic tectonic pulses was the alternation between gravity flow deposition and deposition from suspension fall out. This is observed in cores 661109/09-U-01 and 661109/09-U-2, where grey mudstone (part E of the Bouma sequence) is followed by black mudstone which marks the intervening quiet periods separating the gravity flow events.

1.2. Stratigraphy

Permo-Triassic basin development shows a change in depositional settings from shallow marine to normal marine depositional environments, with carbonates deposited on structural highs (e.g. the Nordland Ridge) and shales deposited in deep marine environments (Figure 2). Bugge et al. (2002) suggested variation in depositional conditions between anoxic and oxic based on variations in the degree of bioturbation observed in Permo-Triassic sediments. The organic-rich shales which are incorporated within the Lower Turbidite Unit (Figure 2) were proposed to have been deposited in the deeper basinal areas under anoxic conditions (Bugge et al., 2002). However, the Permo-Triassic tectonic development and depositional conditions in the area offshore mid Norway are still not well understood thus different analysis techniques were employed for further understanding of the deposits. The current work has used concentrations of element proxies to improve understanding of the depositional conditions in the study area. These elements include sulphur (S) and molybdenum (Mo) which can be used to indicate oxygen levels during deposition (Jones & Manning, 1994; Tribouillard et al., 2006). The S and Mo concentrations are higher in the lower organic-carbon rich interval (black coloured on the studied core) than in the upper organic-carbon-rich interval (with dark grey appearance on core), signifying different oxygen levels during deposition of the two intervals.

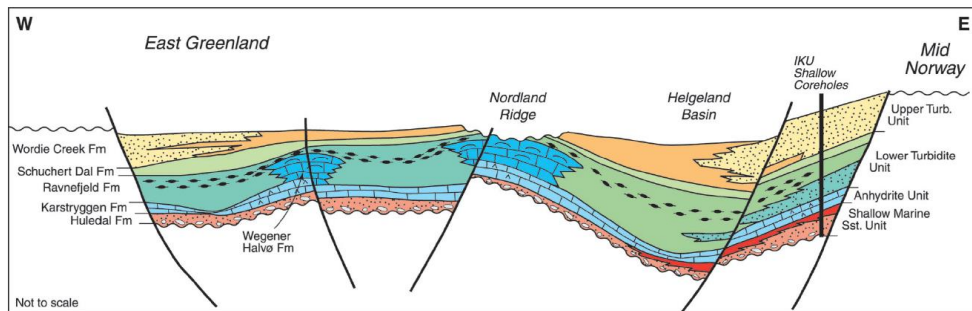


Figure 2. Schematic reconstruction of the Late Permian-Early Triassic basin between Mid Norway and East Greenland (from Bugge et al., 2002).

Previous work found carbonates deposits in the Nordland Ridge and in Greenland (Figure 2), but their presence elsewhere was not known. In this thesis the possible presence of vertically stacked, carbonate build-ups in the Carboniferous-Permian stratigraphy of the Helgeland Basin is reported. Carboniferous-Permian carbonates have also been reported in Greenland, the Barents Sea and Spitsbergen (Stemmerik, 2000; Stoker et al, 2017), indicating widespread distribution and favourable regional depositional conditions for carbonates during that time period. No carbonates of Triassic age were found in the work presented in this thesis. Continued drowning of the area due to late Permian-Early Triassic transgression (Surlyk et al., 1984; Doré, 1992) may have limited carbonate deposition during the time of deposition of the Early Triassic Upper Turbidite Unit.

There is no formal Permo-Triassic stratigraphy of the study area. The available subdivisions are from the works of Bugge et al. (2002) and Müller et al. (2005). Bugge et al. (2002) described four lithological units from the Permo-Triassic successions penetrated by IKU shallow cores 6611/09-U-01 and 6611/09-U-02. These units were correlated to eastern Greenland successions (Figure 2). From bottom to top these are: the Shallow Marine Sandstone Unit, the Anhydrite Unit, the Lower Turbidite Unit, and finally the Upper Turbidite Unit (Figure 2). The Permo-Triassic boundary on the mid Norwegian side was placed at the lithostratigraphic boundary between the Lower and Upper Turbidite Units, while the corresponding boundary on the Greenland side is placed between the Schuchert Dal Formation and the Wordie Creek Formation (Surlyk et al., 1986; Bugge et al., 2002). Müller et

al. (2005) subdivided the Permo-Triassic stratigraphy into five units named units Tr1-Tr5. Descriptions of these units are as follows.

1.2.1. Short descriptions of the stratigraphic units

The brief description of the Permo-Triassic stratigraphic units given here is adapted from Bugge et al. (2002) and Müller et al. (2005). The base of the Shallow Marine Sandstone Unit is formed by a 1 m-thick, poorly sorted, matrix-supported, immature, reddened conglomeratic sandstone, which fines up into massive to cross-laminated, unevenly bioturbated, brick red to brown-grey, fine-grained sandstones. The Shallow Marine Sandstone Unit is overlain by the Anhydrite Unit which contains replacive anhydrite, occurring within a background of laminated, pyritic siltstone; the anhydrite is overlain by massive, grey, carbonate cemented sandstones that have several gypsum-filled fractures. The Anhydrite Unit is overlain by the Lower Turbidite Unit which marks the upper part of the upper Permian interval in the Norwegian Sea area and comprises a succession of fining upward sandstone beds interbedded with unevenly bioturbated, dark-grey siltstone layers. The basal part of each fining-upward bed consists of massive, coarse-grained, locally conglomeratic sandstones, which fine upward into strongly laminated sandstones and siltstones that have soft- and syn-sedimentary deformation structures. The focus of this work was on the two organic-carbon-rich layers within the Lower Turbidite Unit. The Lower Turbidite Unit is equivalent to Unit Tr1 of Müller et al. (2005). Unit Tr1 is dominated by submarine fan deposits and minor marginal marine deposits. Unit Tr2 follows upward, and is dominated by marginal marine deposits. The Early Triassic sedimentation in the Norwegian Sea area led to the deposition of the Upper Turbidite Unit which is dominated by a sequence of dark-grey, locally laminated pyritic siltstone units that are interbedded with massive and fining-upward sandstone beds. Unit Tr3, which was dated as Mid Triassic by Müller et al. (2005), followed deposition of the Lower Triassic interval. Unit Tr3 is continental, as implied by its brownish-red colour, and partly marginal marine as shown by the presence of scattered marine algae. Unit Tr4 follows upward and is dominated by marine deposition, examples of which are the Lower Salt and Upper Salt deposits. These salt deposits are localized in the Helgeland Basin; they could not be found in the Froan Basin. This is explained by occurrence of a short marine incursion during the Middle Triassic (Müller et al., 2005). The marine incursion is believed to

have come from the north since the Middle and Upper Triassic interval is fully marine in the southwestern Barents Sea (Hamann et al., 2005). Müller et al. (2005) suggested either eustatic sea level rise or local tectonics during the Middle Triassic. A local tectonic event, which occurred in the Helgeland Basin during the Middle Triassic, has been recognized in this work. It is possible that uplift and erosion characterised this local tectonic event, leading to an angular unconformity that has been found in the area between the Helgeland and Froan basins. A Middle Triassic angular unconformity was mentioned by Brekke (2000) but no further details were given. The local tectonic event was followed by a period of thermal subsidence that is also found in this work. Müller et al. (2005) described unit Tr5 as the youngest Triassic interval in the study area. This unit is lacustrine and contain extensive mud deposits at its basal part. Sandstone beds alternating with mudstones and coal beds follow upward and continued into the Lower Jurassic Åre Formation (Dalland et al., 1988).

CHAPTER 2: METHODS USED

Three main techniques have been used to accomplish this work. These are core logging, geophysical techniques on seismic, and element proxies. Geophysical techniques on seismic involved both qualitative and quantitative interpretations and Intercept-Gradient (IG) crossplotting. Only a short description is given here to indicate how each method has been used in accomplishing this thesis, to avoid too much repetition of details that are found in the three attached papers that describe individual topics in detail.

2.1. Data Sources

Data used to accomplish this work consist of a combination of:

- Data from the Equinor database including seismic and well log data sets,
- IKU shallow drilling core core 6611/09-U-01, and
- Open source data from the Norwegian Petroleum Directorate (NPD) fact pages.

2.2. Core logging

Part of core 6611/09-U-01 has been logged to interpret Permo-Triassic sedimentological processes and depositional mechanisms. This core was drilled on the eastern margin of the Helgeland Basin (Figure 1). The purpose of the core logging was to understand sedimentary deposits and grain size variations that may reflect changes in depositional mechanisms and sediment input.

2.3. Seismic interpretation

Petrel software was used to accomplish the seismic interpretation of the Trøndelag Platform, specifically the Nordland Ridge and the Helgeland and Froan basins. Equinor inhouse software (AVOCADO) was used for the IG crossplotting.

2.3.1. Qualitative seismic interpretation

Qualitative seismic interpretation involved mapping of the subsurface reflectors/horizons and demarcations of sedimentary fill geometries that were essential for identification of upper

Devonian – Upper Triassic tectonic phases (an example is shown in Figure 3). The identified sedimentary fill geometries were key in recognition of late Devonian - Late Triassic tectonic phases in the study area.

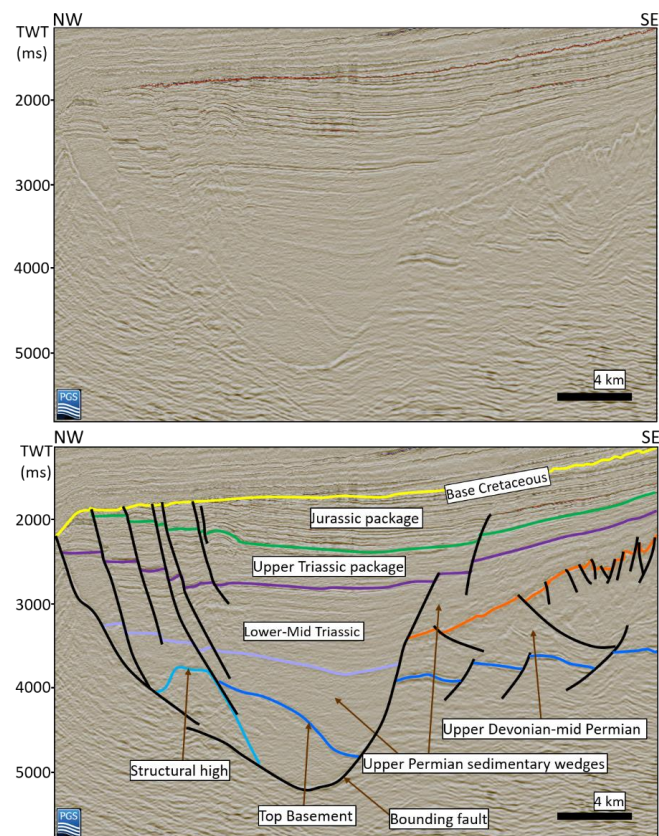


Figure 3. Uninterpreted and interpreted 3D inline 6607 of the PGS14005 survey in the Froan Basin. The study area contains fault-ward thickening sedimentary deposits. An example of this is shown by the upper Permian sedimentary wedges.

2.3.2. Quantitative seismic interpretation

Quantitative seismic interpretation involved identification of characteristic seismic expressions of organic rich sediments following the work of Løseth et al. (2011a, 2011b), analysis of amplitude variation with angle/offset (AVA/AVO) anomalies on seismic to identify AVA/AVO classes indicative of organic-carbon-rich sediments, and analysis of IG crossplots to identify organic-rich sediments.

Figure 4 shows an example of characteristic expressions of organic rich rocks on a seismic profile in the Helgeland Basin. Organic-carbon-rich shales may be recognised on seismic as areas with strata bound listric faults and slide blocks that have glided down on top of one another, mostly in tilted areas (Løseth et al., 2011a). Also, high negative reflection (red/yellow horizon in this context) may indicate the presence of organic-carbon-rich intervals (Løseth et al., 2011b). High negative amplitude reflectors with slide blocks (Figure 4) and strata bound listric faults have been found in the Helgeland and Froan basins. The presence of these structures allowed the recognition of upper Permian organic-carbon-rich rocks in the study area.

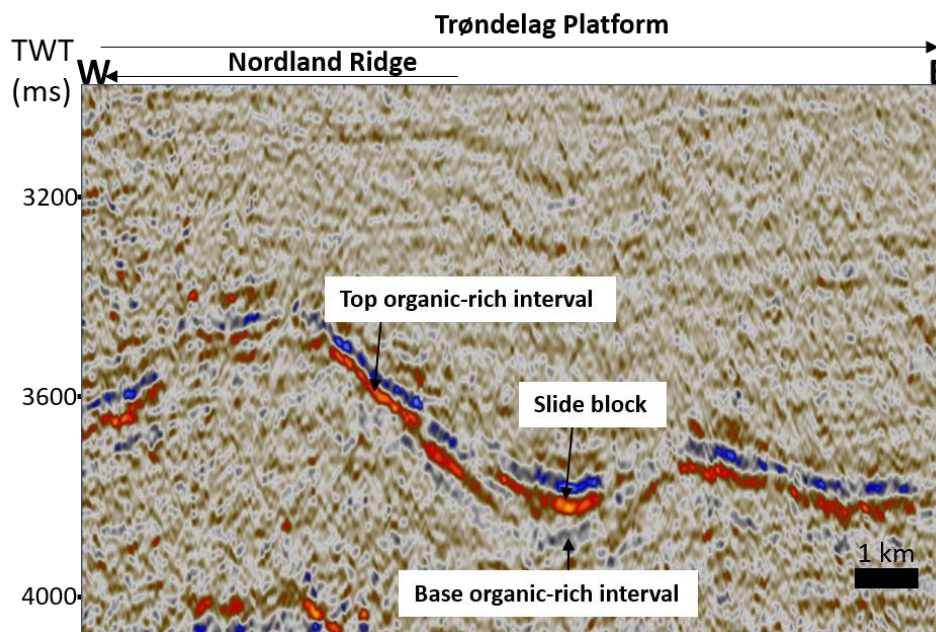


Figure 4. Seismic line MNR-7314 (see Figure 1 for location) showing an upper Permian organic-carbon-rich interval that slid down in the Helgeland Basin. Here the upper Permian organic-rich interval is a high amplitude negative reflector.

2.3.2.1. AVO anomalies on seismic

Proper scaling and phase matching of the analysed seismic profiles are important for a successful and meaningful AVA/AVO investigation. The scaling and phase matching were done to avoid misinterpretations. The purpose was to compare amplitudes of the same interval on two different lines acquired from different angles/offsets and thus amplitude

variation with angle/offset. Amplitudes and frequencies must be comparable (Figure 5) and adjusted when necessary in order to ensure correct interpretations.

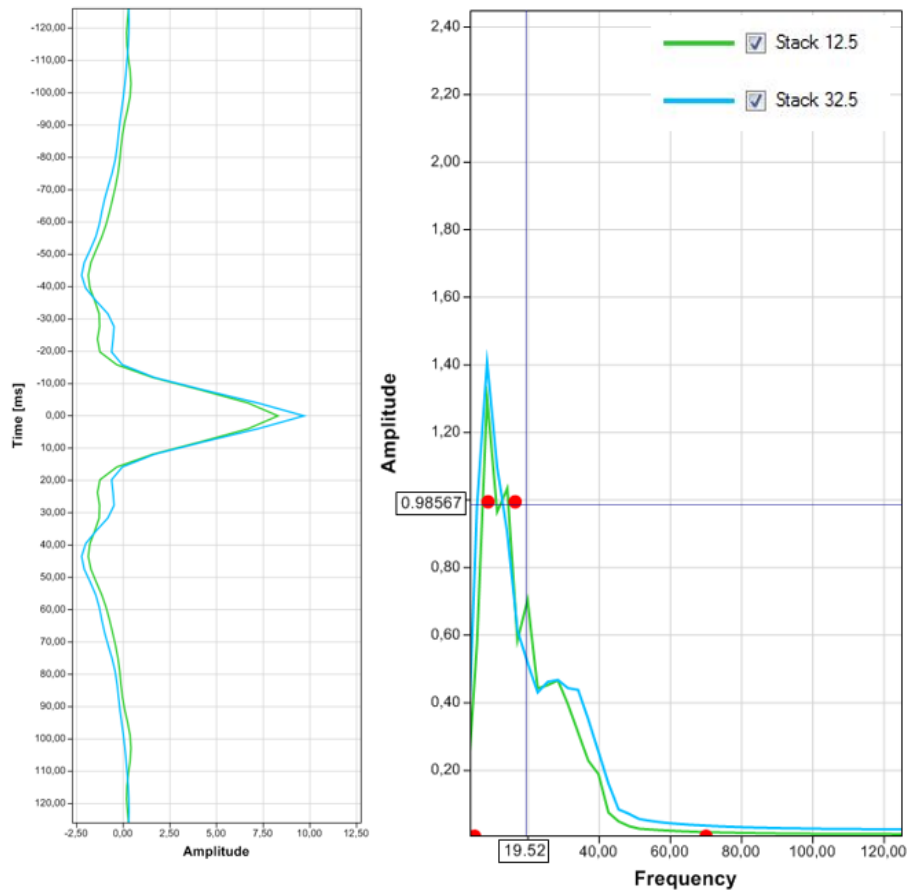


Figure 5. Amplitude (left) and frequency (right) matching (right) between near and far angles on one of the analysed seismic lines.

An AVA/AVO anomaly class is due to subsurface variation in reflection coefficients with angle of incidence which causes either amplitude dimming or brightening with angle/offset (see Figure 6). Traditionally, the AVA/AVO classes have been used to identify gas and oil sands based on the contrast in acoustic impedance between rock layers (Rutherford & Williams, 1989; Castagna & Swan, 1997). More recently the classes have also been used to identify other deposit types, including OCR deposits (Løseth et al., 2011b; del Monte et al., 2018).

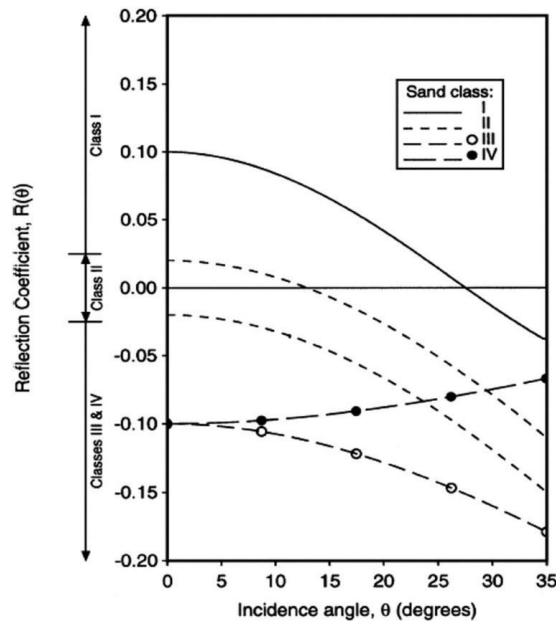


Figure 6. AVA/AVO anomaly classes (from Castagna & Swan, 1997).

2.3.2.2. IG crossplotting

The AVA/AVO technique depends on the variability of amplitudes of the reflection coefficients based on angles/offsets (Ostrander, 1984; Avseth et al., 2005). Crossplots of intercept (I) against gradient (G) can be used to enable AVA/AVO analysis (Castagna & Swan, 1997; Avseth et al., 2005). The idea of IG crossplotting follows Shuey's (1985) approximations to the Zoeppritz equations. Shuey (1985) simplified the Zoeppritz equations into a two term approximation (Equation 1). Gradient (G) is defined as the magnitude of the rate of change of amplitude with angle/offset (Rutherford & Williams 1989) while intercept (I) is the normal incidence trace (see Ross & Kinman, 1995).

$$R(\theta) = I + G \sin^2(\theta) \quad (1)$$

where R = reflection coefficient, θ = angle of incidence, I = AVA/AVO intercept, and, G = AVA/AVO gradient.

It is known that seismic reflections and their intensities are due to contrasts in acoustic impedance between sedimentary layers. An extension of acoustic impedance to non-normal angle of incidence, to create a noise free isotropic medium, is called elastic impedance (Whitcombe et al., 2002). The elastic impedance (EI) can be modified by using a Chi angle that

allows the evaluation angle to vary from -90° to 90° (Whitcombe et al., 2002). The modification of EI by using a Chi angle results in extended elastic impedance (Whitcombe et al., 2002). Extended elastic impedance (EEI) enables the assessment of different areas where fluid and lithology trends can be imaged and separated when an appropriate Chi angle (χ value) is known. Separation of different lithologies, and sometimes fluids, at different χ angles is the basis for lithology background trends in IG crossplotting. The IG crossplots have their trendlines oriented at Chi angles for either lithologies (Litho, Chi) or fluids (Fluid, Chi).

The AVA/AVO classes on IG crossplots are defined based on their positions relative to lithology and fluid (background) trends on the plots. The IG crossplot has four quadrants (Figure 7).

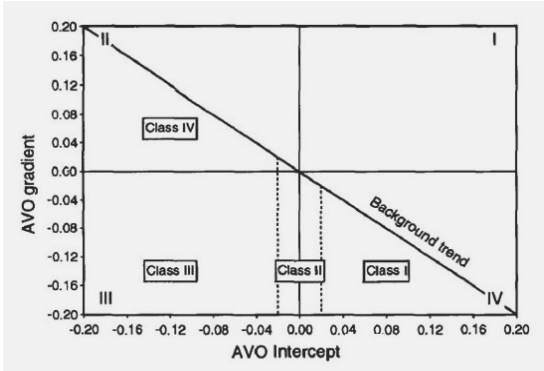


Figure 7. IG crossplot showing AVO classes I-IV (from Castagna and Swan, 1997). The crossplot has four quadrants (I-IV).

Table 1 summarizes the definitions of AVA/AVO classes that are applied in this thesis. The AVA/AVO classes and their relative positions in quadrants of the IG crossplots (Figure 7) are due to contrasts in acoustic impedance between rock layers. The product of $R(0)$ and G (AVO product) determines the AVA/AVO plotting position in the IG crossplot.

Table 1. AVO classes after Rutherford and Williams (1989), Castagna & Swan (1997) and Ross and Kinman (1995). This table is slightly modified from Avseth et al. (2005). Plus (+) and minus (-) signs stand for positive (increased) and negative (decreased) acoustic impedances respectively.

Class	Impedance	Quadrant	R(0)	G	AVO product
I	High-Impedance	4 th	+	-	Negative
IIp	No or low contrast	4 th	+	-	Negative
II	No or low contrast	3 rd	-	-	Positive
III	Low impedance	3 rd	-	-	Positive
IV	Low impedance	2 nd	-	+	Negative

The Chi angle, varying from -90° to 90° (Figure 8), allows imaging and separation of fluids and lithological components (Whitcombe et al., 2002) of a particular interval on seismic by using IG crossplotting. The analysis tool needs a brine filled interval (or clean shale layer) and known organic rich interval as inputs whose reflectivity are analysed to yield Chi angles for background trends (Figure 8). The known organic-rich interval is needed for tool calibration. The analysis tool is calibrated on a known organic-rich interval to be sure that the organic-rich interval plots on a class IV position. Light blue and brown vertical lines (Figure 8) are at Chi angles for fluid and lithology background trends respectively. These Chi angles are the angles of the IG crossplot trendlines separating different components (an example is shown in Figure 9)

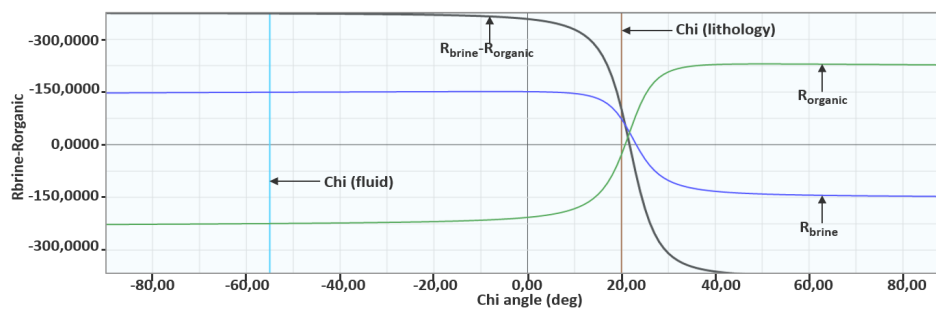


Figure 8. Reflectivity of brine filled sandstone (R_{brine}), organic-carbon-rich interval ($R_{organic}$) and $R_{brine} - R_{organic}$ plotted against Chi angle to identify fluid and lithology components and separate them. $R_{organic}$ and R_{brine} stand for reflection coefficients of organic-rich sediments and brine filled sands respectively.

Figure 9 shows an example of the IG crossplots where the Spekk Formation, a proven organic-rich interval (Dalland et al., 1988), is plotted together with brine filled sandstone. The Spekk Formation shows strong class IV anomaly and weak class II anomaly.

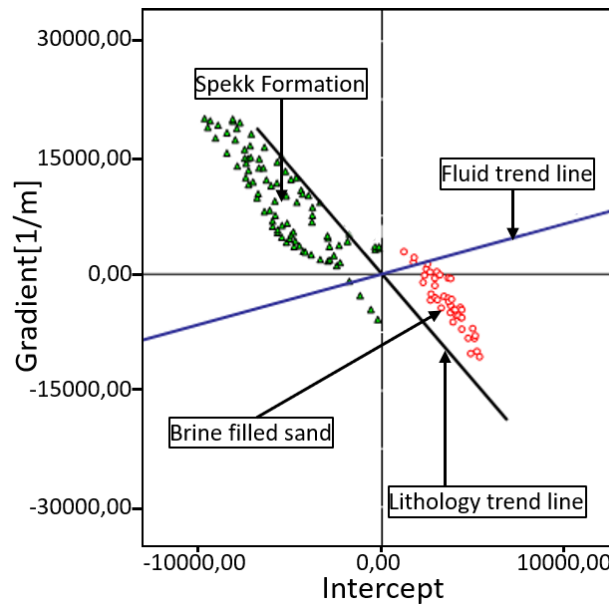


Figure 9. IG crossplot showing the Spekk Formation plotting on the class IV position.

The IG crossplots were combined with the analysis of amplitude variation with angle/offset and characteristic expressions of organic-rich sediments on seismic to interpret the presence of upper Permian organic-carbon-rich rocks in the Helgeland and Froan Basins.

2.4. Element proxies

Element values can be used as proxies for the interpretation of palaeoenvironmental conditions at the time of deposition. Changes in these conditions are determined (normally qualitatively) based on increases and decreases of element values across the studied deposits (Dymond et al., 1992; Calvert & Pedersen, 1993; Jacot des Combes et al., 1999; Algeo and Maynard, 2004; Tribovillard et al., 2006; Friis et al., 2007; Poulsen et al., 2007). Major, minor and trace elements incorporated within sedimentary deposits are of multiple origins (Calvert

& Pedersen, 1993; Jacot des Combes et al., 1999; Nijenhuis et al., 1999; Tribovillard et al., 2006). These elements can be delivered from detrital fluxes, hydrothermal sources and authigenic and biogenic minerals (Calvert & Pedersen, 1993; Tribovillard et al., 2006). The authigenic component of trace and minor elements is distributed to the sediments due to variation in oxygen levels during deposition (Calvert and Pedersen, 1993). Different element fluxes can dominate different depositional environments (Murray & Leinen, 1993). Examples of elements that can be used as proxies for palaeodepositional conditions are given in sections 2.4.1 and 2.4.2.

2.4.1. Concentration of Mo, Ni, Cu, Zn, Al, Fe, K, Ti, Zr, Si and T

Ni, Cu and Zn are commonly found in sedimentary deposits as disseminated sulphides (Calvert & Pedersen, 1993; Calvert & Pedersen, 2007). Calvert and Pedersen (1993) report high Cu, Ni and Zn contents in anoxic surface water, and in sedimentary deposits accumulated under anoxic bottom water underlying oxic waters due to diffusion of these elements from the oxic surface to the anoxic bottom sediments. Thus, depletion of Cu, Ni and Zn in sedimentary deposits indicates deposition under oxic conditions (Calvert and Pedersen, 1993). For sediments deposited under euxinic conditions, Cu precipitation is more favoured than Zn due to differences in the solubility products of their sulphides (Hallberg, 1976; Jones & Manning, 1994). However, Zn content may approach Cu content if the initial depositional conditions were oxic (Jones & Manning, 1994). High contents of minor and trace elements under euxinic conditions are explained by the fact that most of these elements exhibit multiple valence states and are more readily complexed with organic acids under reducing conditions that are found in oxygen deficient environments (Algeo & Maynard, 2004). Anoxic conditions may also be indicated by elevated Mo concentration within sedimentary deposits (Francois, 1988; Tribovillard et al., 2006). Permanently anoxic basins record the highest Mo values (Calvert & Pedersen, 2007).

Al, Fe, K, and Ti are usually related to terrigenous input (Jacot des Combes et al., 1999). Sedimentary Zr, Si and T occur mostly as heavy minerals zircon ($ZrSiO_4$), quartz and Ti oxides respectively (Calvert & Pedersen, 2007). These minerals are resistant to weathering and can withstand several transportation and deposition episodes and that is why Zr, Si and Ti have been used as proxies for aeolian input (Calvert & Pedersen, 2007). Resistance to diagenetic

remobilization of these minerals suggests that sediments delivered from the same source area should be expected to have more or less uniform values. Rapid variability in concentrations of elements incorporated in the resistant heavy minerals implies a change in provenance area or change in mineralogy of the source area.

2.4.2. Barium (Ba) and Phosphorus (P) versus productivity

Ba incorporated into marine micro-organisms is released due to sulphate oversaturation during bacterial decay of organic matter (OM) and precipitates commonly as barite (Dymond et al., 1992; Jacot des Combes et al., 1999). Barite (BaSO_4) is stable under surface oxic conditions but it dissolves under oxygen depleted conditions mainly due to sulphate reduction (equations 2 & 3) following microbial degradation of OM (Von Breyman et al., 1992; McManus et al., 1998).



The usefulness of biogenic barium $[\text{Ba}]_{\text{bio}}$ and barite as palaeoproductivity proxies has been assessed by several workers (Dymond et al., 1992; Von Breyman, et al., 1992; Dymond & Collier, 1996; Jacot des Combes et al., 1999; McManus et al., 1999; Henkel et al., 2012). Jeandel et al. (2000) report a consistency between $[\text{Ba}]_{\text{bio}}$ fluxes and primary productivity and measured carbon export in the tropical NE Atlantic. However, $[\text{Ba}]_{\text{bio}}$ should be used with care as a proxy for palaeoproductivity because $[\text{Ba}]_{\text{bio}}$ may accumulate due to high fluxes of organic matter, but it may undergo post depositional migration due to sulphate reducing conditions and get incorporated into sediments that accumulated under areas with very low primary productivity (Tribovillard et al., 2006). It should be understood that trace and minor element mobility during diagenesis can give patterns and distributions that do not reflect palaeodepositional conditions (e.g. oxygen levels and primary productivity) and trace and minor elements should be used as proxies for palaeodepositional redox levels if the biogenic component is dominant over other sources like detrital and hydrothermal components (Von Breyman et al., 1992; Tribovillard et al., 2006).

Phosphorus (P) is an essential nutrient for the growth of marine organisms (Slomp et al., 2004). Much of phosphorus exported to the seafloor, in contrast to TOC, may be preserved in

sediments and thus may serve as a palaeoproductivity proxy (Latimer & Filipelli, 2003) but local richness of P in sediments is not a certain indication of high primary productivity (Tribovillard et al., 2006).

2.4.3. Elements analysed

In the current work, element distributions recorded from core 6611/09-U-01 were studied in order to interpret Permo-Triassic depositional conditions in the Helgeland Basin. The elements were measured by using a Niton XL3t GOLDD+ handheld X-ray fluorescence scanner (Figure 10) to be able to study changes in the chemistry of the analysed deposits. These changes were important in indicating changes or lack thereof in provenance mineralogy, oxygen levels, and influence of terrestrial and fluvial input during deposition. The 40 elements Nd, Pr, Ce, La, Ba, Sb, Sn, Cd, Ag, Mo, Nb, Th, Zr, Y, Sr, U, Rb, Bi, Au, Se, As, Pb, W, Zn, Cu, Ni, Co, Fe, Mn, Cr, V, Ti, Ca, K, Al, P, Si, Cl, S, and Mg were measured. The element distributions, combined with grain size variations, deposit types and presence of organic-rich rocks, were used to identify tectonic pulses and changes in basin conditions that facilitated deposition and preservation of the upper Permian organic-rich sediments in the Helgeland Basin. Matlab scripts used to plot and analyse the recorded elements are given in Appendix 1.



Figure 10. Niton XL3t GOLDD+ handheld X-ray fluorescence scanner used to scan core 6611/09-U-01 for element distribution.

2.4.3.1. PXRf element recording mechanism

The working mechanism of the PXRf is summarized in Figure 11. The summary is based on the explanation from Thermo Fisher Scientific (2019) of the PXRf technology. The X-ray generating tube has a silver (Ag) anode (X-ray source, see Figure 11) which can reach up to 50 kV and 200 μ A when in operation. When an atom is irradiated with this high energy X-ray beam, an electron from the inner orbital shell is ejected from its position provided that the supplied energy is greater than the atom's binding energy. The number of electron shells depends on the atomic number of a particular element; in Figure 11 an example is shown of an atom with three electron shells (K, L and M). The electron's ejection destabilizes the atom; thus, another electron has to fill the vacancy left by the ejected electron. This vacancy is filled

by an electron from the higher energy orbital shells. The electron dropping to fill the vacancy releases X-ray fluorescence whose energy is recorded by the PXRF as an energy peak. These energy peaks are the ones that are used by the PXRF processor to identify contents of different elements on the sample.

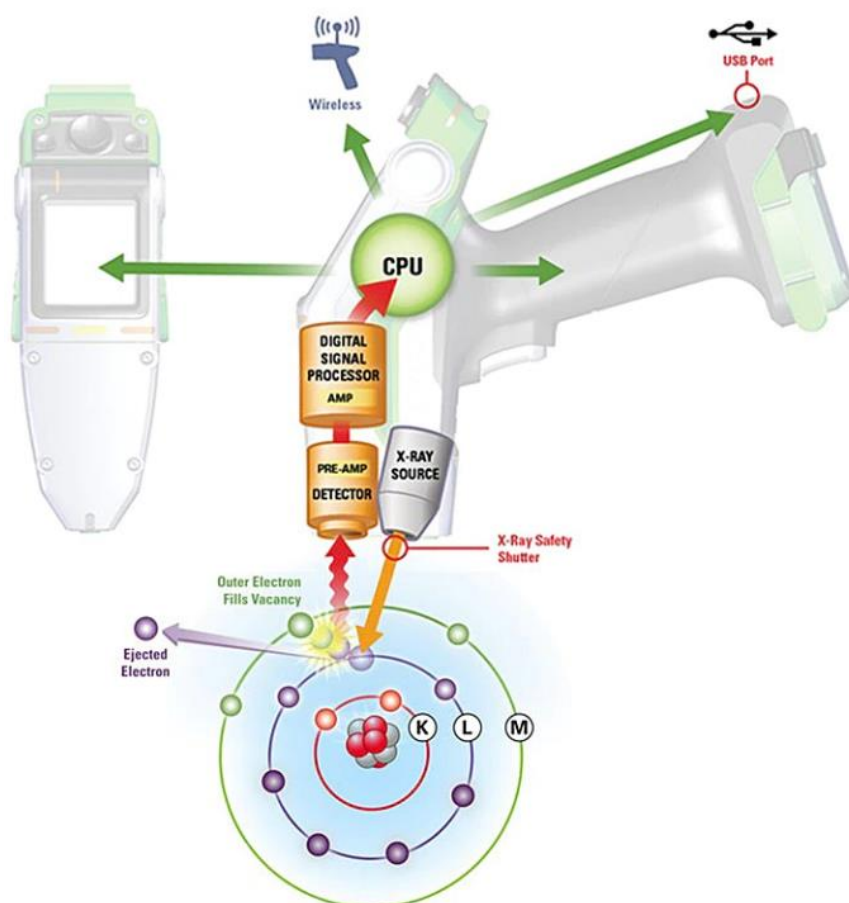


Figure 11. Schematic diagram of the working of the X-ray fluorescence tool. Image from Thermo Fisher Scientific website: <https://www.thermofisher.com/no/en/home/industrial/spectroscopy-elemental-isotope-analysis/spectroscopy-elemental-isotope-analysis-learning-center/elemental-analysis-information/xrf-technology.html>. Accessed on 13th Dec, 2019.

2.4.3.2. Cluster analysis and element distributions

Multivariate statistical analysis (Parks, 1966; Cloutier et al., 2008) was done on the concentration values of the recorded elements to determine elements with similar distribution trends. Pearson correlation coefficients (see Benesty et al., 2009), factor analysis,

dendrograms (Parks, 1966; Cloutier et al., 2008), and crossplots were used to cluster linked elements. Correlation coefficients between elements and distribution plots for the studied elements are shown in the results in section 4.3. Other examples of element crossplots and distributions across the studied deposits are shown in Appendices 2 and 3 respectively.

CHAPTER 3: RESULTS AND DISCUSSION

The main results of this thesis work are presented as separate manuscripts (included in section 4) submitted for publication as research papers in scientific journals. However, some of the issues that cross-reference the work could not be addressed in the individual manuscripts. These issues will be discussed below.

3.1. Upper Permian-organic-carbon rich layers

Tectonic activities and variation in fluvial input were key to the development of anoxic conditions that facilitated preservation of these upper Permian organic-carbon-rich intervals. Two upper Permian organic-carbon-rich intervals have been found in two cores on the eastern margin of the Helgeland Basin (core 6611/09-U-1) and in the Sør High (6507/6-4 A) of the Nordland Ridge (see Figure 1 for location). However, the AVO results (section 4.2) show only one interval in the Helgeland Basin. Furthermore, the IG crossplots and AVA/AVO anomalies on seismic indicated two upper Permian organic-carbon-rich intervals in a small area in the Froan Basin. The identification of one interval in the Helgeland Basin suggests either merging of the two intervals in the deeper basinal areas or significant thinning of these rocks to the extent that they were below the resolution of the used seismic data. Thin organic rich intervals cannot be identified at the given depth of investigation on the analysed seismic data. The presence of the upper Permian organic-carbon-rich rocks in a small area of the Froan Basin is interpreted to have been caused by either patchy distribution of these rocks due to anoxia not having developed equally in every sub-basin during deposition, or low TOC content which may have caused absence of characteristic seismic expressions of the upper Permian organic-rich rocks in some parts of the Trøndelag Platform. These factors could be the reason for the indication of one interval in the Helgeland Basin and presence of the upper Permian organic-rich rocks in a small area of the Froan Basin (see section 4.2 with the AVO results).

The Trøndelag Platform contains several Permo-Triassic sub-basins (Figure 3, also covered in detail in section 4.1, basin development) some of which accommodate the upper Permian deposits (reported in section 4.2, AVA/AVO results). In the current work, seismic interpretation and a combination of core logging and analysis of element proxies has led to the suggestion that some of the sub-basins were disconnected and isolated from the main

ocean leading to restricted conditions, and limited oxygen supply (sections 4.1 basin development and 4.3 core work). This in turn caused oxygen levels to vary from one sub-basin to another leading to varied preservation potential and consequently deposition of sediments with varied TOC during deposition of the lower organic-carbon-rich interval.

Deposition of the lower organic carbon interval was followed by an oxic regime that is reflected by a reduction in organic content and by bioturbation of an interval separating the two organic-rich intervals (section 4.3, core analysis). This indicates that the basin was not constantly anoxic. This oxic regime was followed by anoxia during deposition of the upper organic carbon rich interval. This second period of anoxia is reflected by an increase in TOC, change in mudstone colour from grey to dark grey and disappearance of bioturbation in the sediments. Deposition of the upper organic rich interval has been interpreted to have been associated with an increase in fluvial input. Fluvial input caused stratification in the water column and finally development of anoxia that was key to preservation of organic carbon during deposition of the upper organic-rich interval. The intervening oxic conditions may also suggest either the absence of organic rich rocks or presence of intervals with low TOC content in areas where organic-carbon-rich rocks were not indicated by seismic (section 4.2, AVA/AVO results).

3.2. Number of tectonic phases

Different parts of the work in this thesis were on different scales. Because of this, the results are not always directly comparable. In the course of this PhD work, a combination of seismic interpretation and core logging led to the identification of two late Permian and two Early Triassic tectonic pulses in the Norwegian Sea basin (sections 4.1 and 4.3 respectively). Core logging indicated two late Permian tectonic pulses while analysis of sedimentary fills based on interpretation of seismic data indicated one late Permian tectonic pulse. The challenge in identifying the second late Permian tectonic pulse from seismic data is mainly due to scale and resolution issues with seismic. The late Permian tectonic pulses, deduced from core logging, are reflected by sedimentary deposits that are a few metres thick that are below seismic resolution. Restricted thickness of deposits from tectonic phases (section 4.3, core analysis) might also be a reason why the second Early Triassic tectonic phase could not be identified on seismic lines crossing the Helgeland Basin (section 4.1). This suggests that

several other local episodic tectonic pulses might have resulted in deposits that cannot be identified based on seismic interpretation alone. Further work on the available cores (6611/09-U-1 and 6611/09-U-2) will improve the current understanding of the tectonic development during the Permo-Triassic.

3.3. Influence of tectonics on organic rocks distribution

AVA/AVO results (section 4.2) indicate that the distribution of the upper Permian organic-rich rocks was influenced by tectonics. This was mainly due to the upper Permian deposits following the orientation of the Helgeland Basin. Core logging and analysis of element proxies (section 4.3) show that the late Permian tectonic event indeed influenced deposition of the upper Permian organic-carbon-rich deposits. The major influence was in creating sub-basins that were disconnected from the main ocean, causing limited oxygen supply and consequently anoxia development for preservation of organic matter.

3.4. Alternation of organic rich rocks and carbonates

Dome structures seen on the seismic lines that were investigated during the determination of basin history (section 4.1) have been interpreted tentatively in that section as upper Permian carbonate build-ups. This interpretation was based on geometric criteria although an alternative interpretation was that the structures are intrusions. The interpretation of carbonates is strengthened by results of the AVA/AVO work (section 4.2). IG crossplots show the likely presence of carbonates in the organic-carbon-rich intervals, so that there was a lateral alternation of the two lithologies. Interfingering of upper Permian organic-rich rocks in the structural highs was suggested by Bugge et al. (2002) based on correlations with eastern Greenland geology. The results of the seismic interpretation (section 4.1) and the AVA/AVO work (section 4.2) show that the same may have occurred in the deeper parts of the Helgeland Basin.

CHAPTER 4: RESEARCH PAPERS

Further details of the integrated methodology, results and discussion are found in the three attached papers.

4.1. Paper I

“Permo-Triassic sedimentary fills and tectonic phases off mid Norway: seismic investigation of the Trøndelag Platform”

Emily Barnabas Kiswaka¹ and Maarten Felix¹

¹NTNU Norwegian University of Science and Technology, Norway (emily.kiswaka@ntnu.no)

Accepted for publication by Norwegian Journal of Geology

4.1.1. Author contributions

My contribution to this paper involved intensive literature review, qualitative seismic interpretation and writing.

Maarten Felix was involved in text editing and provided relevant scientific discussion and recommendations.

Permo–Triassic sedimentary fills and tectonic phases off mid Norway: seismic investigation of the Trøndelag Platform

Emily Barnabas Kiswa¹ and Maarten Felix¹

¹NTNU Norwegian University of Science and Technology, N-7491, Trondheim, Norway

Email: emily.kiswa@ntnu.no

Abstract

Seismic interpretation (2D and new 3D surveys) has been used to investigate sedimentary fills and timing of tectonic activity offshore mid Norway. This study was focussed on upper Permian and Lower Triassic sedimentary basin fills, but a longer stratigraphic interval (Devonian–Upper Triassic) was analysed in order to get a broad understanding of what happened prior to, during and after deposition of the upper Permian–Lower Triassic successions. The ages of the sedimentary fills were partly constrained by well ties. Seismic reflectors and sedimentary successions below the upper Permian interval are of Late Devonian–mid Permian age. Six sedimentary fill geometries (fill type A – F) were identified. These are (A) fault-ward thickening packages with internal strata thickening towards bounding faults, (B) wedge shaped packages whose internal strata have more or less uniform thickness, (C) sedimentary fills containing fill type A overlain by sedimentary strata with more or less uniform thickness, (D) gently dipping packages that thicken towards deeper areas of the basin, and downlap onto pre-existing topography, (E) gently dipping strata filling depressions, and (F) sedimentary wedge with rotated internal strata and folded top. These fill types were used to determine phases of active tectonics and quiescent phases. Based on temporal changes of the fill types, five late Palaeozoic–Triassic unconformities have been mapped: a nonconformity where the Palaeozoic strata onlap onto the basement, a mid Permian unconformity, two Early Triassic unconformities and a Middle Triassic angular unconformity. Results show that Devonian– Permian, mid Permian, late Permian, Early Triassic, late Early Triassic, and Mid–Late Triassic rifts influenced sedimentation offshore mid Norway. Some tectonic pulses occurred on a local scale and are not reflected by sedimentary fills in all sub-basins of the Trøndelag Platform.

Key words: Sedimentary fill, sedimentary wedge, Trøndelag Platform, Helgeland Basin, Froan Basin, Nordland Ridge, tectonic phase, Norwegian-Greenland seaway

1. Introduction

The Norwegian-Greenland seaway opened as the result of multiple tectonic episodes that started in the Carboniferous (Brekke, 2000) and ended with the final separation during the late Palaeocene (Surlyk, 1990). Three main rifting episodes related to the opening have been recognised regionally; these are events during the late Carboniferous to early Permian (Blystad et al., 1995), middle Permian (Surlyk et al., 1984; Surlyk, 1990; Doré, 1992; Seidler, 2000; Oftedal et al., 2005; Guarnieri et al., 2017), and Early Triassic (Seidler et al., 2004; Müller et al., 2005). The late Palaeozoic tectonics created the framework for the tectono-sedimentary development of the Norwegian Sea basin (Brekke, 2000). Minor block movements in the late Permian are considered to mark initial stages of the Early Triassic rifting that created several sub-basins which were controlled by major faults (Müller et al., 2005; Redfern et al., 2010). Müller et al. (2005) reported that a short lived marine incursion occurred during the Middle Triassic, suggesting local tectonics or eustatic sea level rise during that time period.

Not all tectonic pulses affected the entire area though, and several pulses have been recognised only in individual basins, indicating different developments in different basins (Müller et al., 2005). These local tectonic pulses occurred outside the major phases mentioned above. For example, two Early Triassic marine rifting events are recorded from eastern Greenland outcrops (Seidler et al., 2004; Guarnieri et al., 2017), but offshore mid Norway only one Early Triassic tectonic event has been reported based on Lower Triassic basin infill geometries (Müller et al., 2005). The local tectonic developments are not as well known as the regional development and are sometimes only suggested in the literature (e.g. Müller et al., 2005) rather than described in detail.

The upper Palaeozoic and Lower Triassic deposits of eastern Greenland have been widely studied (Surlyk et al., 1984; Surlyk et al., 1986; Christiansen et al., 1993; Stemmerik et al., 1993; Kreiner-Møller & Stemmerik, 2001), made possible because they are exposed onshore. Less work has been done on the Permo–Triassic successions of the Norwegian Sea basin that are deeply buried in the Trøndelag Platform (Fig. 1). Earlier work on the Permo–Triassic deposits of the Norwegian Sea area has focussed on cores (especially 6609/7-1, 6611/09-U-01 6611/09-U-02, and 6608/8-1), interpretation of 2D seismic data (most of which have

limited quality) and correlation with eastern Greenland (Blystad et al., 1995; Brekke, 2000; Bugge et al., 2002; Müller et al., 2005).

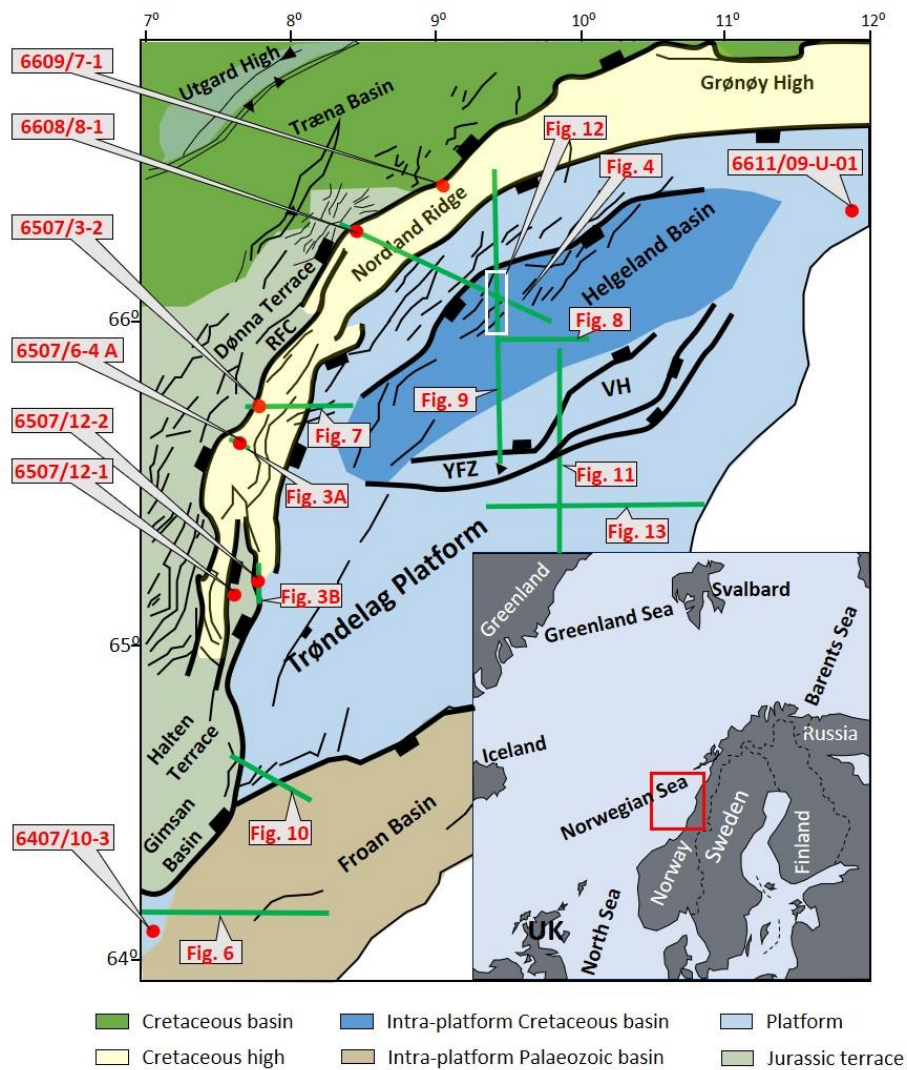


Figure 1. Structural element map of the Trøndelag Platform area with the locations of key cores and seismic lines used to illustrate the findings. Major extensive faults are shown by thick black lines while small faults are shown by the thin black lines. Main map sourced from NPD FactMaps (http://npdwms.npd.no/npdwmsmap_wqs84.asp?; accessed on 13th March 2018). Insert map modified after Bugge et al. (2002). Structural elements modified from Blystad et al. (1995). RFC – Revfallet Fault Complex, VH – Vega High and YFZ – Ylvingen Fault Zone.

In the current study, seismic investigation of the Trøndelag Platform including its subsidiary elements the Frøya High, Nordland Ridge, Helgeland Basin and Froan Basin (Fig. 1), and similarities with eastern Greenland geology, have been used to study sedimentary fill geometries and faults to improve the understanding of the tectono-sedimentary development of the deeper parts of the study area, and determine the effects of both regional and local tectonic phases, which has until now been unclear. This work was aimed at studying the upper Permian and Lower Triassic successions, but older and younger intervals were also studied for a fuller understanding of the basin development. New 3D surveys were used that were unavailable for previous work, which allowed looking into the deeper parts of the basin and improved the confidence in recognition of the structures present.

1.1. Stratigraphy of the study area

A formal stratigraphic subdivision of the rocks in the area does not exist, but Bugge et al. (2002) and Müller et al. (2005) have subdivided the deposits into multiple units (see Fig. 2). Description of cores 6611/09-U-01 and 6611/09-U-02 allowed Bugge et al. (2002) to report four Permo–Triassic lithological units on the eastern margin of the Helgeland Basin. These are, from oldest to youngest: Shallow-Marine Sandstone Unit, Anhydrite Unit, Lower Turbidite Unit, and Upper Turbidite Unit (Fig. 2). These units were correlated with formations encountered in eastern Greenland (Fig. 2).

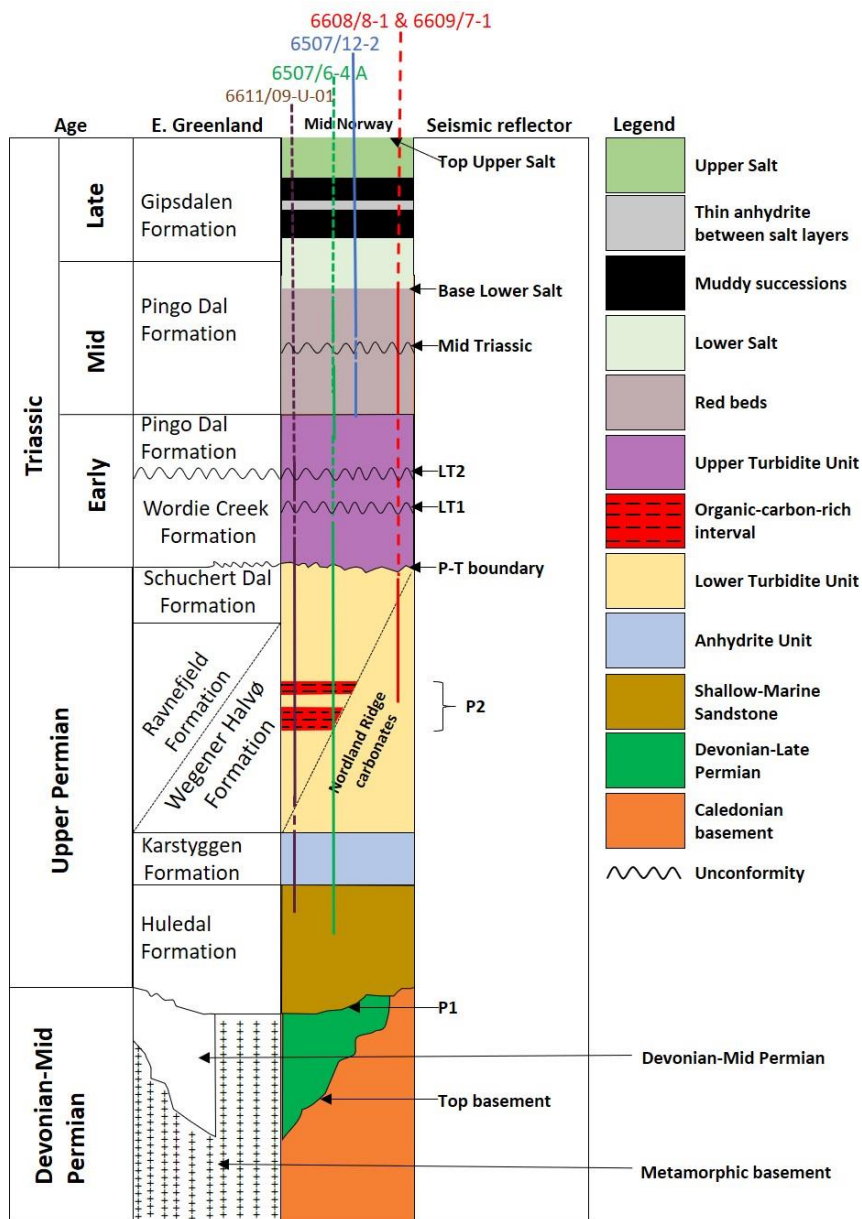


Figure 2. Correlated chronostratigraphic schemes between the Helgeland Basin and eastern Greenland with vertical positions of the major reflectors (see main text for further description). The exact position of P2 is uncertain therefore the possible range is shown. Dashed vertical lines show intervals that were not penetrated by wellbores. Stratigraphic columns have been modified after Jacobsen & van Veen (1984), Surlyk (1990), Stemmerik et al. (1993), Stemmerik et al. (1997), Seidler (2000), Bugge et al. (2002), Seidler et al. (2004), Müller et al. (2005), Guarnieri et al. (2017), and Andrews & Decou (2019). P1 – mid Permian unconformity, P2 – late Permian reflector and LT1 and LT2 are the Lower Triassic reflectors.

The Shallow-Marine Sandstone Unit marks the base of the Permo–Triassic stratigraphy in core 6611/09-U-01 and rests most likely on crystalline basement (Bugge et al., 2002). The Anhydrite Unit follows upward and contains abundant gypsum-filled fractures and anhydrite nodules (Bugge et al., 2002). The Lower Turbidite Unit is overlain by the Upper Turbidite Unit, and their boundary was placed at the Permian–Triassic boundary. A possible hiatus exists between the upper Permian and the Lower Triassic (Bugge et al., 2002; Müller et al., 2005). This unconformity may be regional as the Permo–Triassic boundary in eastern Greenland has been described as unconformable in places (e.g. Stemmerik et al., 1997; Guarnieri et al., 2017). The Early Triassic, offshore mid Norway, began by deposition of the Upper Turbidite Unit, which is correlated with the Wordie Creek Formation of eastern Greenland (Bugge et al., 2002). The sediments in eastern Greenland also consist of deep water gravity flow deposits, and the sequence there contains erosional surfaces associated with an Early Triassic rifting event (e.g. Surlyk et al., 1986; Seidler, 2000; Seidler et al., 2004).

Müller et al. (2005) subdivided the Triassic stratigraphy offshore mid Norway into five sedimentological units based on seismic interpretation and core logging. These authors named the units Tr1 to Tr5, and described them as follows. Unit Tr1 is dominated by submarine fan deposits and minor marginal marine deposits. This depositional unit is the same as the Upper Turbidite Unit of Bugge et al. (2002). Unit Tr2 is dominated by marginal marine deposits. Unit Tr3 is continental, as implied by its brownish-red colour, and partly marginal marine as shown by the presence of scattered marine algae. Müller et al. (2005) dated this depositional unit as Mid Triassic. Unit Tr4 is dominated by marine deposition as shown by the presence of evaporites. These evaporites consist of two thick halite beds (called Lower Salt and Upper Salt) separated by a thick mudstone succession which contains a thin anhydrite (Jacobsen & van Veen, 1984; Müller et al., 2005). The youngest Triassic interval was named unit Tr5 and its base is marked by an extensive mud-dominated deposit thought to have been deposited in a shallow lacustrine basin (Müller et al., 2005). The seismic boundary between unit Tr4 and Tr5 is marked by a strong amplitude reflector (top Upper Salt). The upper part of Unit Tr5 is characterised by thick sandstones, interbedded with greenish-grey mudstones and thin coal beds (Müller et al., 2005). This alternation marks the transition into the Lower Jurassic Åre Formation (Dalland et al., 1988).

2. Dataset and methodology

Over one hundred 2D seismic lines and two 3D seismic cubes have been used for the interpretation of the study area. Wellbores 6507/6-4 A and 6608/8-1 have penetrated the upper Permian reflectors and upper Permian sedimentary packages (Müller et al., 2005; NPD, 2013) on the margins of the Trøndelag Platform (Fig. 1). These reflectors and packages have been followed from where the seismic lines cross the wellbores to the deeper basinal areas. The specific amplitude characteristics of the reflectors were used in their identification on the different lines, ensuring a correct description especially where reflectors were difficult to follow. On these lines, nine major reflectors were interpreted to identify the stratigraphic positions of different basin fills and to study the tectonic development of the area. These reflectors are, from oldest to youngest (Fig. 2): the top of the basement, two Permian reflectors (called P1 and P2), and six Triassic reflectors. The Triassic reflectors are: a Permo–Triassic (P-T) reflector (most likely the Permo–Triassic boundary, as discussed below), two Lower Triassic reflectors (LT1 and LT2), the Mid Triassic reflector, the base Lower Salt, and top Upper Salt reflectors (Fig. 2). Age assignment for the reflectors in the deeper parts of the Froan Basin is limited by the absence of well control. The ages of the P2 reflector, base Lower Salt reflector and top Upper salt reflector were established from well ties (Figs. 3 & 4). The ages of reflectors below P1 as well as the ages of P1, LT1 and LT2, are assigned tentatively, based on their seismic stratigraphic positions (above or below) relative to the P2 and base Lower Salt reflectors, and based on onlap features. The absence of good time control means that the assignments can only be tentative, and future work may result in some shifts when better time control becomes available. All deposits below the studied reflectors are assumed to be of Upper Devonian to mid Permian age.

Different stratal relationships (onlap, downlap and toplap) were key to identifying unconformities in the studied succession. The identification of the unconformities was based on definitions and findings of Mitchum et al. (1977) and Kyrkjebø et al. (2004). An unconformity was identified as an onlap or downlap surface in the interiors of the sub-basins and as an angular unconformity in the platform highs (also see Kyrkjebø et al., 2004).

The term unconformity is used here despite the lack of firm time control, meaning that the surface referred to could be an actual unconformity, a diastem, or a more complex surface. This use of terminology follows previous descriptions of the stratigraphy in the area, but may

need to be changed in the future if better information becomes available. Unconformities have traditionally been considered to be timelines/barriers that separate younger deposits from older strata (Mitchum et al., 1977), but recently it has been shown that these surfaces can be composite and diachronous and do not always separate younger strata from older rocks (Kyrkjebø et al., 2004; Holbrook and Bhattacharya, 2012; Gani, 2017). A composite surface is defined by Gani (2017) as “an amalgamation of many surfaces, simultaneously representing surfaces of deposition, erosion, nondeposition and/or sediment bypass along that surface”. Understanding the underlying complexity, the unconformities presented in the current work will be limited to the geometrical relationships reflecting these periods of deposition, erosion and nondeposition based on a respective tectonic position. The time aspect of the unconformities was not the focus of this work, instead ages of the unconformities will be established tentatively from the available well data.

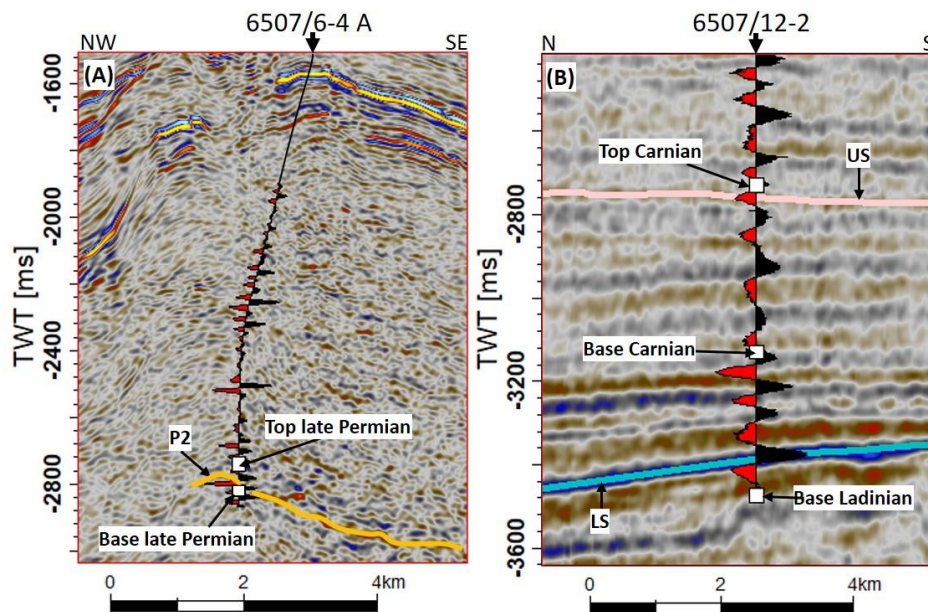


Figure 3. Well ties used to constrain ages of the analysed interval. In this figure, negative and positive seismic responses are shown by red and blue/black colours respectively. (A) 3D inline 9240 of the ST13M09 survey constraining the P2 age on core 6507/6-4 A in the Nordland Ridge. Here the P2 reflector was traced on a negative reflector. (B) 2D seismic line crossing well 6507/12-2 constraining the ages for the base Lower Salt (LS) and top Upper Salt (US) reflectors in the Trøndelag Platform. TWT – two-way-travel time.

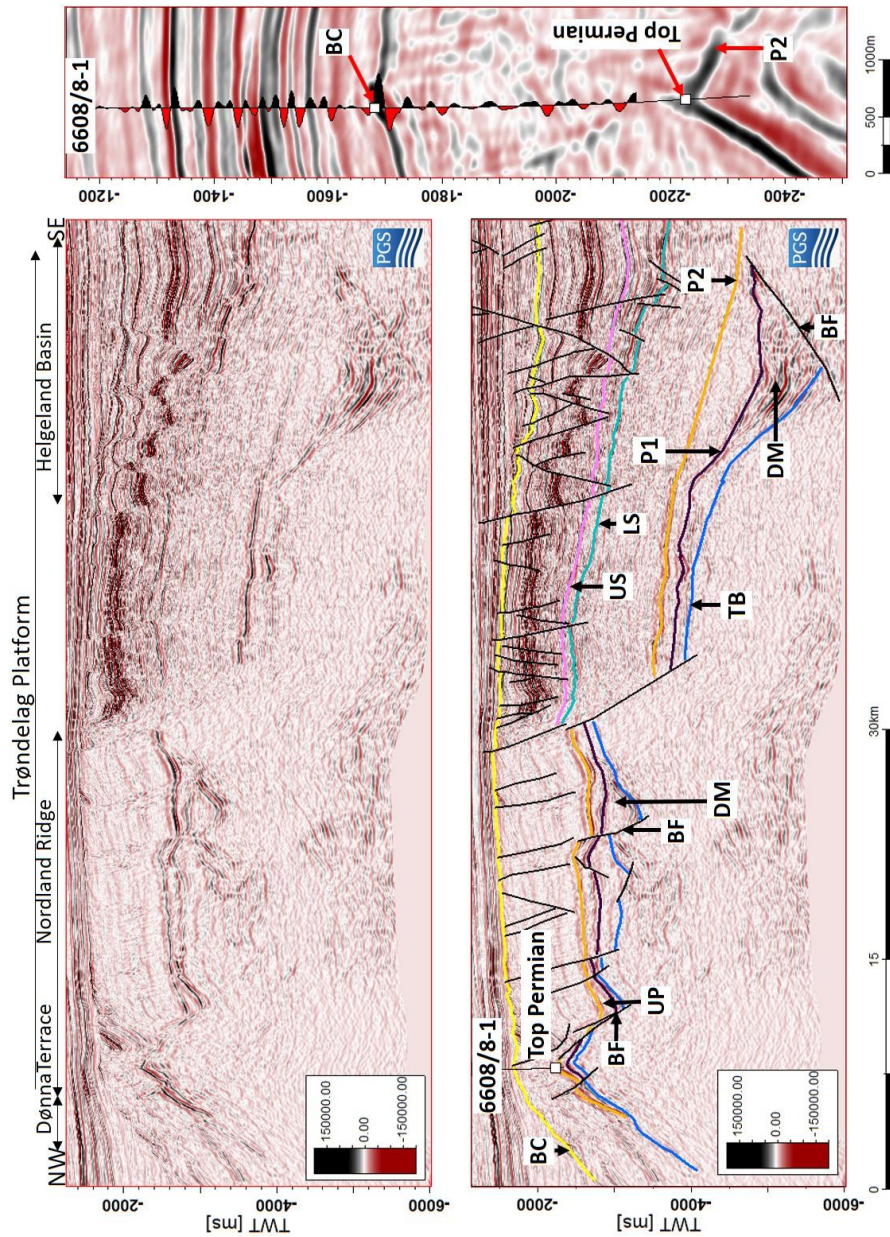


Figure 4. Uninterpreted and interpreted 3D inline 38198 of the PGS16005 survey (see Fig. 1 for location). Wellbore 6608/8-1 has penetrated the late Permian reflector (P2). A box to the right shows a zoomed seismic area of the interval penetrated by the wellbore 6608/8-1. The P2 reflector is part of the upper Permian wedge in the Nordland Ridge. Sedimentary wedges below the upper Permian wedges (UP) are tentatively assigned an Upper Devonian–mid Permian age (DM). The base Lower Salt (LS) and top Upper Salt (US) reflectors are only present in the Helgeland Basin. Both DM and UP are fill type A shown in Fig. 5. TB – Top basement, BC – Base Cretaceous, BF – bounding fault.

3. Results and interpretations

In this section, the main findings from the 3D and 2D conventional seismic interpretation will be presented using eight 2D lines and two lines from the 3D data sets (the locations of these lines are shown in Fig. 1). The other lines show similar results, and were in addition used for correlation of reflectors across the Trøndelag Platform. In the presented results, the terms positive and negative reflector stand for increased and decreased acoustic impedances respectively.

3.1. Sedimentary fill types

The interpretation of active tectonics versus quiescent phases has been based on different basin fill geometries. The studied interval contains six sedimentary fill geometries (Fig. 5). Fill geometry A is characterised by a wedge shape, i.e. thickening of the total fill towards the bounding fault, and by a thickening of the internal strata toward the bounding fault. This stratal pattern reflects syn-rift sedimentation (Nøttvedt et al., 1995; Ravnås & Bondevik, 1997; Steel, 1998; Elliott et al., 2017). Fill type A was recognised in the Upper Devonian–mid Permian, upper Permian–Lower Triassic and Upper Triassic successions (Figs. 4, 6, 7, 8 & 9).

Fill type B in Fig. 5 is also wedge-shaped, but in this case the internal strata have more or less uniform thickness and are normally gently dipping to flat-lying. This pattern means deposition did not take place during the movement of the fault but was a later process that infilled existing topography (Nøttvedt et al., 1995). It is therefore indicative of a post-rift quiescent period. This fill type is shown by some of the Middle-Upper Triassic intervals (Fig. 10).

A third wedge type (fill type C) is a combination of fill types A and B, where the fill is composed of two parts, with a lower part where strata thicken towards the bounding fault as shown by fill type A (thus indicating fill during active fault movement), and an upper part where strata are of more or less uniform thickness (thus indicating fill after the movement on the fault had stopped but before the basin was full). This fill type is seen in the Lower Triassic and Upper Triassic intervals in the Helgeland Basin and the Nordland Ridge (Fig. 7). It is described as a separate type here as it is the only case where a basin has been filled in multiple stages.

Fill type D in Fig. 5 shows a sedimentary fill containing strata that thicken basin-ward and downlap onto pre-existing topography. These strata fill lows in existing basin topography

during a tectonically quiescent period. An example of this is the Upper Devonian– mid Permian fill in Fig. 11, where the strata downlap onto the basement.

Fill type E shows a sedimentary fill containing deposits interpreted to have filled a saucer shaped depression that is not influenced by faulting. The strata are thickest in the middle of the depression and thinnest toward the flanks, which implies fill of a thermally subsided basin. This fill type has been observed in the Upper Triassic interval in the Helgeland Basin (Fig. 12).

Fill type F is somewhat different and is characterised by rotated internal strata and has a clear folded top. The package is bounded by a rotated, low angle fault. The folding of the entire package is due to post-fill tectonic deformation. This wedge type accommodates the Upper Devonian– mid Permian sedimentary successions (Fig. 13).

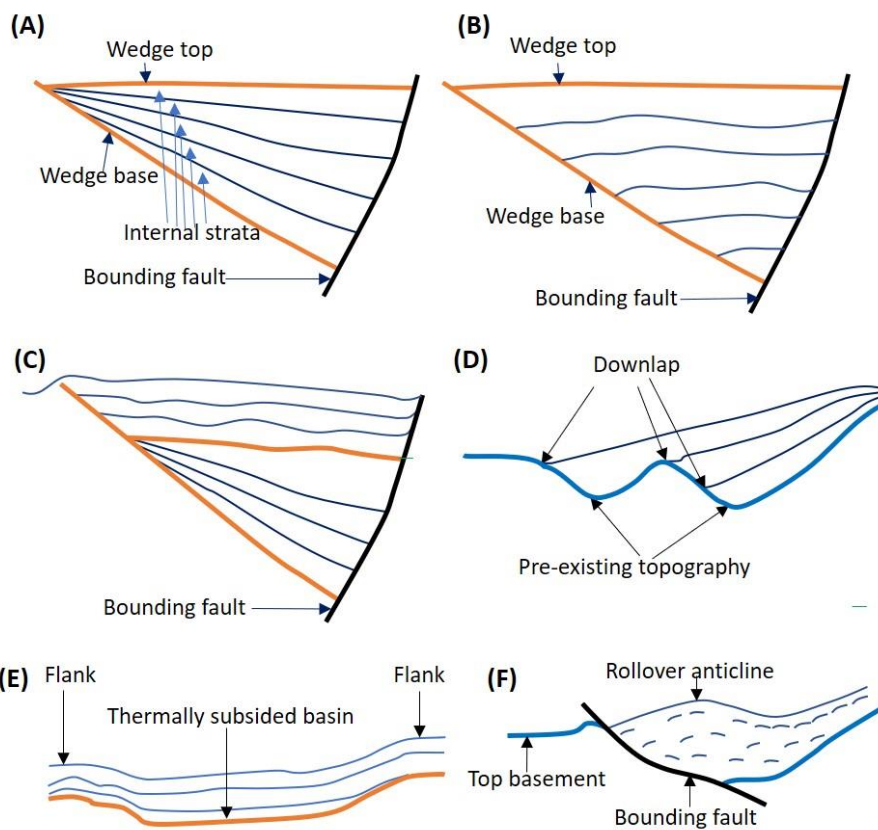


Figure 5. Cartoons illustrating different sedimentary fill geometries identified in the study area. A: syn-rift sedimentation, B: post-rift sedimentation, C: syn-rift followed by post-rift sedimentation, D: infill of existing topography, E: infill of thermally subsided basin, F: tectonic deformation after infill. See main text for discussion.

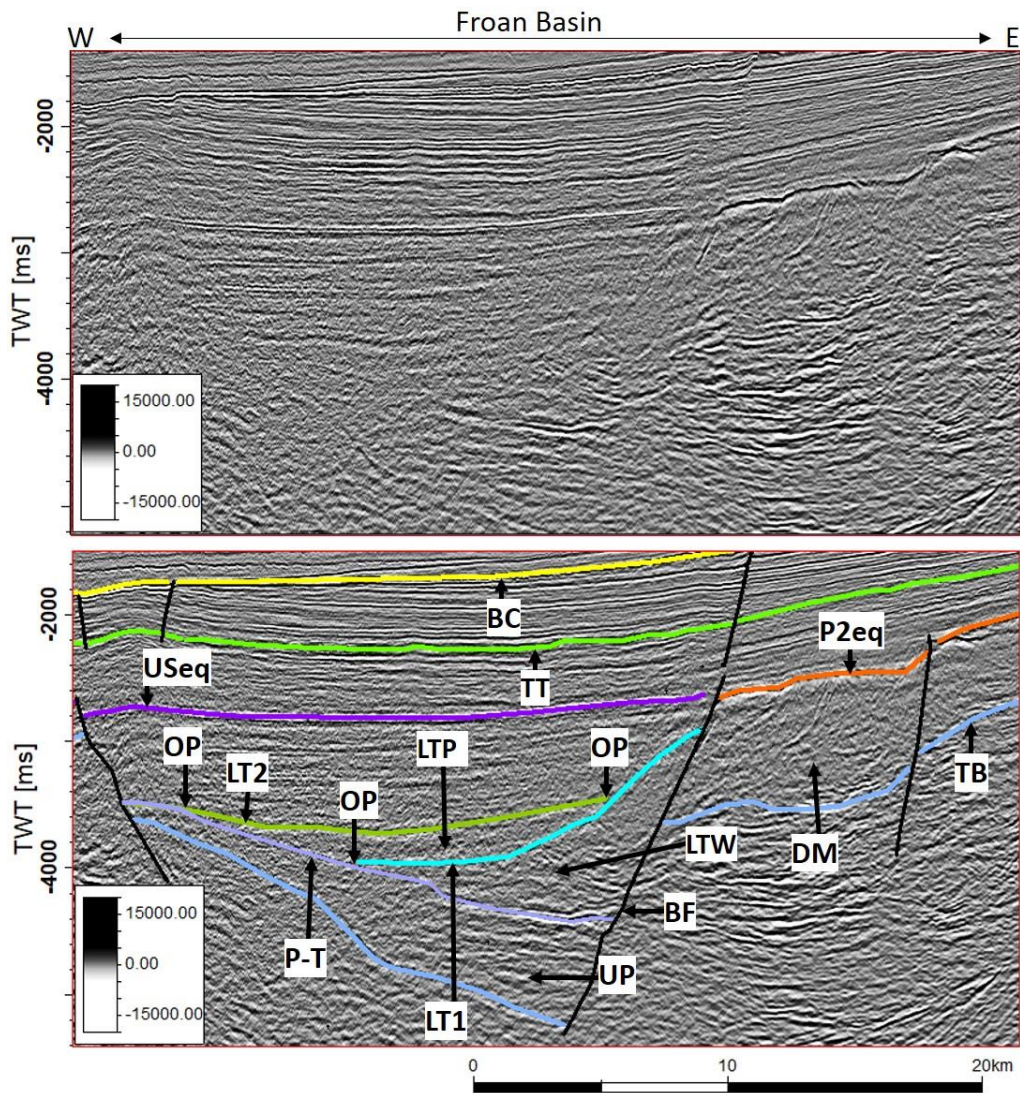


Figure 6. Uninterpreted and interpreted seismic line MNR07-7118 through the Froan Basin (see Fig. 1 for location). Both the upper Permian (UP) and Lower Triassic (LTW) wedges are bounded by a westward dipping major fault (BF). Both UP and LTW are fill type A shown in Fig. 5. P2eq is the top of the Upper Devonian–mid Permian package (DM). The P-T reflector is the top upper Permian. The Lower Triassic reflectors (LT1 and LT2) onlap onto the P-T reflector indicating that the P-T is an unconformity. LT2 onlaps onto LT1 indicating an unconformity between LT1 and LT2. The top Upper Salt equivalent reflector (USeq) has been mapped in the Froan Basin. OP – onlap, BC – base Cretaceous, TB – top basement, LTP – Lower Triassic package.

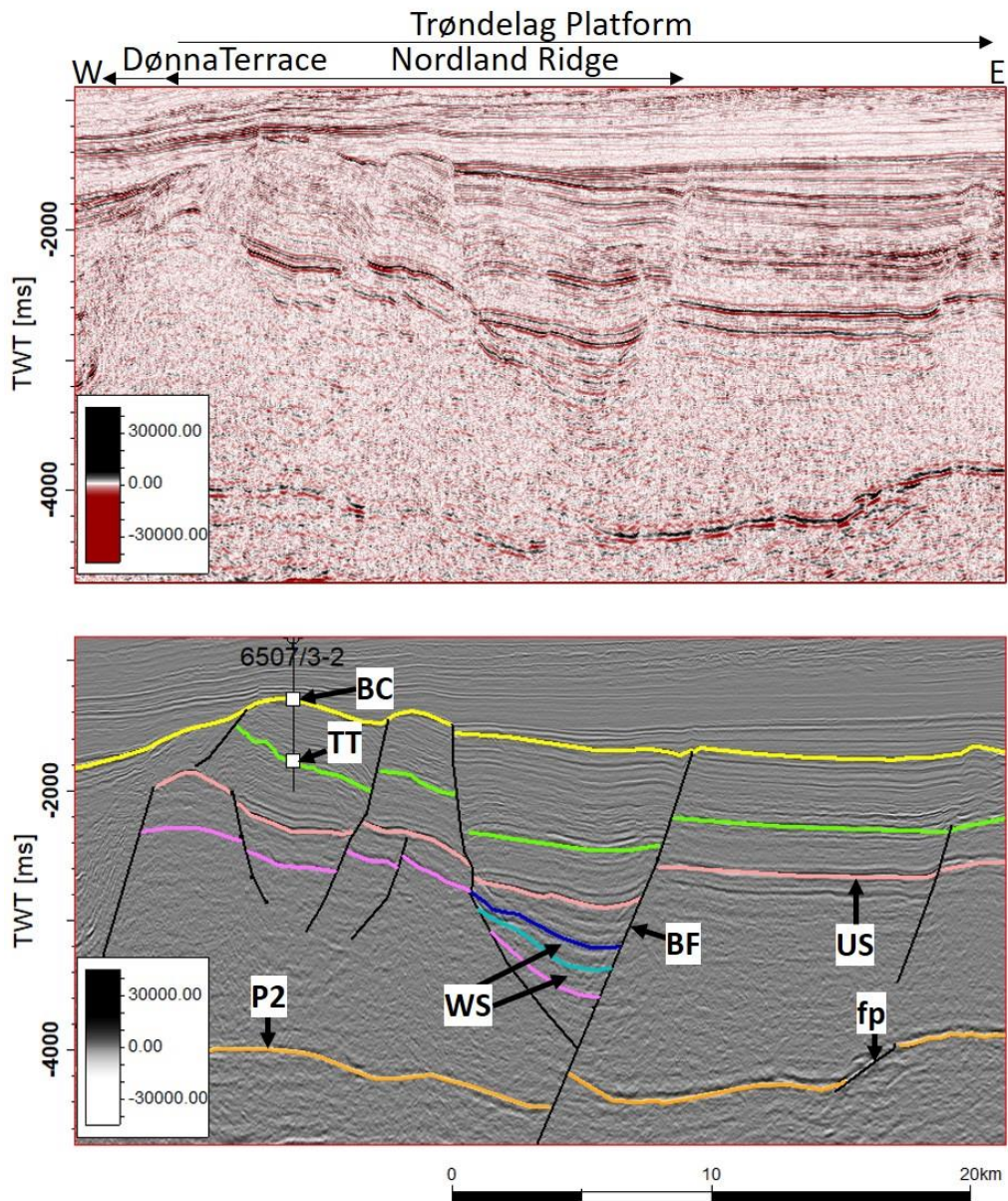


Figure 7. Seismic line MNR07-7294 showing that the P2 reflector, which is discontinued by multiple faults, can be followed all the way through the Nordland Ridge (see Fig. 1 for location). This figure also shows a sedimentary wedge thickening towards a bounding fault (BF). The wedge internal strata (WS) up to the top Upper Salt (US) thicken toward the bounding fault as shown by fill type A in Fig. 5. The top of the wedge is marked by US; thus, the wedge is assigned to the Upper Triassic interval. The strata above the Upper Triassic wedge have uniform thickness. In this line, Triassic top (TT) and base Cretaceous (BC) ages are constrained by wellbore 6507/3-2 (see NPD, 2003 for well information). fp – fault that has discontinued the P2 only, TB – top basement.

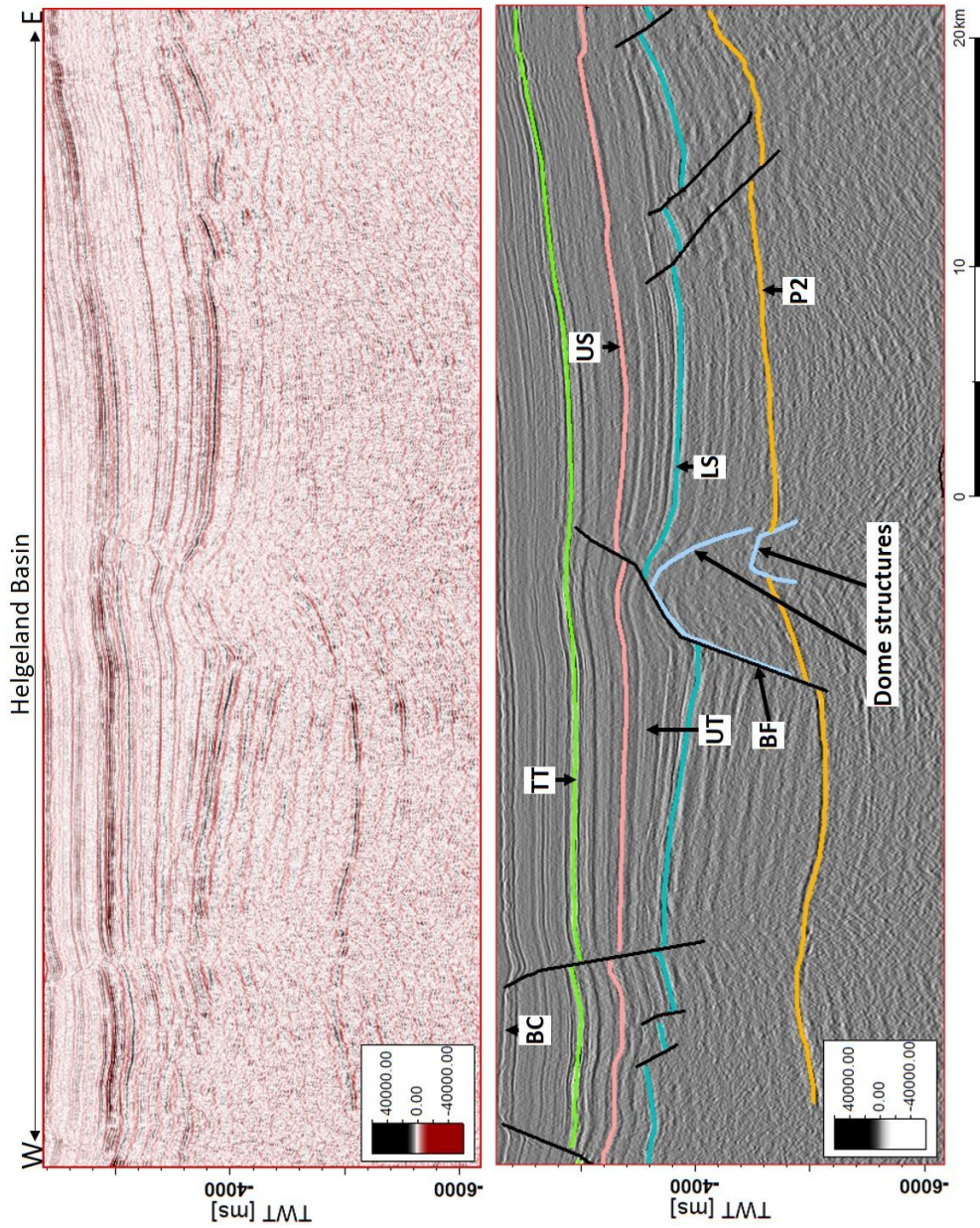


Figure 8. Uninterpreted and interpreted seismic line MNR-7314 in the Helgeland Basin (see Fig. 1 for location). Two dome shaped structures, one on top of the other, are seen. The base Lower Salt (LS) and top Upper Salt (US) reflectors encase a sedimentary deposit (UT) that thickens towards a bounding fault (BF) as shown by fill type A in Fig. 5, although draping onto the dome structure complicates the stratal geometry. The P2 reflector and LS and US have been discontinued by the bounding fault. The bounding fault follows the surface of the upper dome structure. TT – Triassic top.

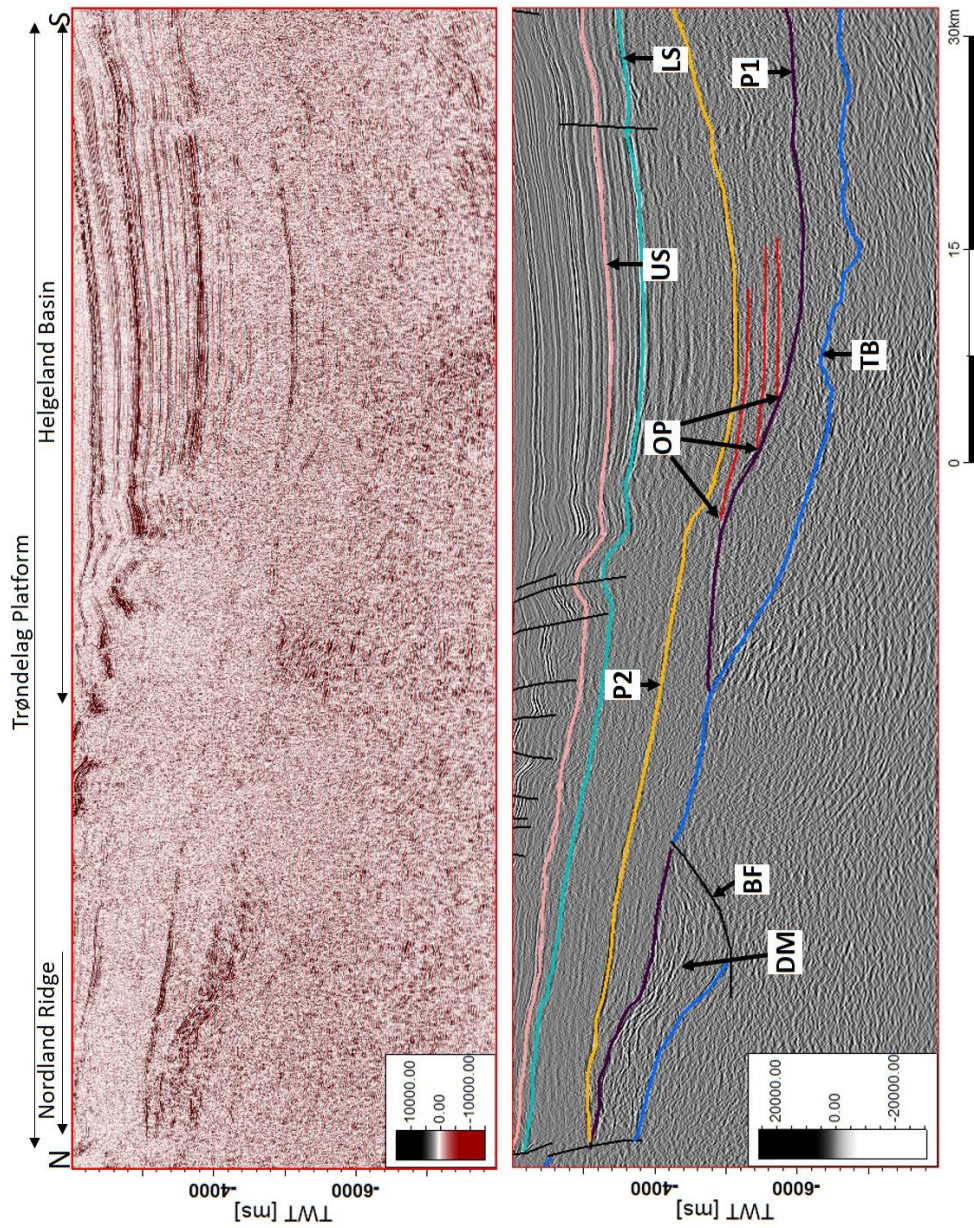


Figure 9. Seismic line MNR08-518 (uninterpreted and interpreted) showing a syn-rift wedge of Upper Devonian–mid Permian age (DM). The top basement (TB), P1 and P2 are discontinued by a bounding fault (BF). P2 is laterally more extensive than P1. P1 onlaps onto the basement (fill type D) and other reflectors (red) onlap (OP) onto the P1. The interval between the base Lower Salt (LS) and top Upper Salt (US) thins towards the Nordland Ridge and is thickest in the Helgeland Basin. DM is a fill type A shown in Fig. 5.

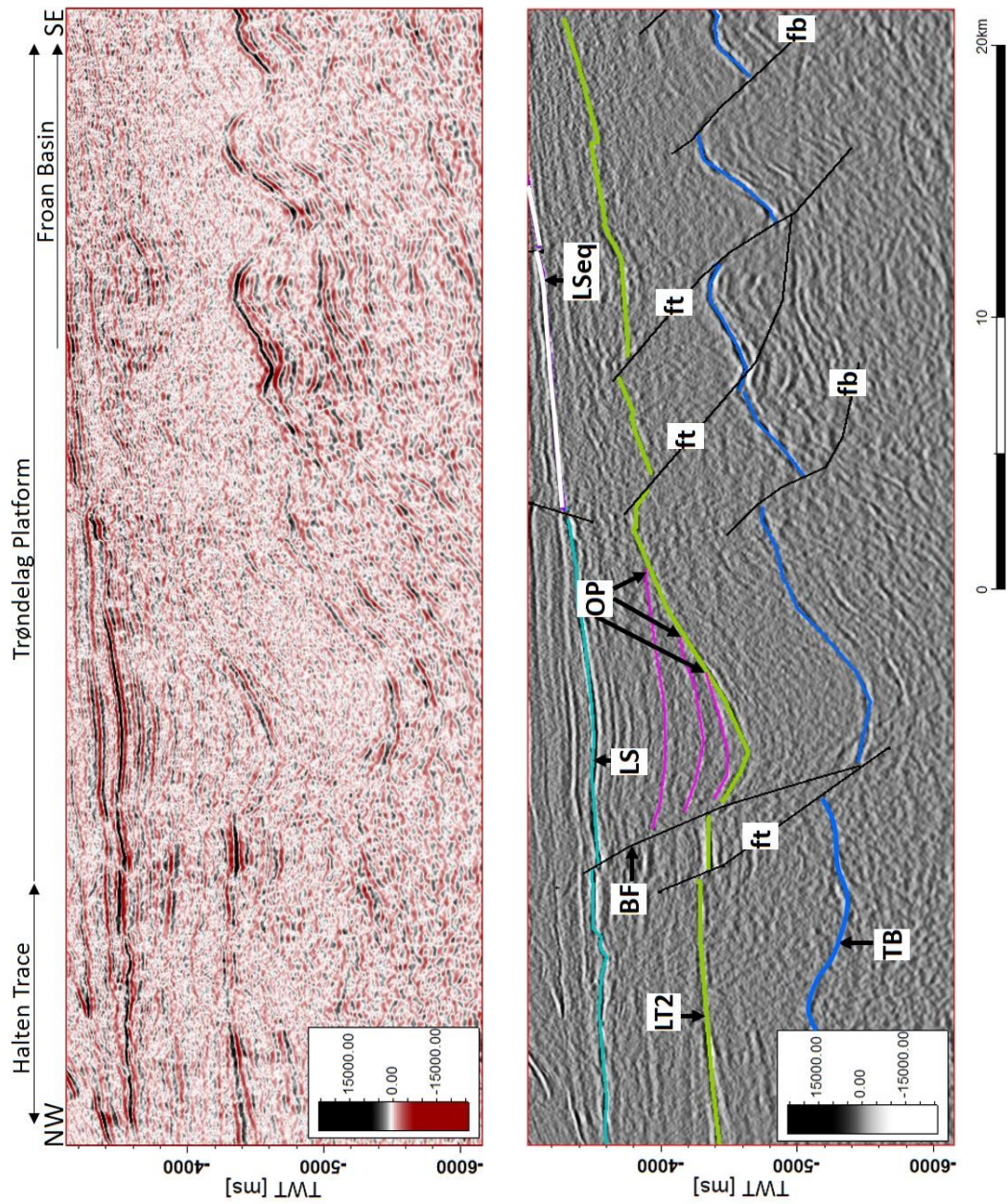


Figure 10. Uninterpreted and interpreted seismic line MNR11-90507 through the Trøndelag Platform (see Fig. 1 for location). Pink reflectors onlap (OP) onto the LT2 reflector, indicating fill type B of Fig. 5. The base Lower Salt (LS) and the overlying strata are characterised by more or less gently dipping strata of uniform thickness. fb – faults that have displaced top basement only, ft – faults that have displaced the top basement- Lower Triassic reflectors, TB – top basement and LSeq is an equivalent of the base Lower Salt reflector in the Froan Basin.

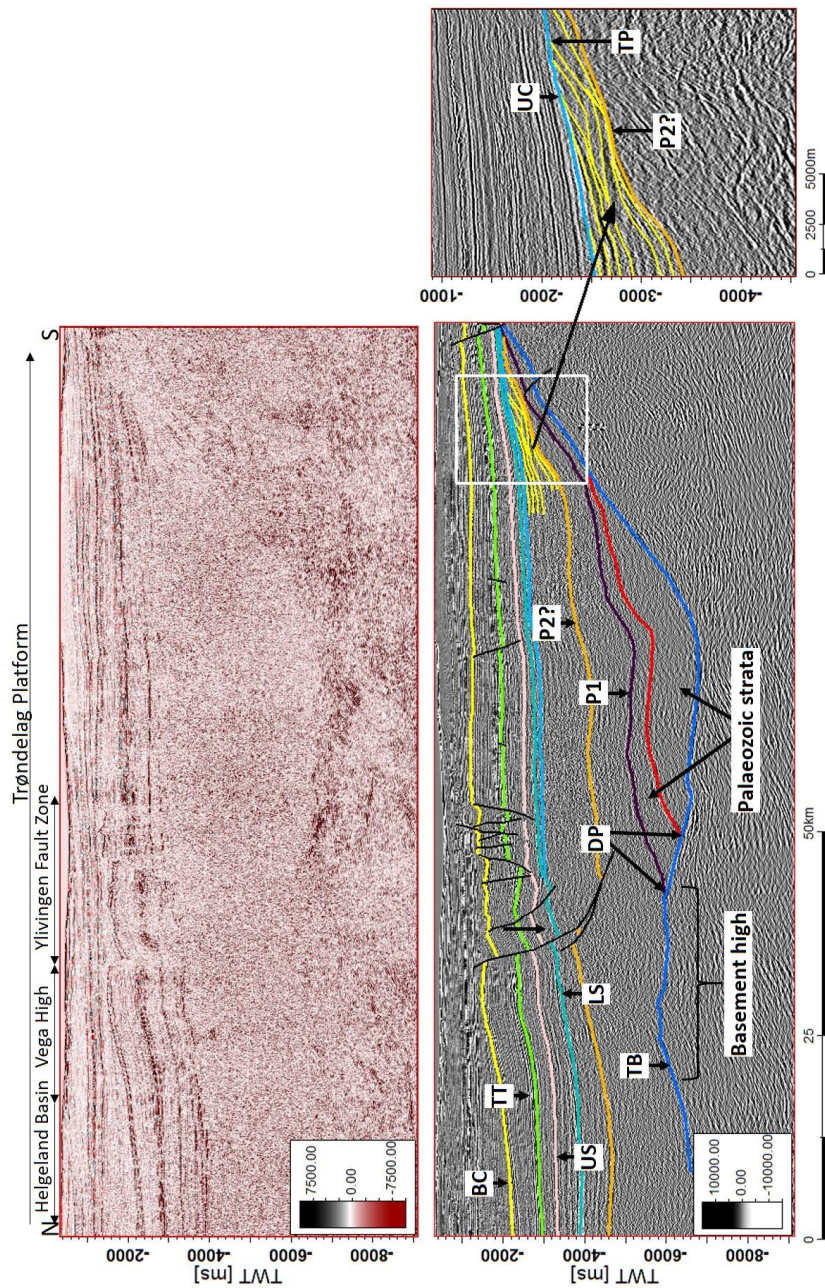


Figure 11. Seismic line MNR07-540 (uninterpreted and interpreted lines) through the Trøndelag Platform (see Fig. 1 for location) showing southward thinning of Palaeozoic strata which downlap (DP) onto the top of the basement (TB) in deeper areas (fill type D in Fig. 5). An interval between the base Lower Salt (LS) and top Upper Salt (US) also thins southward toward a structural high. The insert shows reflectors (yellow) that toplap (TP) at the Middle Triassic unconformity (UC) reflector. TT – top Triassic. A question mark is used where the P2 position is uncertain.

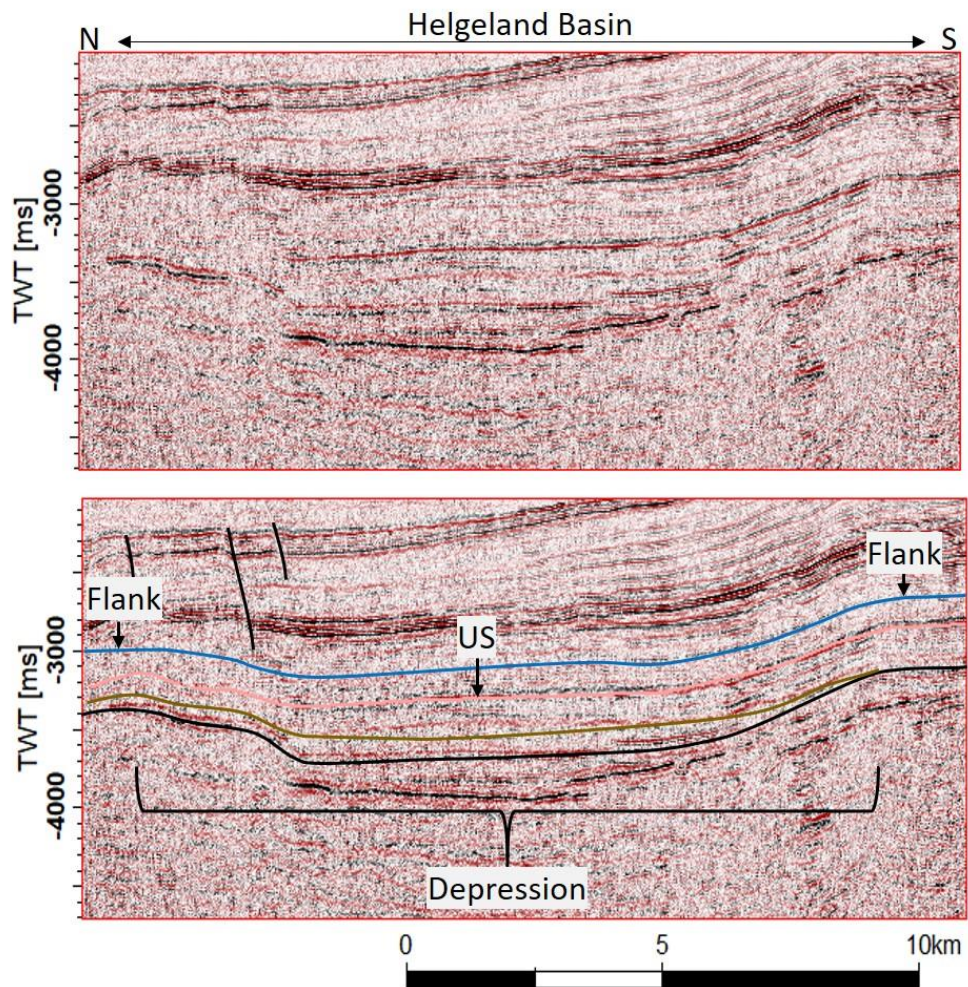


Figure 12. Top and bottom images show uninterpreted and interpreted parts respectively of seismic line MNR07-540 in the Helgeland Basin. The section shows a depression filled by sedimentary deposits. The Upper Salt is part of the successions filling the depression. Other reflectors were traced to show the depression geometry. The depression has a thick sedimentary package in the middle and thin deposits at the flanks. This is fill type E in Fig. 5.

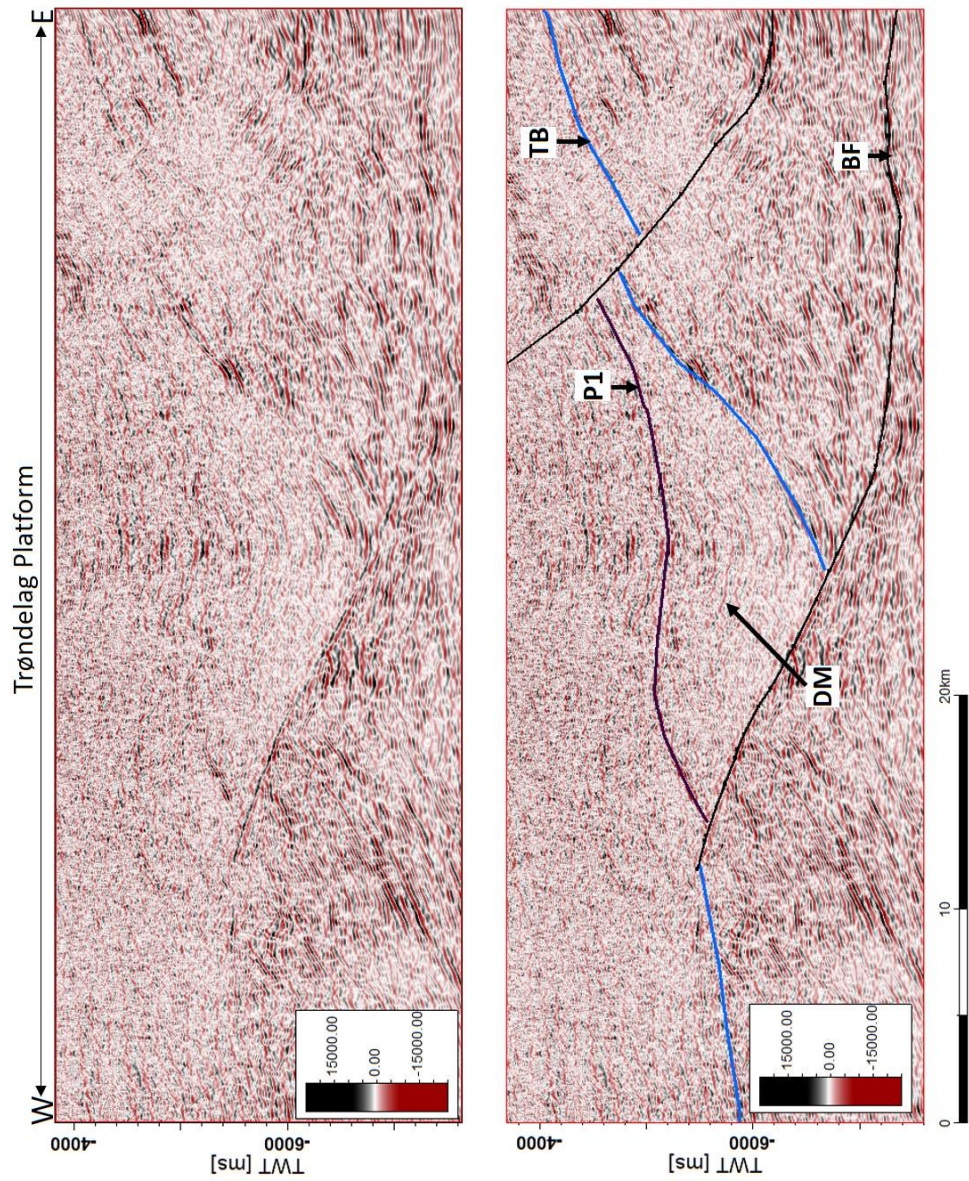


Figure 13. Top and bottom images show uninterpreted and interpreted seismic line MNR06-7260 respectively (see Fig. 1 for location). The Upper Devonian–mid Permian wedge (DM) is bounded by a low angle fault (BF) and contains weak internal reflectors that are rotated (fill type F in Fig. 5). The P1 reflector is weakly folded, marks the top of the upper Devonian–mid Permian wedge and onlaps onto the bounding fault.

3.2. Reflectors and packages

Based on the fill types and the ages of reflectors, the following tectonic development can be seen in the Trøndelag Platform. The description focusses mostly on the indicators of active tectonic phases.

3.2.1. Top basement

The top of the basement is marked by a positive reflector that overlies the bottommost chaotic interval (see Fig. 6) and can be seen in the entire Trøndelag Platform (Figs. 4, 6, 9, 10, 11 & 13). It shows varied relief, such as localised highs (Fig. 11), and is in places offset by faults (Figs. 4, 6, 9, 10 & 13). The localised highs on the basement, which are mostly found in the Helgeland Basin (Fig. 11), show Palaeozoic basement topography.

3.2.2. Palaeozoic strata below the P1 reflector

Various basin fill types can be seen in the Palaeozoic strata. The oldest Palaeozoic strata downlap onto the top basement reflector in the deeper parts of the basin in the south and southeast of the Helgeland Basin (Fig. 11) and thin out from the deep areas toward the margins of the platform (Fig. 11). This is the type of fill shown in Fig. 5D, signifying deposition onto pre-existing topography during tectonic quiescence. The Helgeland Basin and Nordland Ridge contain wedge-shaped sedimentary packages that thicken toward bounding faults (Figs. 4 & 9). These wedges show fill type A (formed during active tectonics) of Fig. 5. South and southeast of the Helgeland Basin, Palaeozoic fill consists of a rotated wedge characterised by rotated internal strata (Fig. 13). The wedge in Fig. 13 is a type F fill of Fig. 5 (fill finished before tectonic deformation).

3.2.3. P1 reflector

The P1 reflector is below P2 (which is a late Permian reflector based on the well tie in Fig. 4). In the northern part of the Trøndelag Platform (including the Nordland Ridge and the Helgeland Basin), P1 is a high amplitude discontinuous reflector that marks the top of the various fill types described above. Some weak reflectors are observed onlapping onto the P1 reflector in the Helgeland Basin (Fig. 9). The combination of overlain basins with different fill types and onlap onto the reflector indicates that P1 is an erosional surface. Because P1 is below P2 in every area where both of them are present, including in locations with well ties,

and because it is an onlap surface, it is thought to mark the mid Permian unconformity which has also been found in eastern Greenland (Fig. 2).

3.2.4. P2 reflector

The P2 is a high amplitude reflector in the Trøndelag Platform. The P2 appears as a negative reflector in the well tie in Fig. 3A but it was traced as a strong positive reflector in the well tie in Fig. 4. That is, the P2 reflector shows intensity variation and polarity change from strong positive in some parts of the Nordland Ridge (Fig. 4) to strong negative in most of the central part of the Helgeland Basin (Fig. 7). Fig. 4 shows a good example of P2 dimming, where the intensity of the reflector decreases as it approaches the sedimentary wedge in the southeastern part of the seismic line in the Helgeland Basin. The intensity variation of the P2 reflector is attributed to the fact that the P2 overlies multiple rock units with different petrophysical properties. The P2 reflector overlies at least four different rock units (units 1-4) as described in the discussion.

The P2 reflector is generally laterally extensive in most of the northern part of the Trøndelag Platform (Figs. 7 & 11), although it is locally discontinuous. For example, it can be followed from west to east across the Helgeland Basin and in some parts of the Nordland Ridge (Fig. 7). The P2 reflector cannot be traced directly from the Helgeland Basin to the Froan Basin but an equivalent reflector in the same stratigraphic position and with the same amplitude characteristics is found in the Froan Basin. This equivalent reflector has been named P2eq (Fig. 6). The P2eq is a high amplitude positive reflector overlying the Upper Devonian–mid Permian package in the Froan Basin (Fig. 6).

Sedimentary wedges (fill type C) containing P2 are interpreted to contain upper Permian successions because P2 is the late Permian reflector (see Fig. 4). In the Helgeland Basin and the Nordland Ridge, the reflectors above P2 are more or less parallel (Fig. 4). An example of this is the uniform thickness of the sedimentary layers between P2 and the base of the Lower Salt from the southeastern end of the Nordland Ridge to the Helgeland Basin (Fig. 4). Such a sedimentary configuration indicates a change from syn-rift sedimentation during the late Permian, as illustrated by fault-ward thickening strata immediately below P2 (e.g. UP in Fig. 4), to post rift sedimentation characterised by more or less uniform thickness strata (fill type B) during the Lower Triassic– Middle Triassic.

3.2.5. P-T reflector

The P-T reflector is identified in the Froan Basin (Fig. 6), as a negative low amplitude reflector, where it marks the top of an upper Permian wedge-shaped sedimentary package (fill type A). The P-T reflector was difficult to follow with certainty in most of the seismic profiles. It is interpreted as the Permo–Triassic boundary because it marks the top of the upper Permian wedge, although as mentioned by Bugge et al. (2002) it is difficult to be clear about the exact depth of this stratigraphic boundary. The P-T reflector is an unconformity since other reflectors onlap onto it (Fig. 6). There is an equivalent P-T reflector in the Helgeland Basin, but it is difficult to follow.

3.2.6. LT1 reflector

The LT1 is a negative low amplitude reflector that is only present in the Froan Basin (Fig. 6). It overlies a steeply dipping wedge that thickens towards the bounding fault (fill type A of Fig. 5, fill during active tectonics). The LT1 onlaps onto both the P-T reflector and the bounding fault. The steeply dipping wedge is assigned a Lower Triassic age because it is just above the upper Permian wedge (LTW in Fig. 6).

3.2.7. LT2 reflector

The LT2, a negative low amplitude reflector, is only present in the Froan Basin and onlaps onto the P-T and LT1 reflectors (Fig. 6). LT2 is the top of the Lower Triassic fill (LTP) that overlies the steeply dipping wedge fill (LTW) in Fig. 6. The LT2 reflector marks the top of the Lower Triassic fill which dips in the same direction as the LTW (Fig. 6). The onlap relations shown by the LT1 and LT2 reflectors indicate either different depositional time, nondeposition and/or erosion, or renewed tectonics.

3.2.8. Middle Triassic

A positive high amplitude toplap reflector is observed in the Trøndelag Platform to the north of the Froan Basin, indicating an angular unconformity. The toplap reflector is a gently northward dipping surface with high amplitude just below the base of the Lower Salt (Fig. 11). The well tie in Fig. 3B gives a Middle Triassic age for the base of the Lower Salt, and thus the toplap surface is interpreted to be of Middle Triassic age in the Trøndelag Platform north of

the Froan Basin. Reflectors which top lap onto the Middle Triassic unconformity are stratigraphically between the late Permian reflector (P2) and the unconformity (Fig. 11).

3.2.9. Upper Triassic

The base of the Lower Salt is marked by a discontinuous positive high amplitude reflector (Figs. 3B & 4). The top Upper Salt is marked by a discontinuous negative high amplitude reflector (Figs. 3B & 4). No salt deposit has been penetrated by wellbores just to the north of the Froan Basin, but the equivalents (in terms of amplitude characteristics and stratigraphic positions) of the base Lower Salt (LSeq) and top Upper Salt (USeq) reflectors can be followed southwards to the Froan Basin (Figs. 6 & 10). In the Frøya High (see Fig. 1 for well location), the USeq overlies a shaly interval penetrated by wellbore 6407/10-3 (NPD, 2004a) rather than Upper Salt, hence the designation as equivalent reflector in the Froan Basin. In the central and northern parts of the Trøndelag Platform, the salt layers thin out toward the structural highs (Figs. 9 & 11): the salt deposits are thickest in the parts furthest away from the shoreline and away from the platform highs. This seismic pattern agrees with well data since correlation between wellbores 6507/12-2 and 6507/12-1 has shown that all layers (thus including the salt layers) thin toward the edges of the Trøndelag Platform (NPD, 2004b). Sedimentary wedges in Figs. 7 & 8 (fill type A of Fig. 5, fill during active tectonics) are Middle-Upper Triassic deposits because they are encased between the Lower and Upper Salts that are of late Mid-Triassic to early Late Triassic age (see the well tie in Fig. 3B).

3.3. Dome shaped structures

The new seismic data show previously undetected dome structures in the deep part of the Helgeland Basin. Two isolated dome shaped structures, one on top of the other (Fig. 8), are observed on three seismic lines in the Helgeland Basin, about 83 km west of the present Norwegian coastline. The lower structure is a topographic relief beneath the upper structure. The bases of these structures are within the Carboniferous–Permian deposits of the Helgeland Basin while the top of the upper structure is within the Upper Triassic strata and ends just below the top Lower Salt reflector. The structures show vertical zones of deteriorated seismic quality. These dome shaped structures can be traced up to about 16 km in a N-S orientation and about 7.5 km E-W. The upper structure is wider than the lower structure. Both dome

shaped structures have steep slopes. Reflectors onlap onto these structures (for example, the P2 reflector onlaps onto the lower structure). At the top of the structure a monocline is observed in faulted superjacent strata.

3.4. Faults

Large-scale faults occur in the study area. They displaced the major reflectors and influence the basin fill patterns. These are the faults active before the late Permian, late Permian faults, and late Permian–Triassic faults. The name of a fault reflects the age of the section that was displaced when the fault was active. For example, the sedimentary wedge in Fig. 8 is confined between the salt reflectors. These salts are of late Mid Triassic to early Late Triassic age (Jacobsen & van Veen, 1984; Müller et al., 2005), thus the bounding fault is named late Triassic fault due to the age of the salt layers.

Faults that were active before the late Permian displaced the top of the basement and bound the Upper Devonian–mid and upper Permian strata (Figs. 4 & 13). These faults are bounding faults for fill types A and F of Fig. 5. The bounding faults for the Upper Devonian–mid Permian sedimentary wedges in the deeper parts of the Trøndelag Platform are flatter than other faults (Figs. 4 & 13).

All faults that have discontinued only the P2 reflector (Fig. 7) are named late Permian faults. These faults have only been found in the Helgeland Basin. The late Permian–Triassic faults bound the upper Permian wedges and Lower Triassic packages (Fig. 6) indicating fault activity during the Permo–Triassic (fill type A of Fig. 5, fill during active tectonics).

4. Discussion

4.1. Dome structures

It is not immediately clear what the dome shaped structures are that are present in strata of Carboniferous to Lower Triassic age in the Helgeland Basin (Fig. 8). Based on observations in areas offshore Norway, one of the two following explanations is most likely. The first possible explanation is that the structures are intrusions. The mid Norway-eastern Greenland separation was accompanied by widespread volcanism during the Palaeocene to Eocene that led to several intrusive magmatic bodies in the Frøya High and the Møre and Vøring basins (Prestvik et al., 1999; Brekke, 2000). However, several intrusion-induced features were not

observed in the analysed seismic images. Missing features include minor faulting (but still observable on seismic) of the immediate strata above the intrusion (Zhao et al., 2014; Zhao et al., 2016) which occurred during intrusion (only a major fault is seen), or saucer and eye shaped structures (e.g. Brekke, 2000; Hansen et al., 2007).

The second possible explanation is that the structures are isolated carbonate build-ups, as the structures show multiple features described by Burgess et al. (2013) to identify such build-ups. Carboniferous–Permian carbonates and carbonate build-ups are known from the Barents Sea (Stemmerik et al., 1999; Elvebakk et al., 2002), the Nordland Ridge (Bugge et al., 2002), eastern Greenland (Surlyk, 1990), and from fragments in the turbidite units (Bugge et al., 2002). The depositional conditions were therefore conducive for carbonate deposition and the domes may be Carboniferous-Permian carbonate build-ups that formed positive relief over which late Permian and Triassic sediments were deposited. From the criteria given by Burgess et al. (2013), the following are observed here. Both dome structures have steep margins. Strata overlying the domes are faulted and folded by a fault that displaces upper Permian–Upper Triassic strata and thus postdates the domes. The faulting and folding are probably due to differential compaction; early cementation of carbonates in the area (Bugge et al., 2002) means that the build-ups would have been more resistant to compaction and faulting as compared to the surrounding deposits. The build-ups in turn formed local highs causing onlap of later deposits, for example the P2 reflector (Fig. 8). The stacking of the two domes indicates a long-lived location, as also found in the Barents Sea by Elvebakk et al. (2002). In addition to the geometric criteria, the width of the structures (about 7.5 and 16 km for the lower and upper structure respectively) fall within the ranges of known carbonate build-ups given by Burgess et al. (2013).

If the interpretation of isolated Carboniferous-Permian carbonate build-ups is correct, then this shows that carbonates were widespread throughout the area during the initial opening of the seaway, extending to east Greenland and the Barents Sea. It is possible that more Carboniferous-Permian carbonate build-ups exist in the area, but it was not possible to identify any more due to the limited quality of the seismic data set. Absence of these carbonates in the Triassic interval may have been caused by an increased clastic supply due to multiple gravity flows that dominated the area during the late Permian– Early Triassic (Bugge et al., 2002) and continued drowning of the area due to late Permian– Early Triassic

transgression (Surlyk et al., 1984; Doré, 1992). However, more research will be needed to confirm whether these structures are carbonates, or whether they are intrusions, or something else.

4.2. P2 reflector intensity

The intensity of the late Permian reflector P2 dims toward the sub-basins of the Trøndelag Platform area (Fig. 4) due to lateral variation in lithological properties. The P2 reflector is interpreted to overlie multiple sedimentary units and that is why its intensity varies, and polarity is reversed, from place to place. A conceptual model was created to show the distribution of these units in the study area (Fig. 14). These units are named units 1-4 and their distributions were based on well reports, the Permo–Triassic deposition model of mid Norway and eastern Greenland of Bugge et al. (2002) and the presence of Upper Devonian sediment offshore and onshore mid Norway (Bugge et al., 2002; Osmundsen et al., 2006).

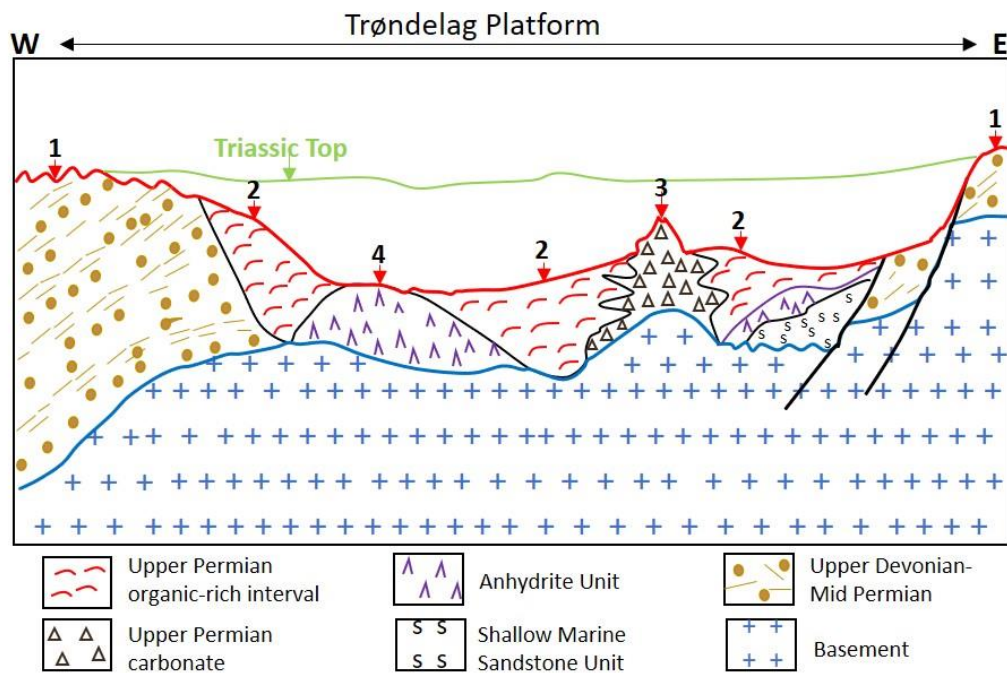


Figure 14. Conceptual Permo–Triassic depositional model showing distribution of the P2 reflector (thick red line). This figure is not to scale. The intensity of the P2 varies depending on what unit is below it. P2 is thought to overlie four different units (1, 2, 3 and 4) which are explained in the main text. The presence of these units is based on NPD wellbore reports, similarities with eastern Greenland, Bugge et al. (2002) and Osmundsen et al. (2006).

Unit 1 contains the Upper Devonian strata and is present in the eastern Trøndelag Platform as inferred from Fig. 6. Devonian clastic strata are documented onshore, directly east of the current study area (Osmundsen et al. 2006). Devonian continental environments were continuous across the area before rifting, and Devonian deposits are present on both sides of the Norway-Greenland seaway (Osmundsen et al. 2006; Guarnieri et al., 2017), so are likely to be present (although unproven) in the interior of the Nordland Ridge (Fig. 4) and Frøya High. Unit 2 consists of upper Permian organic-carbon-rich sediments, based on the description of core 6611/09-U-01 by Bugge et al. (2002) and on the core 6507/6-4 A report (NPD, 2013). Core 6507/6-4 A penetrated sedimentary successions that are age equivalent to Permo-Triassic deposits on core 6611/09-U-01 (NPD, 2013) as indicated in Fig. 2. Unit 3 contains upper Permian carbonates. Upper Permian carbonates have been penetrated by wellbores 6609/7-1 and 6608/8-1 (Bugge et al., 2002; Müller et al., 2005) on the Nordland Ridge (see Fig. 1 for locations). Interfingering of units 2 and 3 is based on the Permo-Triassic depositional model of Bugge et al. (2002). Unit 4 contains the Anhydrite Unit of Bugge et al. (2002). Units 1, 3 and 4 have higher acoustic impedance than unit 2. The units directly above the upper Permian are organic poor (Bugge et al., 2002), thus all successions above P2 can be assumed to have high acoustic impedance. As a result, the P2 is a strong positive reflector when overlying units 1, 3 and 4. The P2 is a strong negative reflector when overlying unit 2 because unit 2 is an organic rich interval with low acoustic impedance and consequently negative reflection.

4.3. Tectonic phases and unconformities

Table 1 summarises the Devonian-Triassic unconformities and rifting events that have controlled sedimentation in the study area. The details of these tectonic phases and unconformities are discussed below.






Interval		Tectonic phase	Location
Triassic	Late	6	Helgeland Basin and Nordland Ridge
	Middle 	6	Between the Froan Basin and northern Trøndelag Platform
	Late Early 	5	Froan Basin
	Early 	4	Froan Basin
Permian	Late	3	Froan Basin, Helgeland Basin, Nordland Ridge
	Middle 	2	Nordland Ridge, Helgeland Basin, an area between the Helgeland Basin and the Froan Basin
	Early	1	
Carboniferous and older		1	
Basement		1	Nordland Ridge, Helgeland Basin and between Helgeland and Froan basins

Table 1. Late Carboniferous–Triassic tectonic phases and unconformities. The unconformities are marked by zigzag lines. Blue arrows show span of the rift episodes.

4.3.1. Devonian–Permian

The late Palaeozoic sub-basins in the Norway-Greenland basin were formed during early extension regimes that led to the initial opening of the Atlantic Ocean (Surlyk et al., 1984). Rifting is reported to have occurred in the south-western Barents Sea during the mid Carboniferous (Gudlaugsson et al., 1998). This rifting episode formed a rift zone that was about 300 km wide and at least 600 km long and was a direct continuation of the north-east Atlantic rift between Greenland and Norway (Gudlaugsson et al., 1998). This continuation suggests that the Devonian–Permian rift occurred on a regional scale.

Different aspects of this period of rifting have also been observed in this work, but not all parts of the Trøndelag platform were affected in the same way. The rifting may have resulted in the basement unconformity shown by the downlap of the Permian strata. Brekke (2000) stated that an early Permian unconformity can be identified in the platform area but did not give further description or supporting references for this. The basement unconformity seen here may be this early Permian unconformity, and it has been mapped in the Nordland Ridge, Helgeland Basin and in the area between the Helgeland and Froan basins. The fact that the bounding faults for the Palaeozoic wedges (Figs. 4 & 13) are flatter than other bounding faults suggests either basement rotation occurred during the Palaeozoic or the presence of low-

angle normal faults in the study area. The presence of low angle normal faults, which have been linked to metamorphic core complexes by Webber et al. (2018), is the most likely interpretation because metamorphic core complexes are present in the study area (see Osmundsen et al., 2005). Formation of these core complexes may have created the basin topography that accommodated Palaeozoic sedimentary fills in the Trøndelag Platform. These Palaeozoic fills thicken toward the deeper parts of the Trøndelag Platform and onlap onto the basement floor (Fig. 11, fill type D of Fig. 5).

The current study has identified Devonian– Permian rift features as indicated by the Upper Devonian– mid Permian wedges that thicken toward the bounding faults (fill type A of Fig. 5) in the Trøndelag Platform (Fig. 4). The Devonian–Permian tectonic events have been reported before (e.g. Blystad et al., 1995) but data and their exact locations in the Trøndelag Platform were not shown. Rifting features of this age are found in most of the central-eastern Trøndelag Platform, to the north of the Froan Basin, in the Nordland Ridge and in a small area to the northwest of the Helgeland Basin (Figs. 4 & 9). The widespread distribution of these features implies rift influence over the entire northern Trøndelag Platform. During the Devonian–Permian rift phase, structural highs could have formed that acted as nucleation sites for carbonate build-ups.

4.3.2. Mid Permian

The second regional tectonic phase has been reported to have taken place during the middle Permian (Brekke et al., 2001). Rifting and erosion characterised the mid Permian in both eastern Greenland, where an extensive mid Permian unconformity has been reported (e.g. Surlyk et al., 1984; Surlyk, 1990; Seidler, 2000; Oftedal et al., 2005; Guarnieri et al., 2017), and the mid Norwegian shelf (Doré, 1992). This unconformity had not been well mapped offshore mid Norway so far.

The P1 reflector is the expression of this tectonic phase in the Trøndelag Platform. The new 3D seismic allowed mapping of this reflector in the Nordland Ridge, Helgeland Basin and in the area between the Helgeland Basin and the Froan Basin. The improved data quality allowed the reflector to be followed from the Nordland Ridge to the Helgeland Basin (Fig. 4). That P1 is an unconformity as shown by the onlap of weak reflectors onto the P1 reflector (Fig. 9), indicating either erosion or non-deposition and consequently an unconformity, basin tilting

after deposition, or both. Basin tilting after deposition indicates rifting during the mid Permian.

4.3.3. Late Permian

The late Permian tectonic phase affected the entire Trøndelag Platform. Late Permian faults and syn-rift deposits, which have been reported previously (Müller et al., 2005), have been mapped in more detail due to the availability of new high-quality 3D data. The 3D data allowed identification of late Permian rift features (faults and syn-rift deposits) in the Nordland Ridge and the tracing of these features from the Nordland Ridge to the deeper parts of the Helgeland Basin (see Fig. 4), thus showing their widespread occurrence which was not clear before. The late Permian rift features (upper Permian wedges, fill type A) are also found in the Froan Basin (Fig. 6) showing that the late Permian tectonic event occurred over all parts of the Trøndelag Platform. In the study area, the occurrence of rifting during the late Permian is also indicated by the late Permian faults (Fig. 7). These faults have been interpreted to indicate a late Permian tectonic event because they only displace the P2 reflector.

4.3.4. Early Triassic

Müller et al. (2005) reported an Early Triassic rifting event offshore mid Norway while two Early Triassic marine rifting events have been reported from eastern Greenland outcrops (Seidler et al., 2004). In the current work, two Early Triassic rift phases were recognised in the Froan Basin in contrast to the one which has been reported previously (Müller et al., 2005).

The two Lower Triassic unconformities were mapped in the Froan Basin based on the onlap relationships between the P-T, LT1 and LT2 reflectors. Both LT1 and P-T reflectors are onlap surfaces interpreted to represent unconformities sensu Mitchum et al. (1977). The onlapping of LT1 onto the P-T reflector shows an equivalent of merging unconformities of Kyrkjebø et al. (2004). The possible existence of a hiatus between Permian and Triassic deposits (in the Helgeland Basin) has also been discussed by Bugge et al. (2002) and Müller et al. (2005) based on description of core data, but here it cannot be differentiated to which of the two Froan Basin unconformities the hiatus in the Helgeland Basin corresponds. Another hiatus is proposed between the two Lower Triassic packages shown in Fig. 6 based on the onlap relationship between them. Onlapping of the Lower Triassic package onto the Lower Triassic

wedge suggests the existence of an unconformity between the two Lower Triassic intervals. These two onlaps indicate the existence of two Early Triassic unconformities in the Froan Basin (Table 1).

Two explanations are possible for the presence of one Early Triassic rift feature (fill type A of Fig. 5) in the Helgeland Basin (Müller et al., 2005), instead of the two rift features (syn-rift deposits and faults) found in the Froan Basin. The first possible explanation is that one of the two Early Triassic rifts did not occur in all sub-basins in the Norway-Greenland Basin. The second possible explanation is that the two rifts occurred over the entire Trøndelag Platform but one of them could not be identified in the Helgeland Basin due to these rift features being thin and below resolution of the current seismic data set. Further analysis on cores penetrating the Lower Triassic interval will be necessary to confirm the presence/ absence of the second Early Triassic syn-rift deposits and faults in the Helgeland Basin, otherwise one Early Triassic rifting episode is considered to have occurred there suggesting localization of tectonic events during that time.

The LT1 and LT2 could not be traced to the Helgeland Basin because they occur in the isolated sub-basins in the Froan Basin, but age equivalent deposits exist since the Lower Triassic sedimentary successions are present in the Helgeland Basin (Bugge et al., 2002; Müller et al., 2005).

4.3.5. Middle-Late Triassic

A local Middle Triassic unconformity limited to the Trøndelag Platform was mentioned by Brekke (2000) without supporting evidence. A Middle Triassic angular unconformity is shown in the current work by the toplap of Lower-Middle Triassic strata against the Middle Triassic reflector at the southern margin of the Helgeland Basin (Fig. 11), north of the Froan Basin.

Block faulting is reported to have occurred during the Mid-Late Triassic to the east of the Nordland Ridge and the Frøya High (Blystad et al., 1995) indicating a Mid-Late Triassic tectonic event. In the current work, Mid-Late Triassic rift features are mapped in the Helgeland Basin and the Nordland Ridge. The Middle-Late Triassic rifting is indicated by the sedimentary wedges (Figs. 7 & 8) indicative of syn-rift sedimentation (fill type A of Fig. 5). These rift features were not found in the Froan Basin, implying a localised rift event within the

Trøndelag Platform. Internal strata of the Upper Triassic wedge that drape onto the upper dome (Fig. 8) imply a change from late syn-rift to early post rift stage. Such changes were explained by Prosser (1993), although dome structures were not part of Prosser's (1993) explanation. The presence of saucer shaped fills in the Helgeland Basin (Fig. 12) suggests that the late Triassic rifting was followed by a period of thermal subsidence. This localised thermal subsidence indication agrees with localization of the Middle Triassic rift phase in the Helgeland Basin.

5. Conclusion

Seismic surveys (2D and 3D) have been used to investigate the Upper Devonian–Triassic sedimentary fill geometries and tectonic development in the Trøndelag Platform and its subsidiary elements, the Nordland Ridge and Froan and Helgeland basins. Based on seismic interpretation, six major sedimentary fill geometries have been identified. These are (A) wedge shaped deposits containing fault-ward thickening internal strata, (B) wedge shaped deposits containing strata of uniform thickness, (C) sedimentary wedges that thicken towards the bounding faults, overlain by gently dipping-more or less flat lying strata, (D) gently dipping strata that thicken towards the deeper basinal areas and onlap onto pre-existing topography, (E) sedimentary packages filling depressions, and (F) sedimentary wedges that are bounded by flatter faults, and contain rotated internal strata and a folded top. Onlap and angular unconformities characterise part of the Palaeozoic-Triassic basin fill offshore mid Norway. Five Palaeozoic–Triassic unconformities have been identified in the study area based on the onlap and toplap features of seismic reflectors. These unconformities are a basement unconformity, a mid Permian unconformity, two Early Triassic unconformities and a Middle Triassic unconformity. These sedimentary fill geometries and unconformities have allowed identification of six rifting episodes that have controlled the Palaeozoic-Triassic sedimentation in the Trøndelag Platform. These rifts are Devonian–Permian, late Permian, two Early Triassic and Mid-Late Triassic rifting events. One of the Early Triassic and the Mid–Late Triassic rift episodes could not be identified everywhere in the Trøndelag Platform, indicating the occurrence of localised rifting events during the basin development. This work has also allowed the identification of two possible Carboniferous–Permian isolated carbonate build-ups in the Helgeland Basin, but more work needs to be done to confirm and improve

the understanding of the existence and distribution of the Carboniferous–Permian carbonate deposition in the study area.

6. Acknowledgements

This work was funded by EnPe-Norad under the ANTHEI (Angola Tanzania Higher Education Initiative) scholarship scheme. Equinor provided geophysical data and working facilities to accomplish the project. MNR lines are reproduced by courtesy of SpectrumGeo and TGS. The 3D surveys were reproduced with permission from PGS. Discussions with Halvor Bunkholt and Koen van den Bril are highly appreciated and led to improvement of the work. Jan Einar Ringås and Valentin Zuchuat are thanked for their constructive reviews.

References

- Andrews, S. D. & Decou, A. 2019: The Triassic of Traill Ø and Geographical Society Ø, East Greenland: Implications for North Atlantic palaeogeography. *Geological Journal* 54, 2124-2144.
- Blystad, P., Brekke, H., Færseth, R.B., Larsen, B.T., Skogseid, J. & Tørudbakken, B. 1995: Structural elements of the Norwegian Continental Shelf Part II: The Norwegian Sea Region. Norwegian Petroleum Directorate Bulletin 8.
- Brekke, H. 2000: The tectonic evolution of the Norwegian Sea Continental Margin with emphasis on the Vøring and Møre basins. In A. Nøttvedt (ed.): *Dynamics of the Norwegian Margin*, Geological Society, London, Special Publication 167, 327-378.
- Brekke, H., Sjulstad, H. I., Magnus, C., & Williams, W. R. 2001. Sedimentary environments offshore Norway - an overview. In O. J. Martinsen and T. Dreyer (eds.): *Sedimentary Environments Offshore Norway-Palaeozoic to Recent*, Norwegian Petroleum Society Special Publication 10, 7-37.
- Bugge, T., Ringås, J. E., Leith, D. A., Mangerud, G., Weiss, H. M., & Leith, T. L. 2002: Upper Permian as a new play model on the mid-Norwegian continental shelf: Investigated by shallow stratigraphic drilling. *American Association of Petroleum Geologists*, Bulletin 86, 107-127.
- Burgess, P. M., Winefield, P., Minzoni, M., & Elders, C. 2013: Methods for identification of isolated carbonate buildups from seismic reflection data. *American Association of Petroleum Geologists*, Bulletin 97, 1071-1098.

- Christiansen, F. G., Piasecki, S., Stemmerik, L., & Telnæs, N. 1993: Depositional Environment and Organic Geochemistry of the Upper Permian Ravnefjeld Formation Source Rock in East Greenland. *American Association of Petroleum Geologists, Bulletin* 77, 1519-1537.
- Dalland, A., Worsley, D., & Ofstad, K. 1988: *A lithostratigraphic scheme for the Mesozoic and Cenozoic succession offshore mid- and northern Norway*. Norwegian Petroleum Directorate, Bulletin 4, 65 pp.
- Doré, A. G. 1992: Synoptic palaeogeography of the Northeast Atlantic Seaway: late Permian to Cretaceous. In J. Parnell (ed.): *Basins on the Atlantic Seaboard: Petroleum Geology, Sedimentology and Basin Evolution*. Geological Society, London, Special Publication 62, 421-446.
- Elliott, G. M., Jackson, C. A.-L., Gawthorpe, R. L., Wilson, P., Sharp, I. R., & Michelsen, L. 2017: Late syn-rift evolution of the Vingleia Fault Complex, Halten Terrace, offshore Mid-Norway; a test of rift basin tectono-stratigraphic models. *Basin Research* 29, 465-487.
- Elvebakk, G., Hunt, D. W., & Stemmerik, L. 2002: From isolated buildups to buildup mosaics: 3D seismic sheds new light on upper Carboniferous–Permian fault controlled carbonate buildups, Norwegian Barents Sea. *Sedimentary Geology* 152, 7-17.
- Gani, M. R. 2017: Mismatch between time surface and stratal surface in stratigraphy. *Journal of Sedimentary Research*, 87, 1226-1234.
- Guarnieri, P., Brethes, A., & Rasmussen, T. M. 2017: Geometry and kinematics of the Triassic rift basins in Jameson Land (East Greenland). *Tectonics* 36, 602-614.
- Gudlaugsson, S. T., Faleide, J. I., Johansen, S. E., & Breivik, A. J. 1998: Late Palaeozoic structural development of the South-western Barents Sea. *Marine and Petroleum Geology* 15, 73-102.
- Hansen, D. M., Redfern, J., Federici, F., Di-Biase, D., & Bertozzi, G. 2007: Miocene igneous activity in the Northern Subbasin, offshore Senegal, NW Africa. *Marine and Petroleum Geology* 25, 1-15.
- Holbrook, J. M., & Bhattacharya, J. P. 2012: Reappraisal of the sequence boundary in time and space: case and considerations for an SU (subaerial unconformity) that is not a sediment bypass surface, a time barrier, or an unconformity. *Earth-Science Reviews*, 113, 271-302.
- Jacobsen, V. W., & van Veen, P. 1984: The Triassic offshore Norway north of 62 N. In *Petroleum geology of the north European margin*. Springer, Dordrecht, 317-327.
- Kreiner-Møller, M., & Stemmerik, L. 2001: Upper Permian lowstand fans of the Bredehom Member, Schuchert Dal Formation, East Greenland. In O. J. Martinsen and T. Dreyer (eds.): *Sedimentary Environments Offshore Norway - Palaeozoic to Recent*, Norwegian Petroleum Society Special Publication 10, 51-65.

- Kyrkjebø, R., Gabrielsen, R. H., & Faleide, J. I. 2004: Unconformities related to the Jurassic–Cretaceous synrift–post-rift transition of the northern North Sea. *Journal of the Geological Society*, 161, 1-17.
- Mitchum Jr, R. M., Vail, P. R., & Thompson Iii, S. 1977: Seismic stratigraphy and global changes of sea level: Part 2. The depositional sequence as a basic unit for stratigraphic analysis: Section 2. Application of seismic reflection configuration to stratigraphic interpretation.
- Müller, R., Nystuen, J. P., & Lie, H. 2005: Late Permian to Triassic basin infill history and palaeogeography of the Mid-Norwegian shelf-East Greenland Region. In B.T.G. Wandås, J.P. Nystuen, E. Eide, F. Gradstein (eds.): *Onshore-Offshore Relationships on the North Atlantic Margin*, Norwegian Petroleum Society Special Publications 12, 165-189.
- Nøttvedt, A., Gabrielsen, R.H. and Steel, R.J. 1995: Tectonostratigraphy and sedimentary architecture of rift basins, with reference to the northern North Sea. *Marine and Petroleum Geology* 12, 881-901.
- NPD. 2003: Wellbore (6507/3-2)/ Exploration. Retrieved March 26, 2020, from NPD FactPages: <https://factpages.npd.no/en/wellbore/pageview/exploration/all/2954>
- NPD. 2004a: Wellbore (6407/10-3)/ Exploration. Retrieved March 26, 2020, from NPD FactPages: <https://factpages.npd.no/en/wellbore/pageview/exploration/all/1927>
- NPD. 2004b: Wellbore (6507/12-2)/ Exploration. Retrieved March 11, 2018, from NPD FactPages: <http://factpages.npd.no/FactPages/Default.aspx?nav1=wellbore&nav2=PageView|Exploration|All&nav3=437&culture=en>
- NPD. 2013: Wellbore (6507/6-4 A)/ Exploration. Retrieved January 19, 2018, from NPD FactPages: <http://factpages.npd.no/FactPages/Default.aspx?nav1=wellbore&nav2=PageView|Exploration|All&nav3=6753&culture=en>
- Oftedal, B. T., Andresen, A., & Müller, R. 2005: Early Triassic syn-rift sedimentation at Hold with Hope, Northeast Greenland. In B. T. G. Wandås, J. P. Nystuen, E. Eide, F. Gradstein (eds.): *Onshore-Offshore Relationships on the North Atlantic Margin*, Norwegian Petroleum Society Special Publications 12, 191-206.
- Osmundsen, P.T., Braathen, A., Sommaruga, A., Skilbrei, J.R., Nordgulen, Ø., Roberts, D., Andersen, T.B., Olesen, O. and Mosar, J., 2005: Metamorphic core complexes and gneiss-cored culminations along the Mid-Norwegian margin In B. T. G. Wandås, J. P. Nystuen, E. Eide, F. Gradstein (eds.): *Onshore-Offshore Relationships on the North Atlantic Margin*, Norwegian Petroleum Society Special Publications 12, 29-41.
- Osmundsen, P.T., Eide, E.A., Haabesland, N.E., Roberts, D., Andersen, T.B., Kendrick, M., Bingen, B., Braathen, A., and Redfield, T. F. 2006: Kinematics of the Høybakken

- detachment zone and the Møre-Trøndelag Fault Complex, central Norway. *Journal of the Geological Society* 163, 303-318.
- Prestvik, T., Torske, T., Sundvoll, B., & Karlsson, H. 1999: Petrology of early Tertiary nephelinites off mid-Norway. Additional evidence for an enriched endmember of the ancestral Iceland plume. *Lithos* 46, 317-330.
- Prosser, S. 1993: Rift-related linked depositional systems and their seismic expression. In G. D. Williams and A. Dobb (eds.): *Tectonics and Seismic Sequence Stratigraphy*, Geological Society, London, Special Publication 71, 35-66.
- Ravnås, R., & Bondevik, K. 1997: Architecture and controls on Bathonian–Kimmeridgian shallow-marine synrift wedges of the Oseberg–Brage area, northern North Sea. *Basin Research* 9, 197-226.
- Redfern, J., Shannon, P. M., Williams, B. P. J., Tyrrell, S., Leleu, S., Perez, I. F., Baudon, C., Štolfová, K., Hodgetts, D., Van Lanen, X. and Speksnijder, A. 2010: An integrated study of Permo–Triassic basins along the North Atlantic passive margin: implication for future exploration. *Geological Society, London, Petroleum Geology Conference series* 7, 921-936.
- Seidler, L. 2000: Incised submarine canyons governing new evidence of Early Triassic rifting in East Greenland. *Palaeogeography, Palaeoclimatology, Palaeoecology* 161, 267-293.
- Seidler, L., Steel, R. J., Stemmerik, L., & Surlyk, F. 2004: North Atlantic marine rifting in the Early Triassic: new evidence from East Greenland. *Journal of the Geological Society* 161, 583-592.
- Steel, R. R. 1998: Architecture of marine rift-basin successions. *American Association of Petroleum Geologists, Bulletin* 82, 110-146.
- Stemmerik, L., Christiansen, F. G., Piasecki, S., Jordt, B., Marcussen, C., & Nøhr-Hansen, N. 1993: Depositional history and petroleum geology of the Carboniferous to Cretaceous sediments in the northern part of East Greenland. In T. O. Vorren, E. Bergsager, Ø.A. Dahl-Stamnes, E. Holter, B. Johansen, E. Lie, T.B. Lund (eds.): *Arctic Geology and Petroleum Potential*, Norwegian Petroleum Society Special Publications 2, 67-87.
- Stemmerik, L., Clausen, O.R., Korstgård, J., Larsen, M., Piasecki, S., Seidler, L., Surlyk, F. and Therkelsen, J. 1997: Petroleum geological investigations in East Greenland: project 'Resources of the sedimentary basins of North and East Greenland'. *Geology of Greenland Survey, Bulletin* 176, 29-38.
- Stemmerik, L., Elvebakk, G., & Worsley, D. 1999: Upper Paleozoic Carbonate reservoirs on the Norwegian and Arctic Shelf: delineation of reservoir models with application to the Loppa High. *Petroleum Geoscience* 5, 173-187.

- Surlyk, F. 1990: Timing, style and sedimentary evolution of Late Palaeozoic-Mesozoic extensional basins of East Greenland. In R. F. P. Hardman and J. Brooks (eds.): *Tectonic Events Responsible for Britain's Oil and Gas Reserves*, Geological Society, London, Special Publication 55, 107-125.
- Surlyk, F., Piasecki, S., Rolle, F., Stemmerik, L., Thomsen, L., & Wrang, P. 1984: The Permian Base of East Greenland. In A. M. Spencer (ed.): *Petroleum Geology of the North European Margin*, Springer, Dordrecht, 303-315.
- Surlyk, F., Hurst, J. M., Piasecki, S., Rolle, F., Scholle, P. A., Stemmerik, L., & Thomsen, E. 1986: The Permian of the Western Margin of the Greenland Sea-A future Exploration Target. In M. T. Halbouty (ed.): *Future Petroleum Provinces of the World*, American Association of Petroleum Geologists Memoir 40, 629-659.
- Webber, S., Norton, K. P., Little, T. A., Wallace, L. M., & Ellis, S. 2018: How fast can low-angle normal faults slip? Insights from cosmogenic exposure dating of the active Mai'iu fault, Papua New Guinea. *Geology*, 46, 227-230.
- Zhao, F., Wu, S., Sun, Q., Huuse, M., Li, W., & Wang, Z. 2014: Submarine volcanic mounds in the Pearl River Mouth Basin, northern South China Sea. *Marine Geology*, 355, 162-172.
- Zhao, Y., Tong, D., Song, Y., Yang, L., & Huang, C. 2016: Seismic reflection characteristics and evolution of intrusions in the Qiongdongnan Basin: Implications for the rifting of the South China Sea. *Journal of Earth Science*, 27, 642-653.

4.2. Paper II

“Norwegian Sea area Permo-Triassic organic-carbon-rich deposits from seismic”

Emily Barnabas Kiswaka¹ and Maarten Felix¹

¹NTNU Norwegian University of Science and Technology, Norway (emily.kiswaka@ntnu.no)

Accepted for publication by Marine and Petroleum Geology Journal (published online on 13th May 2020. Available from <https://doi.org/10.1016/j.marpetgeo.2020.104463>).

4.2.1. Author contributions

My contribution to this paper involved investigation of the seismic lines, IG crossplotting and interpretation, and writing the paper.

Maarten Felix was involved in editing the text and contributed relevant scientific discussion and recommendations.

Norwegian Sea area Permo-Triassic organic-carbon-rich deposits from seismic

Emily Barnabas Kiswaka¹ and Maarten Felix¹

¹NTNU Norwegian University of Science and Technology, N-7491, Trondheim, Norway

Email: emily.kiswaka@ntnu.no

Abstract

Seismic surveys of the Permo-Triassic successions in Norwegian Sea sub-basins have been studied to determine the distribution of organic-carbon-rich intervals in the deeper basinal areas. Upper Permian to Lower Triassic organic-carbon-rich deposits had been described in cores from the margins of the basin, but their distribution in the deeper parts of the basin was unknown. The distribution of the organic-carbon-rich deposits in the deeper basin areas has been determined using a combination of amplitude versus angle/offset (AVA/AVO) analysis and an assessment of strata-bound deformation structures. AVA/AVO anomaly class IV, which has a negative normal incident reflection coefficient that decreases with angle/offset, has been used to predict the presence of organic-carbon-rich rocks in this work. The intercept (I) and gradient (G) plots (IG-crossplots) together with the Near-Far angle amplitude comparison of the seismic surveys have been used to complement the interpretation. The IG cross-plotting was done by selecting small windows (data probes) along the intervals speculated to be organic-carbon-rich. Any data probe which displayed AVO class IV elements on the IG crossplots and exhibited amplitude dimming with angle has been considered to indicate an organic-carbon-rich layer. The results of this work show the presence of both Upper Permian and Middle Triassic organic carbon rich sediments in the deeper parts of sub-basins within the Froan and Helgeland basins in the Norwegian Sea area.

Two and one organic-rich intervals are indicated in the Froan and Helgeland basins respectively. The distribution of these organic-rich rocks was partly tectonically controlled, resulting in spatially limited deposits in the compartmentalized Froan Basin but more extensive deposits in the Helgeland Basin. None of the Lower Triassic sections examined in this study showed AVA/AVO characteristics indicative of organic-carbon-rich sediments on IG crossplots.

Key words: Organic-carbon-rich sediments; Strata-bound deformation structures; IG crossplot; Permo-Triassic deposits; Amplitude variation; Trøndelag Platform

1. Introduction

Extension related to the opening of the North Atlantic during the Permo-Triassic created several basins between mid Norway and east Greenland (Müller et al., 2005). These basins were depocentres for sediment from various sources (Blystad et al., 1995; Brekke, 2000; Müller et al., 2005; Osmundsen et al., 2005; Redfern et al., 2010), with depositional conditions varying from deep marine to terrigenous, and from oxic to anoxic (Bugge et al., 2002), influenced by both tectonics and climate. During some of the anoxic periods, organic-carbon-rich layers were deposited.

Correlations of the deposits in the Norwegian Sea area with age equivalent deposits onshore eastern Greenland (Bugge et al., 2002) show that similar depositional conditions existed across the basin, both in the east on the Trøndelag platform, and in the west in eastern Greenland. The Upper Permian sequences of eastern Greenland contain organic-carbon-rich

successions that have been extensively studied within the Ravnefjeld Formation (Surlyk et al., 1984; Surlyk et al., 1986; Christiansen et al., 1993; Stemmerik et al., 1993; Kreiner-Møller & Stemmerik, 2001). These organic rich units are marine deposits and were deposited under anoxic conditions during sea level-rise and early highstand when the inorganic sediments were limited to basin margin areas (Piasecki & Stemmerik, 1991; Christiansen et al., 1992; Christiansen et al., 1993; Stemmerik et al., 1998).

Unlike on Greenland, the Permo-Triassic deposits in the Norwegian Sea area are not exposed on land. Hence, the Permo-Triassic period remains relatively under-examined in the Norwegian Sea area, and the spatial distributions of sediment (inorganic and organic) are not well understood. There is a limited number of cores that have penetrated the Permo-Triassic System and other older successions in the Norwegian Sea area. Most of these cores have been drilled on the structural highs, and none of them have reached the deeper parts of the Helgeland and Froan basins. Only two cores, 6507/6-4 A and 6611/09-U-01, are reported to penetrate the equivalent of the Ravnefjeld Formation offshore mid Norway (Bugge et al., 2002; NPD, 2013). These cores were drilled on the Nordland Ridge and eastern margin of the Helgeland Basin (Figure 1).

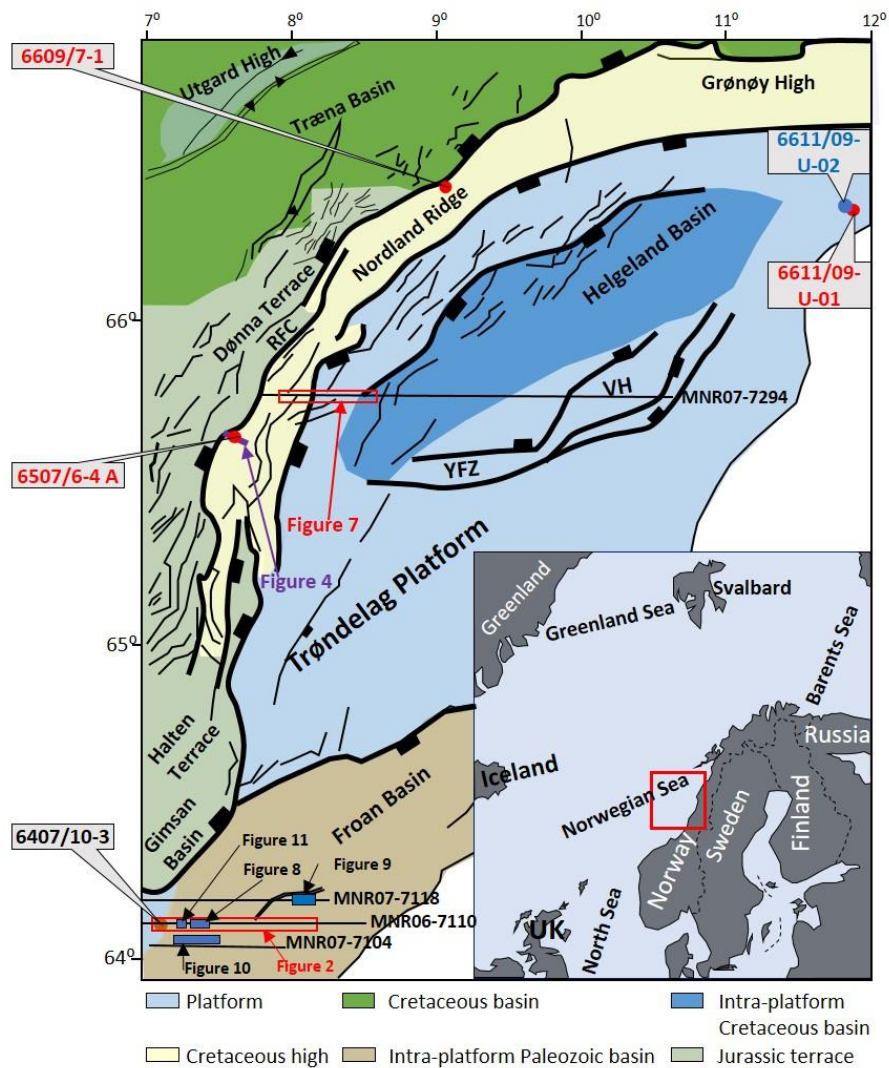


Figure 1. Structural elements of the study area including locations of key cores and seismic profiles. The structural elements map is sourced from NPD FactMaps available at: http://npdwms.npd.no/npdwmsmap_wgs84.asp? (accessed on 12th Jan. 2018). RFC = Revfallet Fault Complex, VH = Vega High and YFZ = Ylvingen Fault Zone. Structural elements after Blystad et al. (1995).

Permo-Triassic sequences from core 6507/6-4 A, on the Sør High, can be correlated to Permo-Triassic successions penetrated by cores 6611/9-U-01 and 6611/9-U-02 on the eastern margin of the Helgeland Basin on the Norwegian continental shelf (NPD, 2013). Two Upper Permian organic-carbon-rich sections have been reported from cores 6507/6-4 A and 6611/9-U-01. The fact that the Helgeland Basin is situated between cores 6611/9-U-01 and 6507/6-4 A (Figure 1) suggests that equivalent Permo-Triassic organic-rich strata might exist in the deeper parts of the Trøndelag Platform area (Bugge et al., 2002; Saxena, 2016). Available seismic surveys indicate the possible presence of deeply buried Palaeozoic intervals within the Helgeland and Froan basins (e.g. Figure 2), but organic-carbon-rich strata have not been identified yet.

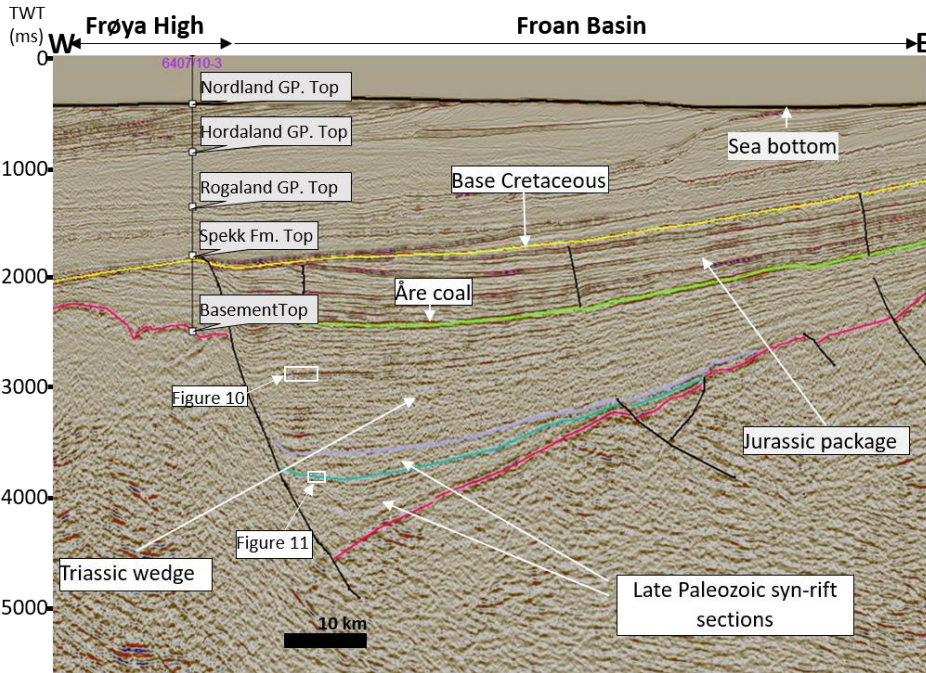


Figure 2. Seismic line MNR 06-7110 crossing well 6407/10-3 showing thick Palaeozoic and Lower Triassic syn-rift deposits in the Froan Basin. See Figure 1 for location.

Here seismic interpretation has been used to investigate deep horizons, between 3-5 seconds (two-way-travel time, TWT) examples of which are shown in Figure 3, to determine the spatial distribution of Permo-Triassic organic-carbon-rich intervals in the deeper parts of the Froan and Helgeland basins (Figure 1). The analysed targets have a patchy distribution (Figure 3). Two main methods have been used: assessment of seismic expressions reported to indicate organic-carbon-rich rocks by Løseth et al. (2011a, 2011b), and intercept and gradient (IG) crossplots to interpret amplitude versus angle/offset (AVA/AVO) anomaly characteristics of the assumed tops of the organic-carbon-rich layers. The presence of a potential organic-carbon-rich section is also interpreted in this study based on the recognition of high amplitude continuous seismic layers that exhibit amplitude dimming with angle. The results presented here will show examples of the main findings from 2D seismic lines MNR07-7294, MNR07-7118, MNR07-7110, MNR07-7104 and 3D seismic inline 9240 of the ST13M09 survey.

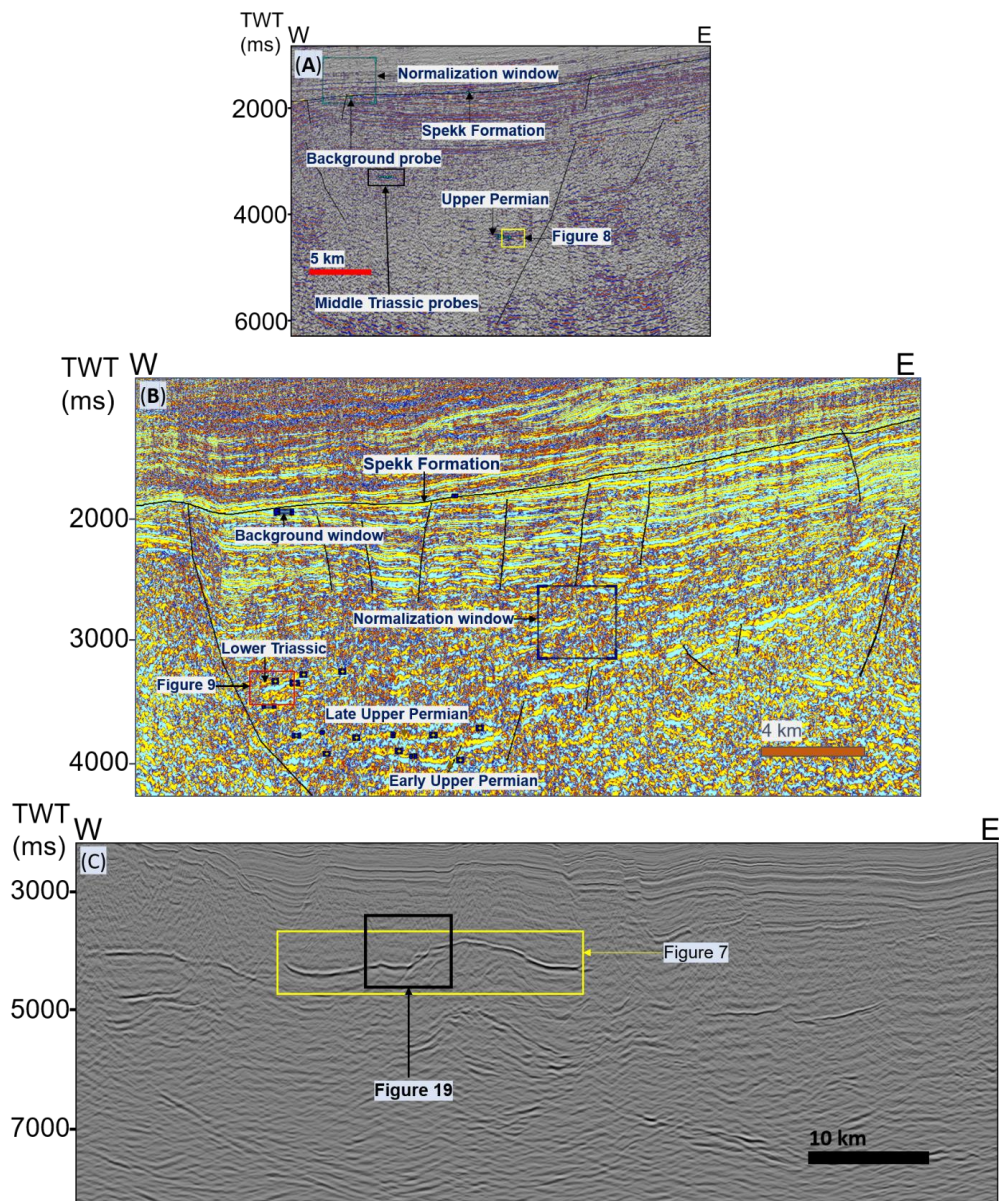


Figure 3. Seismic profiles showing positions of studied horizons. (A&B) Seismic sections MNR07-7118 and MNR07-7104 in the Froan Basin. (C) Seismic section MNR07-7294 across the Helgeland Basin. Small rectangles represent data windows used for IG crossplotting.

2. Geology of the study area

2.1. Tectonic development and structural elements

The shape and orientation of the basins in which Permo-Triassic deposition took place were determined by the tectonic development of the area since the Caledonian orogeny. The Caledonian orogeny resulted in compression in mid Norway during the late Silurian and early Devonian (Blystad et al., 1995). Collapse of the Caledonian orogen in the Middle-Late Devonian was followed by crustal extension with major tectonic rifting in the late Carboniferous and early Permian (Bukovics and Ziegler, 1985; Blystad et al., 1995). The Middle Permian was characterized by regional tectonic rifting, uplift and erosion (Surlyk et al., 1984; Surlyk, 1990; Doré, 1992; Seidler, 2000; Oftedal et al., 2005; Guarnieri et al., 2017). This was followed by extension which lasted into the Triassic (Müller et al., 2005). The Permo-Triassic basin development was continued by block faulting in the Middle-Late Triassic (Blystad et al., 1995). The Permo-Triassic sedimentary basins were mostly controlled by eastward dipping master faults (an example of which is shown in Figure 2), that were largely influenced by Caledonian structural fabrics (Redfern et al., 2010). This resulted in the NE-SW trends of the Froan and Helgeland basins. Some parts of the study area experienced tectonic quiescence in the late Triassic-early Jurassic (Blystad et al., 1995) before tectonic rifting and uplift in the middle Jurassic to earliest Cretaceous (Brekke et al., 2001). The late Jurassic, in the Norway-Greenland area, was characterized by extensional tectonics that culminated in the formation of the central Atlantic (Brekke et al., 2001).

2.2. Depositional environments

The oldest sediments in the Norwegian Sea basin are of uppermost Devonian age, and overlie metamorphic basement (Surlyk, 1990; Bugge et al., 2002). Carboniferous rocks are not found onshore mid Norway but are believed to exist in the deep basinal areas offshore mid Norway (Blystad et al., 1995). About 750 m of Permo-Triassic sediments have been penetrated by cores 6611/09-U-01 and 6611/09-U-02 on the eastern margin of the Helgeland Basin (Bugge et al., 2002). About 2500 m of Triassic sediments, including two Middle Triassic evaporite intervals up to 400 m thick, have been penetrated by wells in the Helgeland Basin (Halland et al., 2011).

During the Permo-Triassic, the basin development showed a change in depositional environments from shallow marine to fully marine (Bugge et al., 2002). The changes in Permo-Triassic depositional environments are similar on both sides of the basin, i.e. the mid Norway basin margin in the east and the eastern Greenland basin margin in the west (Bugge et al., 2002). Shallow marine conditions at the start of the upper Permian, due to late Permian transgression (Swiecicki et al., 1998), resulted in the deposition of gypsum and anhydrite (Christiansen et al., 1993; Bugge et al., 2002). These deposits are the Anhydrite Unit and Karstryggen Formation offshore mid Norway and on eastern Greenland respectively (Christiansen et al., 1993; Bugge et al., 2002). The overlying Permo-Triassic organic-rich rocks in the Norway-Greenland basin have been interpreted to be deep marine sediments that interfinger with age equivalent carbonates along the structural highs (Piasecki & Stemmerik, 1991; Christiansen et al., 1993; Bugge et al., 2002).

The Early Triassic began by submarine fan deposition in a deep marine environment during the active tectonics of the Permo-Triassic extension (Müller et al., 2005). Subsequent

decreasing marine influence is indicated by overlying marginal marine deposits, followed by fine grained, reddish-brown continental sediments towards the Middle Triassic (Brekke et al., 2001; Müller et al., 2005). A short-lived marine incursion, in the Middle Triassic, led to halite and anhydrite deposition in shallow parts of the basin towards the Late Triassic (Müller et al., 2005). Organic-rich sediment may have been deposited in the deeper parts of the Helgeland and Froan basins where anoxia could have been well developed. This is suggested by the sediments in the Helgeland Basin, where the Lower Triassic sequence contains several thin, organic-rich mudstone layers (Bugge et al., 2002). The Late Triassic began by deposition of extensive lacustrine muds, while the uppermost Triassic is characterized by thick fluvial sandstone units interbedded with greenish-grey mudstones and thin coal beds of the Åre Formation (Dalland et al., 1988; Swiecicki et al., 1998; Müller et al., 2005). A sea level rise occurred during the Early to Middle Jurassic, leading to deposition in a shallow shelf environment in the region (Brekke et al., 2001). The Lower Jurassic deposits of the Norwegian Sea area are characterized by coastal plain/ delta plain deposits of the Åre Formation (Dalland et al., 1988; Brekke et al., 2001). The Middle Jurassic is characterized by prograding clastic wedges due to regional and local erosion (Brekke et al., 2001). Marine anoxic bottom water conditions existed during the Late Jurassic, when the Spekk Formation was deposited in the Norwegian Sea area (Dalland et al., 1988). The Spekk Formation contains dark claystones and has a high organic content (Dalland et al., 1988).

3. Dataset and methodology

Two seismic datasets have been used in this work: the 2D MNR and 3D ST13M09 surveys. The MNR data were time processed. Noise removal and multiple attenuation techniques

were employed to improve signal to noise ratio while enhancing clarity for the deeper targets. The ST13M09 data is a post stack mega merge tied to wellbore 6507/6-4 A which was used for tentative age assignment to the studied horizons. Wellbore information was obtained from the Norwegian Petroleum Directorate (NPD) fact pages, Bugge et al. (2002) and Müller et al. (2005).

3.1. Age assignment

A well tie on 3D seismic inline 9240 of the ST13M09 survey (Figure 4) was used to constrain the age of the analysed interval. Ages of the potential Upper Permian organic-rich intervals in the Froan Basin are assigned tentatively based on equivalent layers, in the same stratigraphic position, in the Helgeland Basin. The Upper Permian organic-rich intervals have been cored in the northern part of the Trøndelag Platform (cores 6507/6-4 A and 6611/09-U-01), and from these core locations the intervals have been traced to the deeper parts of the Trøndelag Platform to figure out the spatial distribution of the organic-carbon-rich sediments.

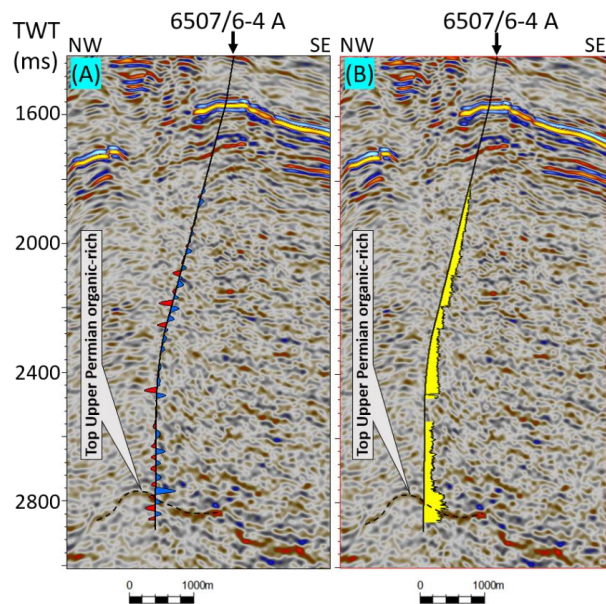


Figure 4. 3D seismic inline 9240 of the ST13M09 survey showing the well tie (wellbore 6507/6-4 A on the Nordland Ridge) used to constrain the age of the analysed interval. (A) Synthetic seismic wiggle showing a negative response (trough) through an Upper Permian organic-rich interval. Sonic and density logs were not available for the shallow depth where the synthetic wiggle is not shown. (B) Acoustic impedance log showing decrease in acoustic impedance across the Upper Permian organic-rich interval.

3.2. Techniques used here

Two main geophysical techniques have been applied to 2D seismic sections to investigate the potential presence of organic carbon rich intervals in the Permo-Triassic successions of the Norwegian Sea area. These techniques are the observation of characteristic seismic expressions of organic-carbon-rich sediments in this area, and interpretation of amplitude variation with angle/offset (AVA/AVO) from seismic profiles and from intercept and gradient (IG) crossplots (as described by Løseth et al. 2011a, 2011b; del Monte et al., 2018). The

amplitudes of the organic rich intervals marked by decreased acoustic impedances, an example of which is shown in Figure 4 B, are compared between near and far angles. In the current work, the analysis was done on 'coloured' inverted profiles. The same colour scale was used in the figures for the compared near and far angle seismic profiles. The coloured inversion converts seismic to relative impedance (Lancaster & Whitcombe, 2000). The top and base of a horizon will after the inversion be seen as one homogeneous layer on the condition that the seismic wavelet contains the lower part of the frequency spectrum, and that noise is properly removed prior to the inversion.

In the images shown here, a yellow/red layer indicates a soft event, and a blue/ black layer a hard event, caused by negative and positive contrast in relative impedances respectively.

3.2.1. Seismic expressions of organic carbon rich shales

Løseth et al. (2011a) described seismic expressions that can be characteristic for organic carbon rich shales and explained their formation. These expressions include deposits showing evidence of gravitational gliding, and strata bound listric faults. Organic-carbon-rich rocks may slide due the high organic content in clays. Organic matter lowers the permeability of clays and hence inhibits the vertical movement of water squeezed due to compaction during early burial. The trapped water accumulates at the base of the organic-rich shale stratum and causes a high pore-fluid pressure. This pressure build-up creates a decollement zone leading to sliding of the organic carbon rich shales. The sliding action is manifested on seismic images as a series of listric faults that segment the upper part of the organic rich interval and terminate at the base of the interval, and by slices of organic-rich-rocks that have slid on top of one another down the fault planes. The gravitational gliding structures are assumed to

have been caused by anisotropic horizontal stresses due to either tilting of the beds or fault related stress release.

The listric faults used to identify organic rich sediments are not diagnostic on their own. For an interval to be regarded as organic rich, apart from displaying listric faults characteristic of organic rich rocks, it should also be a soft event that displays either amplitude dimming with angle/offset or AVA/AVO class IV characteristics on IG crossplots. The combination of these features means the identification of the tops of organic-carbon-rich rocks is reliable.

3.2.2. AVA/AVO classes

The amplitude variation with angle/offset (AVA/AVO) analysis technique (Ostrander, 1984; Avseth et al., 2005; del Monte et al., 2018) has been applied in this work to investigate deeply buried successions. The AVA/AVO technique relies on extracting the amplitudes of the reflection coefficients as a function of angle/offset (Ostrander, 1984; Avseth et al., 2005). AVA/AVO class I represents high impedance sandstones that have high positive reflection coefficients at normal incidence, exhibit amplitude decrease with offset, and experience phase reversal at higher incidence angles (Rutherford & Williams, 1989). Classes II and IIp are both near-zero impedance contrast sandstones (Rutherford & Williams, 1989). Class IIp has a small positive normal incidence reflection coefficient, and exhibits phase reversal with offset, while class II has a negative normal incidence reflection coefficient that brightens with increasing incidence angle (Ross & Kinman, 1995). Class III represents low impedance sandstones that have high negative reflection coefficients, at all angles of incidence, that become more negative (amplitude brightening) with offset (Rutherford & Williams, 1989). Class IV is defined by a negative normal incident reflection coefficient that become less

negative (amplitude dimming) with offset (Castagna & Swan, 1997). Class IV has been used in the current work to predict the presence of organic-carbon-rich intervals in the deeper parts of the Trøndelag Platform. The identification of class IV was done by using both seismic images (comparing amplitudes of layers between different angles) and by using crossplots. On the crossplots are shown lines separating lithologies of different properties, labelled Litho, Chi. Chi refers to the angle with the positive Y-axis and is measured anticlockwise. The Chi (χ) angle varies from -90° to 90° (Whitcombe et al., 2002).

3.2.2.1. AVA/AVO class IV on seismic

On seismic, the AVA/AVO class IV has a high negative reflection coefficient that decreases with angle/offset (Castagna & Swan, 1997). Seismic wedge modelling was done to predict the AVA/AVO response of the Upper Permian organic-rich rocks offshore mid Norway in order to ensure that the method can pick up AVA/AVO class IV at the investigated depths on the available seismic images. The wedge model was created by using the algorithm of Aki & Richards; Ricker wavelets and 12 Hz bandwidth were used in the modelling. The Ricker wavelet matched the phase and bandwidth of the studied seismic data. The seismic modelling was done by creating a wedge model which describes the seismic response of the Upper Permian organic-carbon-rich intervals based on thickness, burial depth and total organic carbon (TOC, for the model derived from average compressional and shear velocities, V_p and V_s respectively, and average density ρ of a layer).

Determining the model input was not entirely straightforward using the possible input data from either core 6507/6-4 A or core 6611/09-U-01. The model input needs TOC values that are high enough to be able to be detected with the seismic methods, i.e. higher than 3 wt.%

according to Løseth et al. (2011b). The model input for thickness and burial depth needs to be representative of the conditions of the rocks under investigation, in this case deeply buried rocks. The problem here was that the deposits from core 6507/6-4 A are buried deep enough but have low TOC values at 0.6-1.2 wt.% (NPD, 2013), while the deposits from core 6611/09-U-01 have high enough TOC values but are not buried deep enough. Therefore, three different scenarios were tested. The first scenario used all input values from core 6507/6-4 A (Table 1). This scenario was run to confirm the lack of response for low TOC values. The second scenario was run on core 6507/6-4 A using TOC input values from core 6611/09-U-01 (Table 1). This scenario was run to show the response for high TOC values. The third scenario was run on core 6507/6-4 A using TOC input values from the Spekk Formation (Table 1) at burial depths that are comparable to the burial depths of the organic-carbon-rich-intervals of core 6507/6-4 A. This scenario was run to show the response when the TOC input values are higher than those of core 6611/09-U-01.

Input parameters	Average Vp (m/s)	Average Vs (m/s)	Average ρ (g/cm ³)
On core 6507/6-4 A	5315	3060	2.7
On core 6611/09U-01	3787.6	2093.6	2.6
Spekk Formation	3564.7	1633.9	2.5

Table 2. Input parameters, average compressional and shear velocities and average density, used in the wedge model.

3.2.2.2. AVA/AVO classes on IG crossplots

Crossplots of intercept against gradient can be used to enable AVA/AVO analysis (Castagna & Swan, 1997; Avseth et al., 2005; del Monte et al., 2018). Gradient (G) is defined as the magnitude of the rate of change of amplitude with angle/offset (Rutherford & Williams 1989),

while intercept (I) is the normal incidence trace (Ross & Kinman, 1995). The background trend for IG crossplots is defined by brine saturated sandstones or clean shales (Castagna & Swan, 1997). In the current work, background data were taken from nearby intervals that did not show any indication of organic rich sediments. Any deviation from the background trend is interpreted to represent an AVA/AVO anomaly that is attributed to fluids and lithological factors. The IG crossplots can be used to distinguish different AVA/AVO anomaly classes, attributed to fluids and lithological factors, based on the location of the AVA/AVO anomaly in the plot (e.g. Figure 5). Different AVA/AVO classes are defined based on their reflection coefficients and their respective variations with angle/offset. The class IV anomaly can be used to indicate organic-carbon-rich intervals upon calibration to a known organic-carbon-rich section. In the current work, calibration for the organic-carbon-rich rocks was done using the Spekk Formation which is an Upper Jurassic organic rich section in the Norwegian Sea area, and the Åre Formation which contains coal layers (Dalland et al., 1988). Calibration is done using known rocks to verify that a known organic-carbon-rich interval plots on the AVA/AVO class IV position. Thus, if values from the Spekk Formation and Åre coal do indeed plot in the expected position of the IG crossplot, then the method works, and values from the Permo-Triassic deposits with elevated organic content should plot at or near this quadrant position and can that way be recognised.

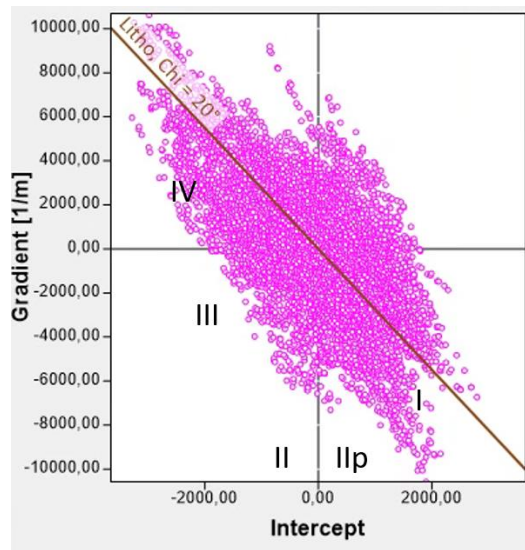


Figure 5. AVA/ AVO classes from a normalization window above the top mid-Triassic organic rich layer on seismic survey MNR06-7110.

In the current work, selected data windows (probes) on seismic profiles have been used for IG crossplotting. Data windows are rectangles covering areas that are analysed for the AVA/AVO anomalies on the seismic sections. The crossplotting was done by using several randomly selected data windows along the potential organic-rich sections so that the results of the same horizon could be compared to one another. The data windows are small rectangles along the targeted horizons, created by using the Petrel blueback special selector tool. A representative IG crossplot was then chosen for presentation if the studied windows taken along the horizon of interest showed similar results. Therefore, the presented IG crossplot results are overall typical for any data window taken along the studied horizon(s).

Different intervals assumed to range from Upper Permian to Middle Triassic have been investigated by moving different selection windows along different layers. The seismic

profiles used for both near versus far angle amplitude investigation and IG crossplotting were bandwidth matched, scaled and time aligned. This was done to make sure the same frequency band was used on both angles, as the same angle stack can have different intensities on the same layer for different frequencies. Variation in intensity of the intervals due to a difference in frequencies can give an incorrect impression of amplitude variation with angle, thus compared angles (near versus far) must be analysed using the same frequency band.

4. Results

A selection of typical results of seismic line interpretation and AVA/AVO analysis (both amplitude comparison and IG crossplotting) is presented here to illustrate the findings (Figure 6-Figure 19). Not all results will be shown, as the results of the other analyses are comparable to the ones presented. Most of the presented results are from the Froan Basin since more organic-carbon-rich intervals were found there than in the Helgeland Basin. The results are summarised in a map (Figure 20) showing the locations of the strata bound deformation structures and the spatial distribution of organic carbon rich layers.

4.1. Wedge model results

Figure 6 shows the results of the seismic wedge model for the studied interval for the three different scenarios. AVA/AVO class IV anomaly, showing high negative amplitude that dims with angle/offset, is one of the characteristic expressions of organic-rich rocks on seismic. The wedge model using all input values from core 6507/6-4 A (Figure 6 A) shows neither high negative amplitude nor a change in amplitude between near and far angles. This is because of the low TOC values of the Upper Permian organic-rich rocks in core 6507/6-4 A. This result

indicates that the Upper Permian organic-rich rocks cannot be identified on the available seismic surveys if the TOC levels across the entire Trøndelag Platform are as low as in core 6507/6-4 A. The wedge model in Figure 6 B was created by importing core 6611/09-U-01 parameters (compressional velocity, shear velocity, and density) in the core 6507/6-4 A model and it shows a high amplitude reflector that dims with angle, indicating a strong class IV anomaly for the organic-rich-interval. This is because the organic-rich intervals in core 6611/09-U-01 have higher TOC levels than those in core 6507/6-4 A, and thus Upper Permian organic-rich intervals can be identified on seismic if their TOC levels are high enough. The wedge model in Figure 6 C was created by importing the Spekk Formation parameters in the core 6507/6-4 A model and it shows a strong negative reflector that dims with angle, indicating a strong class IV anomaly. The intensity of the reflectors in Figure 6 C is higher than in Figure 6 B. This is because the Spekk Formation has higher TOC content than the Upper Permian organic-carbon-rich deposits in core 6611/09-U-01. This indicates that the intensity of the reflector at the top Upper Permian organic-carbon-rich rocks increases when the TOC content increases, and vice versa. The reflectors dim and disappear toward the thin end of the wedges (Figure 6 A-C). Therefore, deeply buried, thin organic-rich intervals cannot be identified on the current seismic, as they are below seismic resolution, no matter how high the TOC content is.

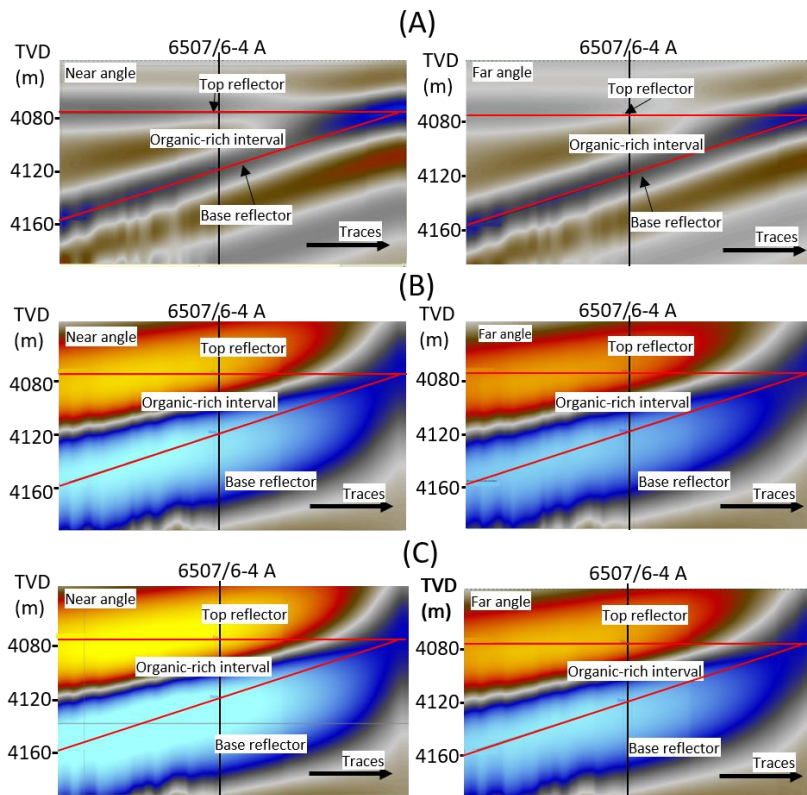


Figure 6. Wedge models for the Upper Permian organic-carbon-rich rocks comparing near (left) and far (right) angles in the Trøndelag Platform. Thick red lines indicate wedge. Colour scale the same for all figures. (A) wedge model for core 6507/6-4 A showing the predicted seismic response of the Upper Permian organic-carbon-rich rocks on seismic. AVA/AVO class IV is not seen in this model. (B) The predicted seismic response of Upper Permian organic-carbon-rich rocks on seismic when properties of the organic rich-rocks on core 6611/09-U-01 are imported in the core 6507/6-4 A model. This model shows amplitude dimming with angle. (C) Predicted seismic response of the Upper Permian organic-carbon-rich rocks on seismic when properties of the Spekk Formation are imported in the core 6507/6-4 A model. This model also shows amplitude dimming with angle, but the top reflector has higher amplitude than model B.

4.2. Seismic amplitude results

The Froan Basin was found to have two Upper Permian intervals with high negative amplitude. These intervals show amplitude dimming with angle, which is indicative of a class IV response and thus possible organic-carbon-rich layers. These intervals are here called the early Upper Permian and late Upper Permian organic-rich intervals. The Helgeland Basin was found to have only one Upper Permian interval showing amplitude dimming with angle, so this one is just called the Upper Permian interval. An example of amplitude dimming with angle for the Upper Permian rocks is shown in Figure 7, for a seismic line in the Helgeland Basin. The organic-carbon-rich intervals also display lateral amplitude variation (e.g. Figure 7 B-D), that is, their intensity is not uniform, as indicated by colour changes from red to yellow and vice versa. The changes in colour of the Upper Permian organic-carbon-rich layers on seismic suggest that the TOC content is not uniformly distributed.

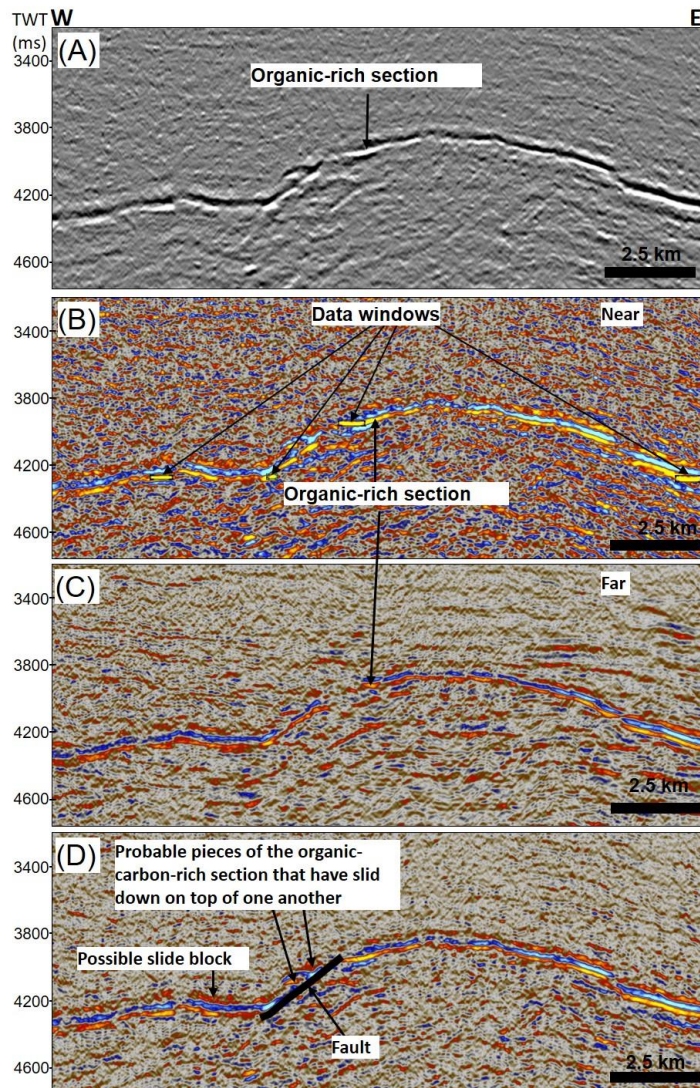


Figure 7. (A) Part of an anomalous amplitude horizon on seismic line MNR07-7294 (see Figure 3 for an overview of the section) interpreted as an Upper Permian organic-carbon-rich layer in the deeper part of the Trøndelag Platform. (B&C) Near (B) versus far (C) angle stacked seismic surveys on line MNR07-7294. (D) The Upper Permian layer is clearly segmented along a fault, indicating gravitational gliding of the organic-carbon-rich interval. See Figure 1 for location.

Not all Upper Permian layers show AVA/AVO class IV behaviour, however. Some areas (an example is shown in Figure 8) instead show amplitude brightening with angle, which is indicative of either AVA/AVO anomaly class II or class III.

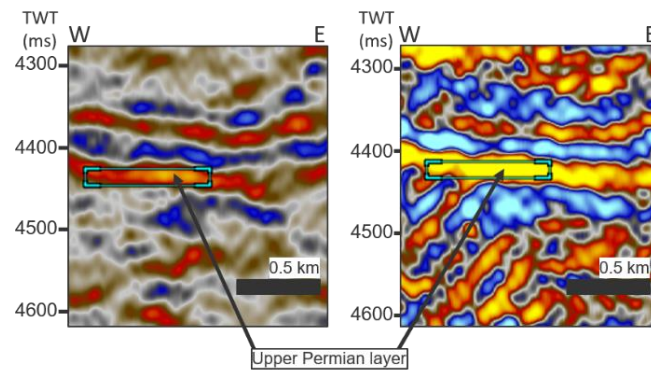


Figure 8. Part of seismic section MNR07-7118 (shown in Figure 3 showing a comparison of the Upper Permian organic-carbon-rich layer from near (left) and far (right) stacked seismic surveys in a small part of the Froan Basin. Rectangles represent data windows for IG crossplot. See Figure 1 for location.

The Lower Triassic interval shows amplitude brightening with angle (an example is shown in Figure 9), indicating AVA/AVO anomaly class II or class III. The Lower Triassic has been studied in both the Helgeland and Froan basins for possible indications of organic-rich layers on seismic images, but none of them showed AVA/AVO anomaly class IV.

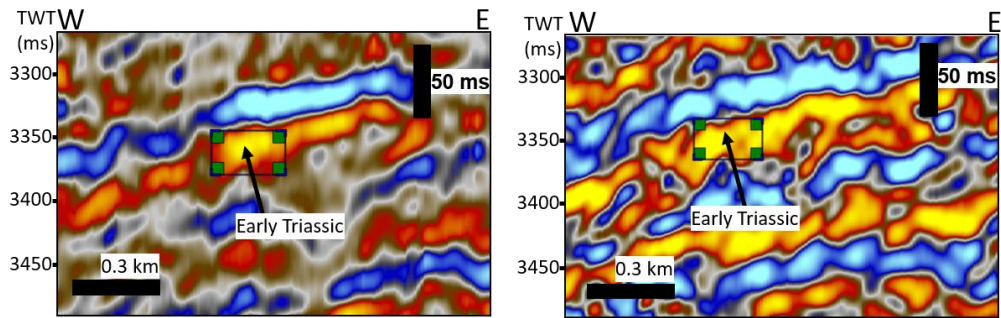


Figure 9. Part of seismic line MNR07-7104 (see Figure 3 for the depth position of this interval on the full seismic section) showing a comparison of the Lower Triassic organic-carbon-rich layer from near (left) and far (right) stacked seismic surveys in the Froan Basin. Rectangles show the positions of data windows for IG crossplots. See Figure 1 for location.

Like the Upper Permian, the Middle Triassic successions include several areas where the layers show amplitude dimming with angle (see example in Figure 10) indicating AVA/AVO class IV anomalies.

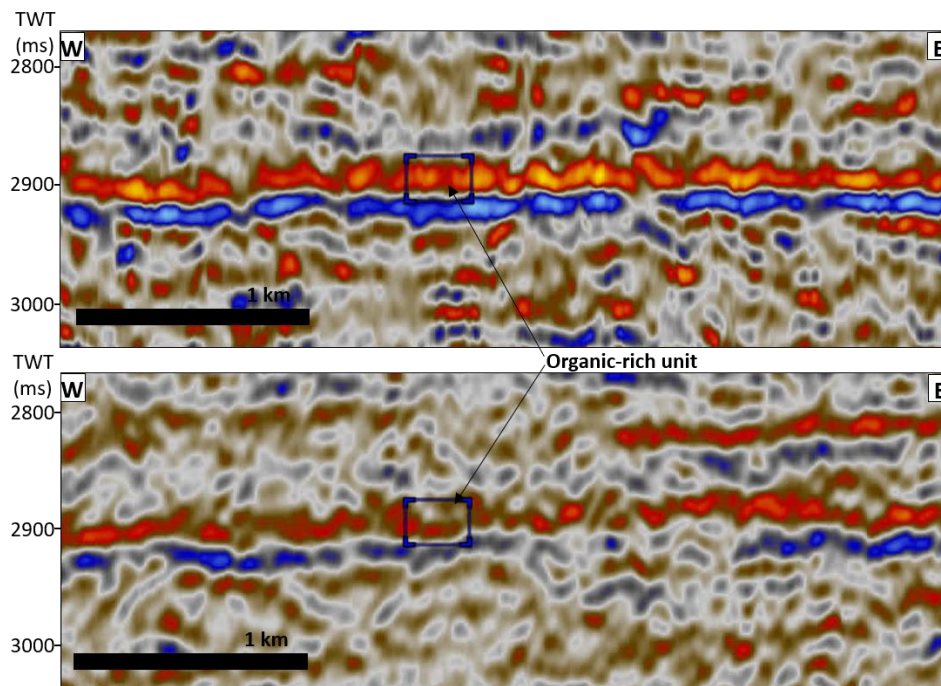


Figure 10. Part of seismic line MNR06-7110 (see Figure 2) showing a comparison of the top Middle Triassic organic carbon rich layer from near stacked angle (top) versus far angle (bottom) in the Froan Basin. Rectangles show the positions of some of the data windows used for the IG crossplotting. See Figure 1 for location.

4.3. Deformation structures on seismic

Two types of deformation structure have been observed in the Upper Permian organic rich intervals that show amplitude dimming with angle/offset in the Helgeland and Froan basins. The presence of both amplitude dimming with offset and deformation structures indicates organic-rich intervals on seismic. The first type of deformation structures is shown by slices of the Upper Permian intervals that have slid on top of one another along the faulted area in the Helgeland Basin (Figure 7 D). The second type are strata-bound deformation structures

where the Upper Permian interval is segmented by several listric faults that terminate at the base of the interval in the Froan Basin (Figure 11). Possible slide blocks of organic rich intervals (Figure 7 D) are localized in tilted areas of the southwestern Helgeland Basin.

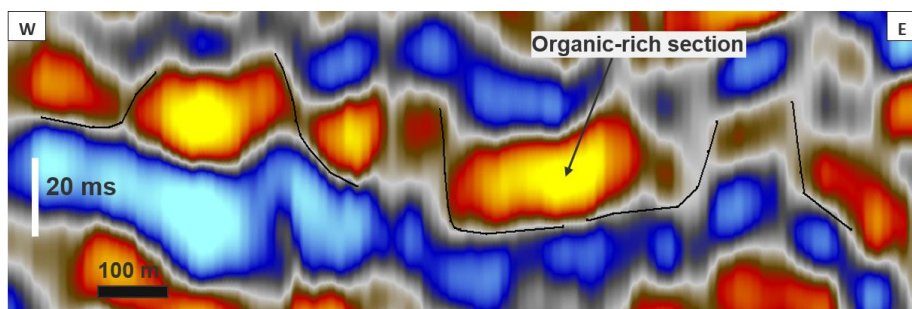


Figure 11. A seismic section showing the Upper Permian organic rich interval. Black lines indicate faults that segment the organic-rich layer and terminate at the base of the organic rich layer on seismic line MNR06-7110 in the Froan Basin (see Figure 2 for the position of this interval).

4.4. AVA/AVO classes on IG crossplots

Calibration results for the IG crossplotting show that the values from the Spekk Formation plot on a class IV position (Figure 12). The Åre coal also has a class IV anomaly, and plots near the Spekk Formation position. This means that organic-carbon-rich intervals will plot on a class IV anomaly position. Different seismic data windows were then studied to identify organic rich intervals in the Permo-Triassic deposits. Examples of data windows that have been used for IG crossplotting are shown in Figure 8-Figure 10.

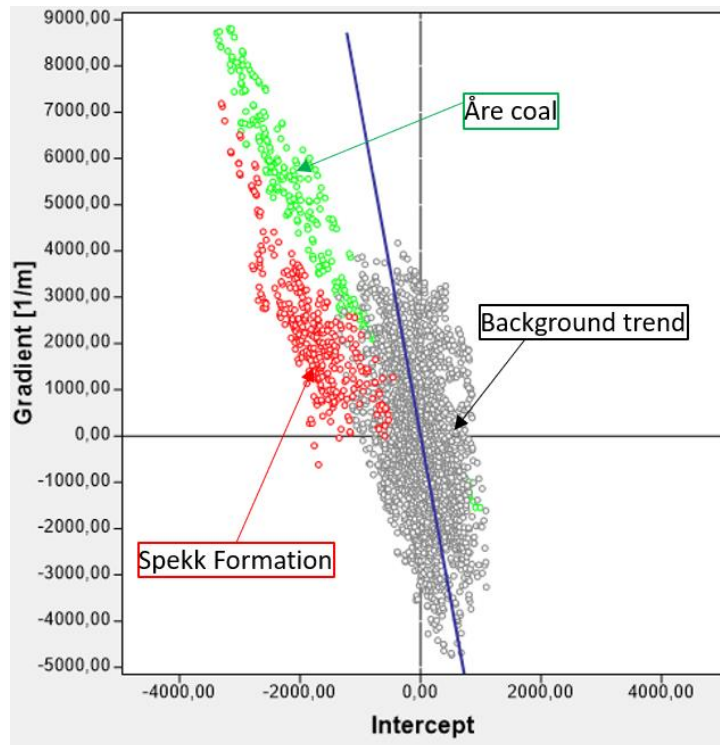


Figure 12. IG crossplot showing the Spekk Formation and Åre coal (both shown in Figure 2) plotting on a class IV position on seismic line MNR06-7110 in the Froan Basin. The Spekk Formation and Åre coal plot in different areas albeit near to each other, due to their difference in TOC values.

The investigated windows of the early Upper Permian and late Upper Permian intervals in the Froan Basin both show a dominance of AVA/AVO class IV anomaly (Figure 13 and Figure 14). These IG crossplots also show weak AVA/AVO classes II and III (Figure 13), which indicates lateral and/or vertical variation in lithological composition within the investigated layers. The variation in AVA/AVO classes may also be due to noise since the current investigation used 2D seismic data of limited quality.

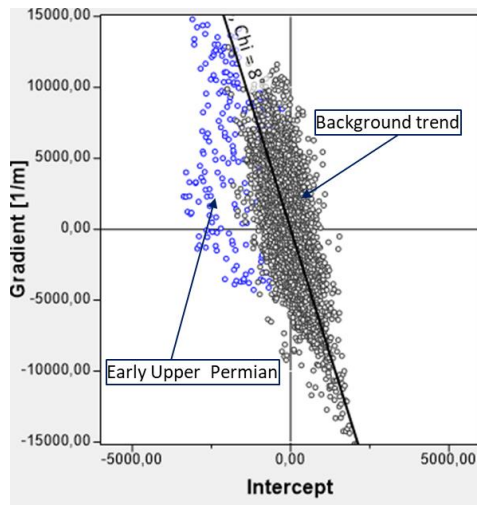


Figure 13. IG crossplot for the data windows along the early Upper Permian organic rich layer on seismic line MNR07-7118 in the Froan Basin. The data window displaying AVO class IV anomaly in this IG crossplot is shown in Figure 8.

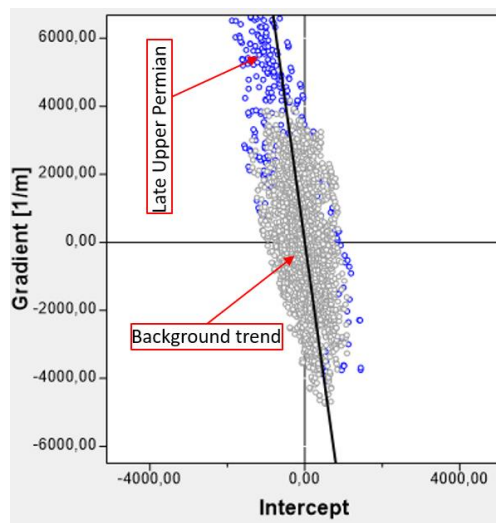


Figure 14. IG crossplot for data windows along the late Upper Permian organic rich layer on seismic line MNR06-7110 in the Froan Basin.

The investigated Upper Permian data windows in the Helgeland Basin display AVA/AVO anomaly class IV (Figure 15 A & B) that is indicative of organic-carbon-rich deposits, a dominant background trend (Figure 15 C), or strong classes IV, III, and II (Figure 15 D).

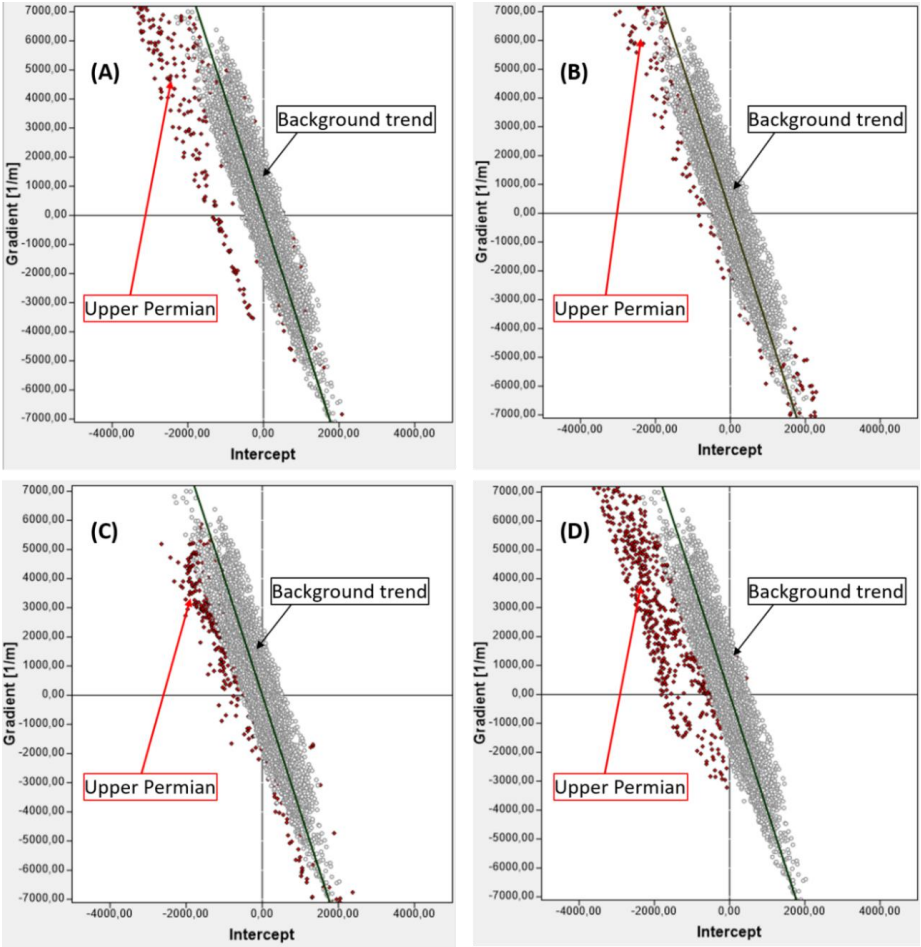


Figure 15. (A-D): IG crossplots for the data windows along the assumed Upper Permian organic-carbon-rich layer on seismic line MNR07-7294 in the Helgeland Basin. A-D are from different data windows along the Upper Permian layer. The data windows displaying AVO class IV trends are shown in Figure 7 (small rectangles). Location of the background probe is shown in Figure 19.

These IG crossplots in Figure 15 indicate lateral variation in lithology and fluid composition for the Upper Permian organic-rich interval in the Helgeland Basin. Upper Permian organic rich rocks were found over a much wider area in the Helgeland Basin than in the Froan Basin (Figure 20).

The Lower Triassic displays very weak AVA/AVO anomaly classes IV, III, and IIp but a strong class II anomaly in both the Helgeland and the Froan Basin (e.g. Figure 16). Thus, this interval is organic poor.

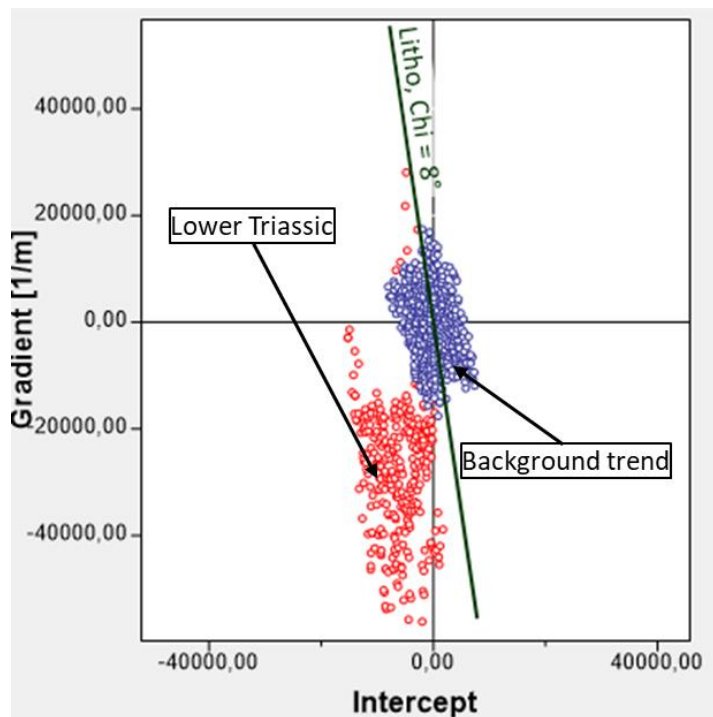


Figure 16. IG crossplot of the Lower Triassic interval on seismic line MNR07-7104 in the Froan Basin.

The data window displaying AVO class IV anomaly in this IG crossplot is shown in Figure 9.

The Middle Triassic interval has strong AVA/AVO class IV and III anomalies (Figure 17 and Figure 18) and a weaker class II anomaly (Figure 18). A strong AVA/AVO class IV anomaly indicates that organic-rich sediments were deposited during the Middle Triassic.

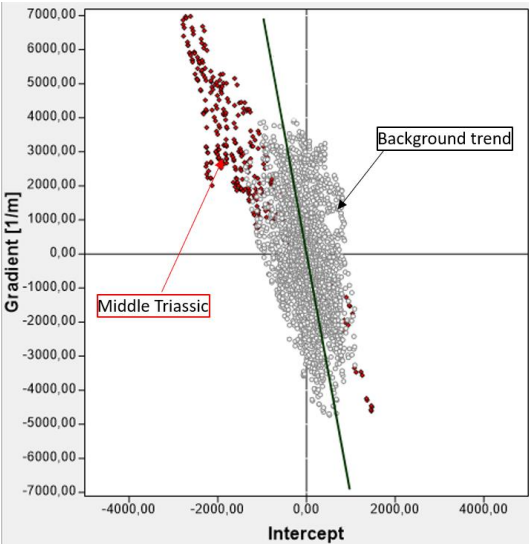


Figure 17. IG crossplot for the data windows along a Middle Triassic Organic rich layer on seismic line MNR06-7110 in the Froan Basin. The data window displaying AVO class IV anomaly in this IG crossplot is shown in Figure 10.

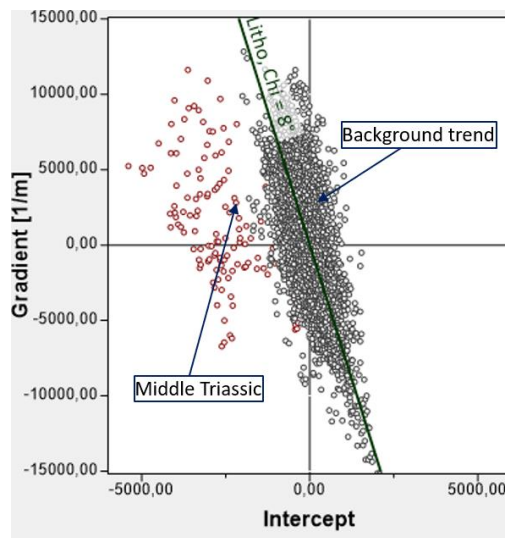


Figure 18. IG crossplot for the data windows along the middle Triassic organic rich interval on seismic line MNRO7-7118 in the Froan Basin. Data windows for the IG crossplots along the Middle Triassic target are shown in Figure 3.

5. Discussion

Using the two seismic methods, organic rich intervals have been found in both the Froan and the Helgeland basins (Figure 20). Two Upper Permian intervals and one Middle Triassic organic-rich interval have been found in the Froan Basin while the Helgeland Basin has one Upper Permian organic-rich interval.

The results in Figure 20 show a minimum distribution only, as not all organic carbon rich rocks can be recognised due to the limitations of the data set and the methodologies used. Løseth et al. (2011) reported a minimum TOC value of 3-4 wt.% as a condition for an obvious contrast between organic-rich and organic-poor rocks on seismic. Deposits with TOC below this value cannot be determined with the AVA/AVO method. Thus, one of the reasons for

the difficulty of finding organic carbon rich rocks especially in the Froan Basin is that the deposits there may be at the limit of the method.

A further method limitation that means the distribution is a minimum description, is that thin layers are below the seismic resolution and thus cannot be identified. The presence of such layers has been determined by Bugge et al. (2002) for example for the Lower Triassic (see below), but these cannot be identified with the current methods.

Further detection limitations are caused by the properties of organic carbon rich rocks, which can vary significantly because of burial compaction, composition, diagenesis, organic carbon richness, and maturation (Avseth & Carcione, 2015). The variation in these properties can affect the interpretation in some of the deep basinal areas. Various other factors, including a tuning effect (Avseth et al., 2005; Løseth et al., 2011b), elastic anisotropy (Kim et al., 1993; Blangy, 1994; Chen et al., 2001) and noise and multiples, can affect the AVA/AVO anomaly responses. The influence of these factors, and the magnitude of the associated uncertainties on the presented AVA/AVO response were not quantified as this was beyond the scope of this study. These limiting factors may explain why organic rich layers are missed in some deeper parts of the Helgeland and Froan basins. Nonetheless, previous work has shown the reliability of the method even when faced with these limitations. Firstly, the calibration, for identification of organic-rich rocks on seismic, was done on known organic-rich layers with known responses (the Spekk and Åre formations). The calibration verified that the organic-rich intervals, in the current 2D data set, plot in AVO class IV position. Although the quality of the investigated seismic profiles varies with depth (TWT in this case), Løseth et al. (2011b) showed that the AVO response of the organic rich layers are preserved quite well with depth. In addition, the analysis was done on a dataset that has undergone noise removal and

multiple attenuation to improve signal to noise ratio and enhance clarity for the deeper targets. The works of Løseth et al. (2011a, b) and del Monte et al. (2018) showed that the methods may be applied successfully in different settings despite the discussed weaknesses.

5.1. Upper Permian

The distributions of the Upper Permian organic matter are not the same in the Helgeland and Froan basins. The Upper Permian organic rich interval is widely distributed in the Helgeland Basin but locally distributed in the Froan Basin (Figure 20). A likely explanation for this is that the Froan Basin contained several isolated sub-basins at the time of deposition, while the Helgeland Basin was a larger single basin. If anoxic conditions did not develop in every sub-basin of the Froan Basin, organic carbon would have been preserved in a patchier distribution than in the Helgeland Basin. However, as mentioned above, the absence of Upper Permian organic rich rocks in most of the Froan Basin could also be due to TOC values being below the detection limit or due to thin layers. The Upper Permian organic-rich rocks, in both the Helgeland and Froan basins, show lateral variation in petrophysical properties, based on their varied seismic intensities and lateral variation in AVA/AVO classes in IG crossplots. Such lateral variation of petrophysical properties may be explained by lateral variation of lithology. Co-occurrence of organic-rich-rocks and another lithology can be seen in the seismic line and IG crossplot in Figure 19. This figure shows that the Upper Permian organic-rich-rocks and another lithology plot as two different populations separated by a background trend on the IG crossplot. The Upper Permian organic-rich shales were deposited at the same time as carbonates (Bugge et al., 2002), hence this other lithology is likely to be carbonate.

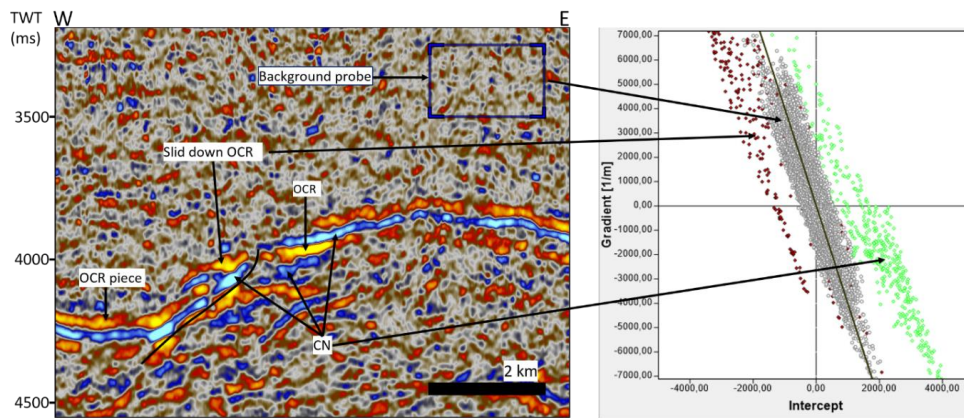


Figure 19. Seismic line MNR07-7294 (see Figure 3 for the position of this seismic interval) in the Trøndelag Platform (left) showing the investigated Upper Permian organic-carbon-rich (OCR) rocks. The OCRs occur together with a second lithology, possibly Upper Permian carbonates (CN, see main text for discussion). The IG crossplot (right) shows that the OCRs (red dots) and possible Upper Permian carbonates (green dots) plot on different sides of the background trend that separates different lithologies. The OCRs have class IV characteristics.

The background trend in Figure 19 separates different lithologies. Therefore, the variation in AVA/AVO classes and intensities of the horizon is not necessarily only due to variation in TOC levels and thicknesses of the organic-rich layers, but also possibly due to alternating deposits (horizontal changes) of organic-rich shales and the Upper Permian carbonates that are known to be present in the area. This means that the interpreted widely distributed Upper Permian organic-rich rocks in the Helgeland Basin (Figure 19) contain patchily distributed organic-carbon-rich intervals (separated by carbonate deposition) that have varied TOC levels and thicknesses.

The distributions of the Upper Permian organic carbon rich rocks and the strata bound deformation structures in the Helgeland Basin follow the basin shape, which was tectonically

influenced (Figure 1). The organic-carbon-rich sediments are aligned with the deepest part of the basin, i.e. oriented SW-NE. The sliding features indicative of organic carbon-rich-rocks are found in the faulted area in the southwest of the Helgeland Basin (Figure 20). In the Froan Basin, the Upper Permian organic-rich rocks and the strata-bound listric faults indicative of gliding of organic carbon rich layers are found in the deep parts of the sub-basin (Figure 20).

The distribution of the Upper Permian organic-rich-rocks presents some issues that cannot be resolved with the current data set. Only one organic-carbon-rich interval was seen on the seismic lines crossing the Helgeland Basin even though two intervals have been cored on the two opposite sides of the Helgeland Basin (cores 6507/6-4 A and 6611/09-U-01). The fact that only one interval can be seen from the seismic profiles would suggest either that one interval has low TOC content in the deeper parts of the basin, merging of the two intervals in the deeper parts of the Trøndelag Platform, or a tuning effect because both layers (as seen in core) are thin and the layers are only a few metres apart vertically. The AVA/AVO response can be diminished due to compaction, diagenesis and maturation of the incorporated organic matter leading to identification of just one interval in the Helgeland Basin.

The Upper Permian organic-rich rocks would have been expected to be continuous across the Helgeland Basin since they are proven in two cores (6507/6-4 A and 6611/09-U-01, see Figure 1 for location) on either side of the Helgeland Basin, but these rocks were not seen over a big area that is demarcated by the purple colour bounded by red dashes in Figure 20. There is no Upper Permian geological boundary like a local high, that would explain the absence of these rocks in most of the NE part of the Trøndelag Platform. Again, the limitations of data set and methods would prevent detection of organic carbon rich rocks in this area if the layers are thin and thus below seismic resolution or if TOC content is too low. The resolution of these

issues needs further work on better data sets in terms of seismic quality, true amplitude preservation upon processing and signal to noise ratio at the investigated depths.

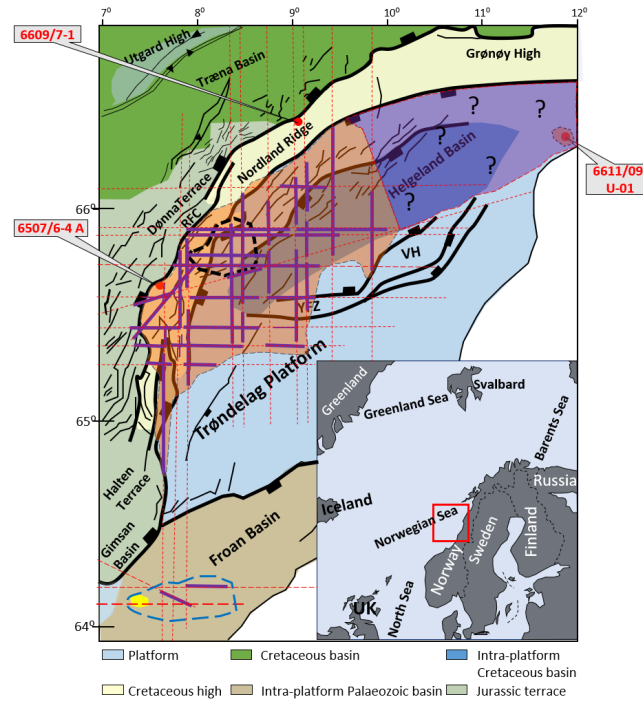


Figure 20. Distribution of Upper Permian and Middle Triassic organic-carbon-rich rocks in the Trøndelag Platform based on seismic interpretation and IG crossplotting. Brown colours and blue dashes indicate the extents of the patchily distributed Upper Permian organic-carbon-rich rocks in the Helgeland and Froan basins respectively. Yellow colour indicates the area where the Middle Triassic organic-carbon-rich rocks have been found in the Froan Basin. Black dashes surround the area where the Upper Permian gliding/sliding structures are found. The Upper Permian strata bound listric faults are found within the area surrounded by blue dashes in the Froan Basin. Purple coloured area (with question marks) shows the region where the Upper Permian organic-rich rocks could not be followed on seismic, although based on the description of core 6611/09-U-01 they would be expected there. Purple lines indicate the parts of the seismic lines where organic-rich intervals have been found while red dotted lines indicate the parts of the seismic lines where organic-rich intervals have not been found.

5.2. Lower Triassic

The Lower Triassic sections studied in this work were not found to show any signatures characteristic of organic-carbon-rich rocks. However, Bugge et al. (2002) reported several thin (typically 0.5–1.5 cm) Lower Triassic organic carbon rich layers at the eastern margin of the Helgeland Basin, with total organic carbon (TOC) of up to 2.8 wt.%. The end Permian biotic crisis caused extinction of most marine species (Stanley & Yang, 1994; Bowring et al., 1998; Kaiho et al., 2001; Knoll et al., 2007; Hochuli et al., 2010) and therefore there would have been limited marine life during the Early Triassic, leading to only thin organic carbon rich deposits when life started to build up again. The deposits in the study area are characterised by turbidites (see Bugge et al., 2002), so the thin organic rich layers reported by Bugge et al. (2002) may have been redeposited by turbidity currents from older deposits, rather than being in situ. Equivalent thin organic rich intervals may exist in the deep basinal areas, but they could not be identified with the current methods.

5.3. Middle Triassic

The middle Triassic in the Froan Basin contains an organic-carbon-rich interval that is indicated on seismic images and IG crossplots. The interval is identified over a small area in a sub-basin in the western part of the Froan Basin (Figure 20). This deposit could have formed during the short lived marine incursion during the Middle Triassic, that led to salt deposition in the Helgeland Basin (Müller et al., 2005). The distribution of the organic-rich sediments in the Froan Basin may indicate basin geometry during deposition of the Middle Triassic sediments, assuming the organic-carbon-rich sediments were deposited in the deepest parts of the sub-basins.

It is not clear why Middle Triassic organic-rich sediments were not found in the Helgeland Basin by using the current seismic data. Either these sediments were not deposited in the studied areas, they were not preserved, or the method limitations prevented detection. As discussed above, the method limitations mean there is some uncertainty in the understanding of the distribution pattern, although it is clear that organic matter is present in the basins.

6. Conclusions

The presence of Permian and Triassic organic carbon rich rocks has been determined in the Froan and Helgeland basins based on analysis and interpretation of seismic sections. Two analysis techniques were used: determination of strata-bound deformation structures, and AVA/AVO analysis. Intercept-Gradient crossplots for the analysed layers show the dominance of AVA/AVO class IV, which is characteristic for organic carbon rich rocks. These layers also show amplitude dimming with angle.

Organic-carbon-rich rocks may be more widespread than could be determined here, as a result of the limitations of the seismic data and methodology used. Further work can resolve this issue and may indicate a larger area for deposition of organic rich sediments. The results show that the spatial and temporal distribution of the organic rich deposits was at least partly controlled by the tectonically induced orientation of the basins. The organic carbon rich deposits were found in the deepest parts of the Helgeland and Froan basins. The Froan Basin contains two Upper Permian and one Middle Triassic organic-carbon-rich intervals, while the Helgeland Basin contains one Upper Permian interval. Lower Triassic organic-rich intervals were not found in either basin.

7. Acknowledgements

This work was funded by EnPe-Norad under the ANTHEI (Angola Tanzania Higher Education Initiative) scholarship scheme. Equinor provided geophysical data and working facilities to accomplish the project. NMR lines are reproduced by courtesy of SpectrumGeo and TGS. Discussions with Olav Kvamme Leirfall and Arve Næss are highly appreciated, and led to improvement of the work. Chris Saville, two anonymous reviewers and the editor are thanked for their comments which helped to improve the manuscript.

References

- Avseth, P., & Carcione, J. M. (2015). Rock-physics analysis of clay-rich source rocks on the Norwegian Shelf. *The Leading Edge*, 34, 1340–1348.
- Avseth, P., Mukerji, T., & Mavko, G. (2005). Quantitative Seismic Interpretation, Applying Rock Physics Tools to Reduce Interpretation Risk. *Cambridge, University Press*, 359 p.
- Blangy, J. P. (1994). AVO in transversely isotropic media—An overview. *Geophysics*, 59, 775-781.
- Blystad, P., Brekke, H., Færseth, R. B., Larsen, B. T., Skogseid, J., & Tørudbakken, B. (1995). Structural elements of the Norwegian continental shelf. Part II: The Norwegian Sea Region. NPD-BULLETIN, No 8, p 5-7.
- Bowring, S. A., Erwin, D. H., Jin, Y. G., Martin, M. W., Davidek, K., & Wang, W. (1998). U/Pb Zircon Geochronology and Tempo of the End-Permian Mass Extinction. *Science*, 280, 1039-1045.

- Brekke, H. (2000). The tectonic evolution of the Norwegian Sea Continental Margin with emphasis on the Vøring and Møre basins. *In* A. Nøttvedt (ed.): *Dynamics of the Norwegian Margin*, Geological Society, London, Special Publication 167, 327-378.
- Brekke, H., Sjulstad, H. I., Magnus, C., & Williams, W. R. (2001). Sedimentary environments offshore Norway - an overview. *In* O.J. Martinsen and T. Dreyer (eds.): *Sedimentary Environments Offshore Norway-Palaeozoic to Recent*, Norwegian Petroleum Society, Special Publication 10, 7-37.
- Bugge, T., Ringås, J. E., Leith, D. A., Mangerud, G., Weiss, H. M., & Leith, T. L. (2002). Upper Permian as a new play model on the mid-Norwegian continental shelf: Investigated by shallow stratigraphic drilling. *American Association of Petroleum Geologists, Bulletin* 86, 107-127.
- Bukovics, C., & Ziegler, P. A. (1985). Tectonic development of the Mid-Norway continental margin. *Marine and Petroleum Geology*, 2, 2-22
- Castagna, J. P., & Swan, H. S. (1997). Principles of AVO crossplotting. *The Leading edge*, 16, 337-342.
- Chen, H., Castagna, J. P., Brown, R. L., & Ramos, A. C. (2001). Three-parameter AVO crossplotting in anisotropic media. *Geophysics*, 66, 1359-1363.
- Christiansen, F. G., Dam, G., Piasecki, S., & Stemmerik, L. (1992). A review of Upper Palaeozoic and Mesozoic source rocks from onshore East Greenland. *In* Spencer, A.M. (ed.): *Generation, Accumulation and Production of Europe's Hydrocarbons II*. Special Publication of the European Association of Petroleum Geologist, 2, 151-161.

- Christiansen, F. G., Piasecki, S., Stemmerik, L., & Telnæs, N. (1993). Depositional Environment and Organic Geochemistry of the Upper Permian Ravnefjeld Formation Source Rock in East Greenland. *American Association of Petroleum Geologists, Bulletin* 77, 1519-1537.
- Dalland, A., Worsley, D., & Ofstad, K. (1988). A lithostratigraphic scheme for the Mesozoic and Cenozoic succession offshore mid- and northern Norway. *Norwegian Petroleum Directorate, Bulletin* 4, 65 p.
- del Monte, A. A., Antonielli, E., De Tomasi, V., Luchetti, G., Paparozzi, E., & Gambacorta, G. (2018). Methods for source rock identification on seismic data: An example from the Tanezzuft Formation (Tunisia). *Marine and Petroleum Geology*, 91, 108-124.
- Doré, A. G. (1992). Synoptic palaeogeography of the Northeast Atlantic Seaway: late Permian to Cretaceous. In J. Parnell (ed.): *Basins on the Atlantic Seaboard: Petroleum Geology, Sedimentology and Basin Evolution*, Geological Society, London, Special Publication 62, 421-446.
- Guarnieri, P., Brethes, A., & Rasmussen, T. M. (2017). Geometry and kinematics of the Triassic rift basins in Jameson Land (East Greenland). *Tectonics*, 36, 602-614.
- Halland, E. K., Gjeldvik, I. T., Johansen, W. T., Magnus, C., Meling, I. M., Mujezinović, J., Riis, F., Rød, R. S., Van T. H., Pham, V.T.H., Tappel, I. (2011). CO₂ atlas for the Norwegian Continental Shelf: The Norwegian Sea. Norwegian Petroleum Directorate. Retrieved June 30, 2019, from:
<https://www.npd.no/contentassets/aa14c3079a47451c88268166ba4e61aa/chapter-5.pdf>

- Hochuli, P. A., Vigran, J. O., Hermann, E., & Bucher, H. (2010). Multiple climatic changes around the Permian-Triassic boundary event revealed by an expanded palynological record from mid-Norway. *Geological Society of America, Bulletin* 122, 884-896.
- Kaiho, K., Kajiwara, Y., Nakano, T., Miura, Y., Kawahata, H., Tazaki, K., Ueshima, M., Chen, Z. and Shi, G.R. (2001). End-Permian catastrophe by a bolide impact: Evidence of a gigantic release of sulfur from the mantle. *Geology*, 29, 815-818.
- Kim, K. Y., Wroldstad, K. H., & Aminzadeh, F. (1993). Effects of transverse isotropy on P-wave AVO for gas sands. *Geophysics*, 58, 883-888.
- Knoll, A. H., Bambach, R. K., Payne, J. L., Pruss, S., & Fischer, W. W. (2007). Paleophysiology and end-Permian mass extinction. *Earth and Planetary Science Letters*, 256, 295-313.
- Kreiner-Møller, M., & Stemmerik, L. (2001). Upper Permian lowstand fans of the Bredehom Member, Schuchert Dal Formation, East Greenland. In O. J. Martinsen and T. Dreyer (eds.): *Sedimentary Environments Offshore Norway - Palaeozoic to Recent*, Norwegian Petroleum Society, Special Publication 10, 51-65.
- Lancaster, S., & Whitcombe, D. (2000). Fast-Track 'coloured' inversion. In: SEG Technical Program Expanded Abstracts 2000. *Society of Exploration Geophysicists*, 1572-1575.
- Løseth, H., Wensaas, I., & Gading, M. (2011a). Deformation structures in organic-rich shales. *American Association of Petroleum Geologists, Bulletin* 95, 729-747.
- Løseth, H., Wensaas, L., Gading, M., Duffaut, K., & Springer, M. (2011b). Can hydrocarbon source rocks be identified on seismic data? *Geology*, 39, 1167-1170.
- Müller, R., Nystuen, J. P., & Lie, H. (2005). Late Permian to Triassic basin infill history and palaeogeography of the Mid-Norwegian shelf-East Greenland Region. In

B.T.G. Wandås, J.P. Nystuen, E. Eide, F. Gradstein (eds.): *Onshore-Offshore Relationships on the North Atlantic Margin*, Norwegian Petroleum Society, Special Publications 12, 165-189.

NPD. (2013). Wellbore (6507/6-4 A)/ Exploration. Retrieved January 19, 2018, from NPD FactPages:
<http://factpages.npd.no/FactPages/Default.aspx?nav1=wellbore&nav2=PageView|Exploration|All&nav3=6753&culture=en>

Oftedal, B. T., Andresen, A., & Müller, R. (2005). Early Triassic syn-rift sedimentation at Hold with Hope, Northeast Greenland. In B.T.G Wandås, J.P. Nystuen, E. Eide, F. Gradstein (eds.): *Onshore-Offshore Relationships on the North Atlantic Margin*, Norwegian Petroleum Society, Special Publications 12, 191-206.

Osmundsen, P.T., Braathen, A., Sommaruga, A., Skilbrei, J.R., Nordgulen, Ø., Roberts, D., Andersen, T.B., Olesen, O. and Mosar, J. (2005). Metamorphic core complexes and gneiss-cored culminations along the Mid-Norwegian margin: an overview and some current ideas. In B.T.G Wandås, J.P. Nystuen, E. Eide, F. Gradstein (eds.): *Onshore-Offshore Relationships on the North Atlantic Margin*, Norwegian Petroleum Society, Special Publications 12, 29-41.

Ostrander, W. (1984). Plane-wave reflection coefficients for gas sands at nonnormal angles of incidence. *Geophysics*, 49, 1637-1648.

Piasecki, S., & Stemmerik, L. (1991). Late Permian anoxia in central East Greenland. In R. V. Tyson and T. H. Pearson (eds.): *Modern and Ancient Continental Shelf Anoxia*, Geological Society, London, Special Publication 58, 275-290.

- Redfern, J., Shannon, P.M., Williams, B.P.J., Tyrrell, S., Leleu, S., Perez, I.F., Baudon, C., Štolfová, K., Hodgetts, D., Van Lanen, X. and Speksnijder, A., (2010). An integrated study of Permo-Triassic basins along the North Atlantic passive margin: implication for future exploration. *Geological Society, London, Petroleum Geology Conference series 7*, 921-936.
- Ross, C. P., & Kinman, D. L. (1995). Nonbright-spot AVO: Two examples. *Geophysics*, 60, 1398-1408.
- Rutherford, S. R., & Williams, R. H. (1989). Amplitude-versus-offset variations in gas sands. *Geophysics*, 54, 680-688.
- Saxena, P. (2016). Play based evaluation of the eastern margin of Nordland Ridge, Norwegian Sea. *University of Stavanger*, unpublished MSc thesis, p 101.
- Seidler, L. (2000). Incised submarine canyons governing new evidence of Early Triassic rifting in East Greenland. *Palaeogeography, Palaeoclimatology, Palaeoecology*, 161, 267-293.
- Stanley, S. M., & Yang, X. (1994). A double mass extinction at the end of the Paleozoic era. *Science*, 266, 1340-1344.
- Stemmerik, L., Christiansen, F. G., Piasecki, S., Jordt, B., Marcussen, C., & Nøhr-Hansen, N. (1993). Depositional history and petroleum geology of the Carboniferous to Cretaceous sediments in the northern part of East Greenland. *In* T.O. Vorren, E. Bergsager, Ø.A. Dahl-Stamnes, E. Holter, B. Johansen, E. Lie, T.B. Lund (eds.): *Arctic Geology and Petroleum Potential*, Norwegian Petroleum Society, Special Publications 2, 67-87.

- Stemmerik, L., Dam, G., Noe-Nygaard, N., Piasecki, S., & Surlyk, F. (1998). Sequence stratigraphy of source and reservoir rocks in the Upper Permian and Jurassic of Jameson Land, East Greenland. *Geology of Greenland Survey, Bulletin 180*, 43-54.
- Surlyk, F. (1990). Timing, style and sedimentary evolution of Late Palaeozoic-Mesozoic extensional basins of East Greenland. *In* R. F. P. Hardman and J. Brooks (eds.): *Tectonic Events Responsible for Britain's Oil and Gas Reserves*. Geological Society, London, Special Publication, 55, 107-125.
- Surlyk, F., Piasecki, S., Rolle, F., Stemmerik, L., Thomsen, L., & Wrang, P. (1984). The Permian Base of East Greenland. *In*: Spencer A.M. (ed.): *Petroleum Geology of the North European Margin*, Springer, Dordrecht., 303-315.
- Surlyk, F., Hurst, J. M., Piasecki, S., Rolle, F., Scholle, P. A., Stemmerik, L., & Thomsen, E. (1986). The Permian of the Western Margin of the Greenland Sea-A future Exploration Target. *In* Halbouty M.T. (ed.): *Future Petroleum Provinces of the World*, American Association of Petroleum Geologists Memoir 40, 629-659.
- Swiecicki, T., Gibbs, P. B., Farrow, G. E., & Coward, M. P. (1998). A tectonostratigraphic framework for the Mid-Norway region. *Marine and Petroleum Geology*, 15, 245-276.
- Whitcombe, D. N., Connolly, P. A., Reagan, R. L., & Redshaw, T. C. (2002). Extended elastic impedance for fluid and lithology prediction. *Geophysics*, 67, 63-67.

4.3. Paper III

“Palaeodepositional conditions of Permian organic-carbon-rich deposits of the Helgeland Basin, mid Norway, based on element proxies and core logging”

Emily Barnabas Kiswaka¹, Maarten Felix¹, and Arve Næss^{1,2}

¹NTNU Norwegian University of Science and Technology, Trondheim, Norway, ²Equinor ASA-Stjørdal, Norway (emily.kiswaka@ntnu.no)

To be re-submitted to scientific journal for publication

4.3.1. Author contributions

My contribution to this paper involved writing, sedimentological core logging and interpretation, element measurements using handheld PXF, plotting of element values, interpretation and writing.

Maarten Felix was involved in writing and providing relevant discussion and recommendations. He provided his scientific expertise in sedimentology and Matlab.

Arve Næss was involved in text editing, but also provided his expertise and scientific knowledge regarding the Permo-Triassic sedimentary conditions of the study area.

This paper is awaiting publication and is not included in NTNU Open

CHAPTER 5: SUMMARY AND CONCLUSIONS

The main results from this thesis work are:

- Both qualitative seismic interpretation and core logging indicated several tectonic pulses, from the late Devonian to late Triassic, in the Trøndelag Platform. These are mid Carboniferous, mid Permian, two late Permian rifts, two Early Triassic rifts, and late Mid Triassic-Late Triassic rifting events.
- Seismic interpretation and a combination of core logging indicate that Permo-Triassic sedimentation in the Helgeland Basin was mostly influenced by tectonics. That is, rifting and uplift created sub-basins and triggered particulate gravity currents that were responsible for deposition of the turbidite units.
- The tectonic pulses that occurred in the late Permian modified the geometries of the basins. This led to the development of conditions that were conducive to the deposition and preservation of the upper Permian organic-carbon-rich rocks in the Helgeland and Froan Basins.
- Upper Permian organic-carbon-rich sediments are present in most of the deeper parts of the Helgeland Basin and some parts of the Froan Basin. The distribution of these organic carbon-rich rocks is aligned with the orientations of the tectonically controlled sub-basins.
- The anoxic conditions during deposition of the LOCR interval were due to restricted basins with limited oxygen supply caused by tectonic isolation of sub-basins from the main ocean.
- Fluvial input was essential for water column stratification and development of anoxia for organic-carbon preservation during deposition of the upper organic-carbon-rich interval (UOCR).

CHAPTER 6: RECOMMENDATIONS AND FUTURE RESEARCH

Future research should focus on expanding the results presented in this thesis and improve the current understanding of the depositional conditions during the Permo-Triassic by applying different analysis techniques. The element analysis was done on a small part of core 6611/09-U-01 only causing the results to lack calibration against other basinal areas. Element analysis on core 6507/6-4 A (see figure 1 in chapter 1 for location and section 4.3 for more text) which has also penetrated the upper Permian organic rich rocks will be a good starting point.

The core analysis (core logging and element analysis) has shown tectonic changes and basin changes during the limited time period limited that was examined. It will be interesting to expand this investigation to the entire length of both core 6611/09-U-1 and core 66111/09-U-2 (which has penetrated the Triassic successions that overlap with core 6611/09-U-1) to determine a longer record of changes in the area.

Laboratory XRF analysis, which involves analysis of homogenized samples, on ambient mudstone is recommended. This will enable recording of element contents whose variations will better reflect oxygen variations, primary productivity, and influence from terrestrial influx during deposition of the organic-carbon-rich sediments. This is because of the complexity of the factors that controlled distribution of the studied elements over the whole interval which contains different deposit types and multiple grain size changes. Grain size change and vertical variations in deposit types have been found to have a significant influence on element distribution over the whole interval. Focusing on ambient mudstones (uniform grain size) will avoid the complexity brought by contributions from various deposit types and changes in grain size.

Determine drainage establishment after the second late Permian tectonic event (reported in Sections 4.1 and 4.3) will be key to understand the abrupt dominance of fluvial input and consequent stratification during deposition of the upper organic-carbon-rich interval. This should also involve a detailed local analysis of the climate conditions during the late Permian. The climate might have varied locally, expanded the drainage system, increased fluvial input and consequently fluvial stratification.

REFERENCES

- Algeo, T. J., & Maynard, J. B. (2004). Trace-element behavior and redox facies in core shales of Upper Pennsylvanian Kansas-type cyclothems. *Chemical Geology*, 206(3-4), 289-318.
- Arthur, M.A., Dean, W.E. and Stow, D.A.V. (1984). Models for the deposition of Mesozoic-Cenozoic fine-grained organic-carbon-rich sediment in the deep sea. In D. A. V. Stow and D. J. W. Piper (eds.): *Fine-grained Sediments: Deep-water Processes and Facies*, Geological Society, London, Special Publications 15, 527-560.
- Avseth, P., Mukerji, T., & Mavko, G. (2005). Quantitative Seismic Interpretation, Applying Rock Physics Tools to Reduce Interpretation Risk. *Cambridge, University Press*, 359 p.
- Benesty, J., Chen, J., Huang, Y., & Cohen, I. (2009). Pearson correlation coefficient. In *Noise reduction in speech processing* (pp. 1-4). Springer, Berlin, Heidelberg.
- Blystad, P., Brekke, H., Færseth, R. B., Larsen, B. T., Skogseid, J., & Tøruðbakken, B. (1995). Structural elements of the Norwegian continental shelf. Part II: The Norwegian Sea Region. *NPD-BULLETIN, No 8*, p 5-7.
- Bøe, R., Fossen, H. & Smelror, M. (2010). Mesozoic sediments and structures onshore Norway and in the coastal zone. *Geological Survey of Norway Bulletin*, 450, 15–32.
- Brekke, H. (2000). The tectonic evolution of the Norwegian Sea continental margin with emphasis on the Vøring and Møre basins. In A. Nøttvedt (ed.): *Dynamics of the Norwegian Margin*, Geological Society, London, Special Publication 167, 327-378.
- Bugge, T., Ringås, J. E., Leith, D. A., Mangerud, G., Weiss, H. M., & Leith, T. L. (2002). Upper Permian as a new play model on the mid-Norwegian continental shelf: Investigated by shallow stratigraphic drilling. *American Association of Petroleum Geologists, Bulletin* 86, 107-127.
- Calvert, S. E., & Pedersen, T. F. (2007). Chapter fourteen elemental proxies for palaeoclimatic and palaeoceanographic variability in marine sediments: Interpretation and application. *Developments in Marine Geology*, 1, 567-644.
- Calvert, S., & Pedersen, T. (1993). Geochemistry of recent oxic and anoxic marine sediments: Implications for the geological record. *Marine Geology*, 113(1-2), 67-88.
- Castagna, J. P., & Swan, H. S. (1997). Principles of AVO crossplotting. *The Leading edge*, 16 (4), 337-344.
- Christiansen, F. G., Dam, G., Piasecki, S., & Stemmerik, L. (1992). A review of Upper Palaeozoic and Mesozoic source rocks from onshore East Greenland. In Spencer, A.M. (ed.): *Generation, Accumulation and Production of Europe's Hydrocarbons II*, The European Association of Petroleum Geologist, Special Publication 2, 151-161.

- Christiansen, F. G., Piasecki, S., Stemmerik, L., & Telnæs, N. (1993). Depositional Environment and Organic Geochemistry of the Upper Permian Ravnefjeld Formation Source Rock in East Greenland. *American Association of Petroleum Geologists, Bulletin* 77, 1519-1537.
- Cloutier, V., Lefebvre, R., Therrien, R., & Savard, M.M. (2008). Multivariate statistical analysis of geochemical data as indicative of the hydrogeochemical evolution of groundwater in a sedimentary rock aquifer system. *Journal of Hydrology*, 353, 294–313.
- Dalland, A., Worsley, D., & Ofstad, K. (1988). A lithostratigraphic scheme for the Mesozoic and Cenozoic succession offshore mid- and northern Norway. *Norwegian Petroleum Directorate, Bulletin* 4, 65 p.
- del Monte, A. A., Antonielli, E., De Tomasi, V., Luchetti, G., Paparozzi, E., & Gambacorta, G. (2018). Methods for source rock identification on seismic data: An example from the Tanezzuft Formation (Tunisia). *Marine and Petroleum Geology*, 91, 108-124.
- Demaison, G., & Moore, G. T. (1980). Anoxic environments and oil source bed genesis, *American Association of Petroleum Geologists, Bulletin* 64, 1179–1209.
- Doré, A. G. (1992). Synoptic palaeogeography of the Northeast Atlantic Seaway: late Permian to Cretaceous. In: J. Parnell (ed.), Basins on the Atlantic Seaboard: Petroleum Geology, Sedimentology and Basin Evolution. *Geological Society, London, Special Publication* 62, 421-446.
- Doré, A.G., Lundin, E.R., Jensen, L.N., Birkeland, Ø., Eliassen, P.E. & Fichler, C. (1999). Principal tectonic events in the evolution of the northwest European Atlantic margin. In Fleet, A.J., & Boldy, S.A.R. (eds.), *Petroleum Geology of Northwest Europe: Proceedings of the 5th Conference*. Geological Society, London, 41–61.
- Dymond, J., & Collier, R. (1996). Particulate barium fluxes and their relationships to biological productivity. *Deep Sea Research Part II: Topical Studies in Oceanography*, 43(4-6), 1283-1308.
- Dymond, J., Suess, E., & Lyle, M. (1992). Barium in deep-sea sediment: A geochemical proxy for paleoproductivity. *Paleoceanography*, 7(2), 163-181.
- Francois, R. (1988). A study on the regulation of the concentrations of some trace metals (Rb, Sr, Zn, Pb, Cu, V, Cr, Ni, Mn and Mo) in Saanich Inlet sediments, British Columbia, Canada. *Marine Geology*, 83(1-4), 285-308.
- Friis, H., Poulsen, M. L., Svendsen, J. B., & Hamberg, L. (2007) Discrimination of density flow deposits using elemental geochemistry-Implication for subtle provenance differentiation in a narrow submarine canyon, Palaeogene, Danish North Sea. *Marine and Petroleum Geology*, 24(4), 221-235.

- Guarnieri, P., Brethes, A., & Rasmussen, T. M. (2017). Geometry and kinematics of the Triassic rift basins in Jameson Land (East Greenland). *Tectonics*, 36(4), 602-614.
- Hallberg, R. (1976). A geochemical method for investigation of palaeoredox conditions in sediments. *Ambio Special Report*, 4, 139-147.
- Hamann, N.E., Wittaker, R.C. & Stemmerik, L. (2005). Geological development of the Northeast Greenland shelf. In Doré, A.G. & Vining, B.A. (eds.): *Petroleum Geology: North-West Europe and Global Perspectives*— Proceedings of the 6th Petroleum Geology Conference. Geological Society, London, 887–902.
- Henkel, S., Mogollon, J. M., Nöthen, K., Franke, C., Bogus, K., Robin, E., Bahr, A., Blumenberg, M., Pape, T., Seifert, R. and März, C. (2012). Diagenetic barium cycling in Black Sea sediments—A case study for anoxic marine environments. *Geochimica et Cosmochimica Acta*, 88, 88-105.
- Jacot des Combes, H., Caulet, J.-P., & Tribovillard, N. P. (1999). Pelagic productivity changes in the equatorial area of the northwest Indian Ocean during the last 400,000 years. *Marine Geology*, 158(1-4), 27-55.
- Jeandel, C., Tachikawa, K., Bory, A., & Dehairs, F. (2000). Biogenic barium in suspended and trapped material as a tracer of export production in the tropical NE Atlantic (EUMELI sites). *Marine Chemistry*, 71(1-2), 125-142.
- Jones, B., & Manning, D. A. (1994). Comparison of geochemical indices used for the interpretation of palaeoredox conditions in ancient mudstones. *Chemical Geology*, 111 (1-4), 111-129.
- Kreiner-Møller, M., & Stemmerik, L. (2001). Upper Permian lowstand fans of the Bredehom Member, Schuchert Dal Formation, East Greenland. In: O. J. Martinsen and T. Dreyer (eds.), *Sedimentary Environments Offshore Norway - Palaeozoic to Recent*, *Norwegian Petroleum Society, Special Publication 10*, 51-65.
- Latimer, J. C., & Filipelli, G. M. (2003). Testing the phosphorus paleoproductivity proxy across a productivity and sedimentology gradient in the Southern Ocean. *AGU Fall Meeting Abstracts*. Online, available at: <http://adsabs.harvard.edu/abs/2003AGUFMPP32C..07L>. Retrieved on 06th Sept. 2019.
- Løseth, H., Wensaas, I., & Gading, M. (2011a). Deformation structures in organic-rich shales. *American Association of Petroleum Geologists, Bulletin* 95, 729-747.
- Løseth, H., Wensaas, L., Gading, M., Duffaut, K., & Springer, M. (2011b). Can hydrocarbon source rocks be identified on seismic data? *Geology*, 39(12), 1167-1170. doi:10.1130/G32328.1

- McManus, J., Berelson, W.M., Klinkhammer, G.P., Johnson, K.S., Coale, K.H., Anderson, R.F., Kumar, N., Burdige, D.J., Hammond, D.E., Brumsack, H.J. and McCorkle, D.C. (1998). Geochemistry of barium in marine sediments: Implications for its use as a paleoproxy. *Geochimica et Cosmochimica Acta*, 62(21-22), 3453-3473.
- McManus, J., Berelson, W. M., Hammond, D. E., & Klinkhammer, G. P. (1999). Barium cycling in the North Pacific: Implications for the utility of Ba as a paleoproductivity and paleoalkalinity proxy. *Paleoceanography and Paleoclimatology*, 14(1), 53-61.
- Murray, R. W., & Leinen, M. (1993). Chemical transport to the seafloor of the equatorial Pacific Ocean across a latitudinal transect at 135°W: tracking sedimentary major, trace, and rare earth element fluxes at the Equator and the Intertropical Convergence Zone. *Geochimica et Cosmochimica Acta*, 57(17), 4141-4163.
- Müller, R., Nystuen, J. P., & Lie, H. (2005). Late Permian to Triassic basin infill history and palaeogeography of the Mid-Norwegian shelf-East Greenland Region. In B.T.G. Wandås, J.P. Nystuen, E. Eide, F. Gradstein (eds.): *Onshore-Offshore Relationships on the North Atlantic Margin*, Norwegian Petroleum Society, Special Publications 12, 165-189.
- Nijenhuis, I. A., Bosch, H. J., Damsté, J. S., Brumsack, H. J., & De Lange, G. J. (1999). Organic matter and trace element rich sapropels and black shales: a geochemical comparison. *Earth and Planetary Science Letters*, 169(3-4), 277-290.
- Oftedal, B. T., Andresen, A., & Müller, R. (2005). Early Triassic syn-rift sedimentation at Hold with Hope, Northeast Greenland. In B.T.G Wandås, J.P. Nystuen, E. Eide, F. Gradstein (eds.): *Onshore-Offshore Relationships on the North Atlantic Margin*, Norwegian Petroleum Society, Special Publications 12, 191-206.
- Ostrander, W. (1984). Plane-wave reflection coefficients for gas sands at nonnormal angles of incidence. *Geophysics*, 49(10), 1637-1648.
- Parks, J. M. (1966). Cluster analysis applied to multivariate geologic problems. *The Journal of Geology*, 74(5), 703-715.
- Peron-Pinvidic, G., Manatschal, G., Osmundsen, P.T. (2013). Structural comparison of archetypal Atlantic rifted margins: a review of observations and concepts. *Marine and Petroleum Geology*, 43, 21–47.
- Peron-Pinvidic, G., Osmundsen, P.T. (2016). Architecture of the distal and outer domains of the Mid-Norwegian rifted margin: insights from the Ran-Gjallar ridges system. *Marine and Petroleum Geology*, 77, 280–299.
- Peron-Pinvidic, G., Osmundsen, P.T. (2018). The Mid Norwegian-NE Greenland conjugate margins: rifting evolution, margin segmentation, and breakup. *Marine and Petroleum Geology*, 98, 162–184.

- Piasecki, S., & Stemmerik, L. (1991). Late Permian anoxia in central East Greenland. *In* R. V. Tyson and T. H. Pearson (eds.): *Modern and Ancient Continental Shelf Anoxia*, Geological Society, London, Special Publication 58, 275-290.
- Poulsen, M. L., Friis, H., Svendsen, J. B., Jensen, C. B., & Bruhn, R. (2007) The application of bulk rock geochemistry to reveal heavy mineral sorting and flow units in thick, massive gravity flow deposits, Siri Canyon Palaeocene Sandstones, Danish North Sea. *In* M. Mange and D. Wright (Eds.): *Heavy minerals in use*, Developments in Sedimentology, 58, 1099-1121.
- Redfern, J., Shannon, P. M., Williams, B. P. J., Tyrrell, S., Leleu, S., Perez, I. F., Baudon, C., Štolfová, K., Hodgetts, D., Van Lanen, X. and Speksnijder, A. (2010). An integrated study of Permo-Triassic basins along the North Atlantic passive margin: implication for future exploration. *Geological Society, London, Petroleum Geology Conference series 7*, 921-936.
- Ross, C. P., & Kinman, D. L. (1995). Nonbright-spot AVO: Two examples. *Geophysics*, 60(5), 1398-1408.
- Rutherford, S. R., & Williams, R. H. (1989). Amplitude-versus-offset variations in gas sands. *Geophysics*, 54(6), 680-688.
- Seidler, L. (2000). Incised submarine canyons governing new evidence of Early Triassic rifting in East Greenland. *Palaeogeography, Palaeoclimatology, Palaeoecology*, 161(1-2), 267-293.
- Seidler, L., Steel, R. J., Stemmerik, L., & Surlyk, F. (2004). North Atlantic marine rifting in the Early Triassic: new evidence from East Greenland. *Journal of the Geological Society*, 161(4), 583-592.
- Shuey, R. T. (1985). A simplification of the Zoeppritz equations. *Geophysics*, 50(4), 609-614.
- Slomp, C. P., Thomson, J., & de Lange, G. J. (2004). Controls on phosphorus regeneration and burial during formation of eastern Mediterranean sapropels. *Marine Geology*, 203(1-2), 141-159.
- Stemmerik, L. (2000). Late Paleozoic evolution of the North Atlantic margin of Pangea. *Palaeogeography, Palaeoclimatology, Palaeoecology*, 161, 95–126.
- Stemmerik, L., Christiansen, F. G., Piasecki, S., Jordt, B., Marcussen, C., & Nøhr-Hansen, N. (1993). Depositional history and petroleum geology of the Carboniferous to Cretaceous sediments in the northern part of East Greenland. *In* T.O. Vorren, E. Bergsager, Ø.A. Dahl-Stamnes, E. Holter, B. Johansen, E. Lie, T.B. Lund (eds.): *Arctic Geology and Petroleum Potential*, Norwegian Petroleum Society Special Publications 2, 67-87.

- Stemmerik, L., Dam, G., Noe-Nygaard, N., Piasecki, S., & Surlyk, F. (1998). Sequence stratigraphy of source and reservoir rocks in the Upper Permian and Jurassic of Jameson Land, East Greenland. *Geology of Greenland Survey, Bulletin 180*, 43-54.
- Stoker, M., Stewart, M., Shannon, P., Bjerager, M., Nielsen, T., Blischke, A., Hjelstuen, B., Gaina, C., McDermott, K., Ólavsdóttir, J. (2017). An overview of the Upper Palaeozoic–Mesozoic stratigraphy of the NE Atlantic region. In Péron-Pinvidic, G., Hopper, J.R., Stoker, M.S., Gaina, C., Doornenbal, J.C., Funck, T., Árting, U. (Eds.): *The NE Atlantic Region: A Reappraisal of Crustal Structure, Tectonostratigraphy and Magmatic Evolution*. vol. 447. Geological Society, London, Special Publications 447, 11–68.
- Surlyk, F. (1990). Timing, style and sedimentary evolution of Late Palaeozoic-Mesozoic extensional basins of East Greenland. In R. F. P. Hardman and J. Brooks (eds.): *Tectonic Events Responsible for Britain's Oil and Gas Reserves*, Geological Society, London, Special Publication 55, 107-125.
- Surlyk, F., Piasecki, S., Rolle, F., Stemmerik, L., Thomsen, L., & Wrang, P. (1984). The Permian Base of East Greenland. In Spencer A. M. (ed.): *Petroleum Geology of the North European Margin*, Springer, Dordrecht, 303-315.
- Surlyk, F., Hurst, J. M., Piasecki, S., Rolle, F., Scholle, P. A., Stemmerik, L., & Thomsen, E. (1986). The Permian of the western margin of the Greenland Sea-A future exploration target. In M. T. Halbouty (ed.): *Future Petroleum Provinces of the World*, American Association of Petroleum Geologists Memoir 40, 629-659.
- Thermo Fisher Scientific (2019) Resources, XRF technology, online source, Available at: <https://www.thermofisher.com/no/en/home/industrial/spectroscopy-elemental-isotope-analysis/spectroscopy-elemental-isotope-analysis-learning-center/elemental-analysis-information/xrf-technology.html>. Accessed on 13th Dec, 2019.
- Tribouillard, N., Algeo, T. J., Lyons, T., & Riboulleau, A. (2006). Trace metals as paleoredox and paleoproductivity proxies: an update. *Chemical Geology*, 232(1-2), 12-32.
- Tsikalas, F., Faleide, J.I., Eldholm, O. & Wilson, J. (2005). Late Mesozoic–Cenozoic structural and stratigraphic correlations between the conjugate mid- Norway and NE Greenland continental margins. In Doré, A.G. & Vining, B.A. (eds.): *Petroleum Geology: North-West Europe and Global Perspectives – Proceedings of the 6th Petroleum Geology Conference*. Geological Society, London, 785–802.
- Tyson, R.V. (2005). The “productivity versus preservation” controversy: cause, flaws, and resolution. In Harris, N.B. (Ed.): *The Deposition of Organic-carbon-rich Sediments: Models, Mechanisms, and Consequences*, SEPM Special Publication 82, 17–33.
- Von Breyman, M. T., Emeis, K. C., & Suess, E. (1992). Water depth and diagenetic constraints on the use of barium as a palaeoproductivity indicator. In C. P.

Summerhayes, W. L. Prell and K. C. Emeis (eds.): *Upwelling Systems: Evolution Since the Early Miocene*, Geological Society, London, Special Publications, 64(1), 273-284.

Whitcombe, D. N., Connolly, P. A., Reagan, R. L., & Redshaw, T. C. (2002). Extended elastic impedance for fluid and lithology prediction. *Geophysics*, 67(1), 63-67.

APPENDICES

Appendix 1. Matlab scripts used to analyse the recorded elements

Appendix 1.1. Plotting element distributions across the scanned core interval

```
% Plot of elemental values for different deposit types

clear variables

elements={'Nd' 'Pr' 'Ce' 'La' 'Ba' 'Sb' 'Sn' 'Cd' 'Ag' 'Mo' 'Nb' 'Th'
'Zr'...
'Y' 'Sr' 'U' 'Rb' 'Bi' 'Au' 'Se' 'As' 'Pb' 'W' 'Zn' 'Cu'...
'Ni' 'Co' 'Fe' 'Mn' 'Cr' 'V' 'Ti' 'Ca' 'K' 'Al' 'P' 'Si' 'Cl' 'S'
'Mg'};
indexes=[4 5 6 7 8 9 10 11 12 13 14 15 16 17 18 19 20 21 22 23 24 25 26 27
28 29 30 31 32 33 34 35 36 37 38 39 40 41 42 43];

% read values from Excel sheet
[num,txt,~] = xlsread('PXRF_Facies_final.xlsx',1);
names=txt(8,:);
depths=num(:,1);

% tops of zones (m)
zone1_b = 312;
zones_t=[305.5 299 282.5 274 266.4 253 246 239.5 231.9...
202.55 196.9 185.1 176 170.9];
text_d=0.5*([zone1_b zones_t(1:length(zones_t)-1)]+zones_t);

for i_el = 1:length(indexes)
    i_element=indexes(i_el);
    elem=num(:,i_element);

    % read ambient mud values from Excel sheet
    [num_am,txt_am,~] = xlsread('PXRF_Facies_final.xlsx',2);
    depths_am=num_am(:,1);
    elem_am=num_am(:,i_element);

    % read turbidite mud values from Excel sheet
    [num_te,txt_te,~] = xlsread('PXRF_Facies_final.xlsx',3);
    depths_te=num_te(:,1);
    elem_te=num_te(:,i_element);

    % read low density turbidite values from Excel sheet
    [num_ldt,txt_ldt,~] = xlsread('PXRF_Facies_final.xlsx',4);
    depths_ldt=num_ldt(:,1);
    elem_ldt=num_ldt(:,i_element);

    % read high density turbidite values from Excel sheet
    [num_hdt,txt_hdt,~] = xlsread('PXRF_Facies_final.xlsx',5);
    depths_hdt=num_hdt(:,1);
    elem_hdt=num_hdt(:,i_element);

    % read debrite values from Excel sheet
    [num_db,txt_db,~] = xlsread('PXRF_Facies_final.xlsx',6);
    depths_db=num_db(:,1);
    elem_db=num_db(:,i_element);
```



```

% read slump values from Excel sheet
[num_sp,txt_sp,~] = xlsread('PXRF_Facies_final.xlsx',7);
depths_sp=num_sp(:,1);
elem_sp=num_sp(:,i_element);

% read slide values from Excel sheet
[num_sli,txt_sli,~] = xlsread('PXRF_Facies_final.xlsx',8);
depths_sli=num_sli(:,1);
elem_sli=num_sli(:,i_element);

% plot values
figure(1), clf

subplot(1,8,1)
max_elem=max(elem);
hold on
fill([0,max_elem,max_elem,0],[266.4 266.4 253 253],[0.9 0.9
0.9],'edgecolor','none')
fill([0,max_elem,max_elem,0],[246 246 239.6 239.6],[0.9 0.9
0.9],'edgecolor','none')
for i=[1,2,3,5,6,7,8,9,11,12,14]
    plot([0 max_elem],[zones_t(i) zones_t(i)],':k')
end
for i=[4,10,13]
    plot([0 max_elem],[zones_t(i) zones_t(i)],'-k')
end
plot(elem,depths,'k')
if (i_el == 5) % Ba=5 has large spikes
    xlim([0 0.075])
end
if (i_el==8) % Sr=8 has large spikes
    xlim([0 0.05])
end
hold off
set(gca,'ydir','reverse'), ylim([170 312]), title(names(i_element))
ylabel('depth [m]')

subplot(1,8,2)
hold on
fill([0,max_elem,max_elem,0],[266.4 266.4 253 253],[0.9 0.9
0.9],'edgecolor','none')
fill([0,max_elem,max_elem,0],[246 246 239.6 239.6],[0.9 0.9
0.9],'edgecolor','none')
for i=[1,2,3,5,6,7,8,9,11,12,14]
    plot([0 max_elem],[zones_t(i) zones_t(i)],':k')
end
for i=[4,10,13]
    plot([0 max_elem],[zones_t(i) zones_t(i)],'-k')
end
plot(elem_am,depths_am,'.k')
hold off
set(gca,'ydir','reverse','yticklabel',[]), ylim([170 312]), title('AM')

subplot(1,8,3)
hold on
fill([0,max_elem,max_elem,0],[266.4 266.4 253 253],[0.9 0.9
0.9],'edgecolor','none')
fill([0,max_elem,max_elem,0],[246 246 239.6 239.6],[0.9 0.9
0.9],'edgecolor','none')
for i=[1,2,3,5,6,7,8,9,11,12,14]

```

```

        plot([0 max_elem],[zones_t(i) zones_t(i)],':k')
    end
    for i=[4,10,13]
        plot([0 max_elem],[zones_t(i) zones_t(i)],'-k')
    end
    plot(elem_te,depths_te,'.k')
    hold off
    set(gca,'ydir','reverse','yticklabel',[], ylim([170 312]),
title('T_E'))

    subplot(1,8,4)
    hold on
    fill([0,max_elem,max_elem,0],[266.4 266.4 253 253],[0.9 0.9
0.9], 'edgecolor','none')
    fill([0,max_elem,max_elem,0],[246 246 239.6 239.6],[0.9 0.9
0.9], 'edgecolor','none')
    for i=[1,2,3,5,6,7,8,9,11,12,14]
        plot([0 max_elem],[zones_t(i) zones_t(i)],':k')
    end
    for i=[4,10,13]
        plot([0 max_elem],[zones_t(i) zones_t(i)],'-k')
    end
    plot(elem_ldt,depths_ldt,'.k')
    hold off
    set(gca,'ydir','reverse','yticklabel',[], ylim([170 312]),
title('LDT'))
    xlabel('%')

    subplot(1,8,5)
    hold on
    fill([0,max_elem,max_elem,0],[266.4 266.4 253 253],[0.9 0.9
0.9], 'edgecolor','none')
    fill([0,max_elem,max_elem,0],[246 246 239.6 239.6],[0.9 0.9
0.9], 'edgecolor','none')
    for i=[1,2,3,5,6,7,8,9,11,12,14]
        plot([0 max_elem],[zones_t(i) zones_t(i)],':k')
    end
    for i=[4,10,13]
        plot([0 max_elem],[zones_t(i) zones_t(i)],'-k')
    end
    plot(elem_hdt,depths_hdt,'.k')
    hold off
    set(gca,'ydir','reverse','yticklabel',[], ylim([170 312]),
title('HDT'))

    subplot(1,8,6)
    hold on
    fill([0,max_elem,max_elem,0],[266.4 266.4 253 253],[0.9 0.9
0.9], 'edgecolor','none')
    fill([0,max_elem,max_elem,0],[246 246 239.6 239.6],[0.9 0.9
0.9], 'edgecolor','none')
    for i=[1,2,3,5,6,7,8,9,11,12,14]
        plot([0 max_elem],[zones_t(i) zones_t(i)],':k')
    end
    for i=[4,10,13]
        plot([0 max_elem],[zones_t(i) zones_t(i)],'-k')
    end
    plot(elem_db,depths_db,'.k')
    hold off
    set(gca,'ydir','reverse','yticklabel',[], ylim([170 312]), title('DB'))
    subplot(1,8,7)

```

```

    hold on
    fill([0,max_elem,max_elem,0],[266.4 266.4 253 253],[0.9 0.9
0.9],'edgecolor','none')
    fill([0,max_elem,max_elem,0],[246 246 239.6 239.6],[0.9 0.9
0.9],'edgecolor','none')
    for i=[1,2,3,5,6,7,8,9,11,12,14]
        plot([0 max_elem],[zones_t(i) zones_t(i)],':k')
    end
    for i=[4,10,13]
        plot([0 max_elem],[zones_t(i) zones_t(i)],'-k')
    end
    plot(elem_sp,depths_sp,'.k')
    hold off
    set(gca,'ydir','reverse','yticklabel',[], ylim([170 312]), title('SP'))

    subplot(1,8,8)
    hold on
    fill([0,max_elem,max_elem,0],[266.4 266.4 253 253],[0.9 0.9
0.9],'edgecolor','none')
    fill([0,max_elem,max_elem,0],[246 246 239.6 239.6],[0.9 0.9
0.9],'edgecolor','none')
    for i=[1,2,3,5,6,7,8,9,11,12,14]
        plot([0 max_elem],[zones_t(i) zones_t(i)],':k')
        text(1.1*max_elem,text_d(i),num2str(i))
    end
    for i=[4,10,13]
        plot([0 max_elem],[zones_t(i) zones_t(i)],'-k')
        text(1.1*max_elem,text_d(i),num2str(i))
    end
    plot(elem_sli,depths_sli,'.k')
    hold off
    set(gca,'ydir','reverse','yticklabel',[], ylim([170 312]), title('SL'))

    print(char(elements(i_el)),'-djpeg','-r600')
    print(char(elements(i_el)),'-depsc')
end

```

Appendix 1.2. Matlab script used to compare element variations with deposit types and element distribution for the whole core interval

```

% Plot of element values

clear variables

xls_column_indexes=[4 5 6 7 8 13 16 18 20 25 27 28 29 31 32 35 36 37 38 ...
    39 40 41 42 43];

% read values from Excel sheets
%pkg load io
[num_all,txt,~] = xlsread('PXRF_Facies_final.xlsx',1);
[num_am,~,~] = xlsread('PXRF_Facies_final.xlsx',2);
[num_te,~,~] = xlsread('PXRF_Facies_final.xlsx',3);
[num_ldt,~,~] = xlsread('PXRF_Facies_final.xlsx',4);
[num_hdt,~,~] = xlsread('PXRF_Facies_final.xlsx',5);
[num_db,~,~] = xlsread('PXRF_Facies_final.xlsx',6);
[num_sp,~,~] = xlsread('PXRF_Facies_final.xlsx',7);
[num_sl,~,~] = xlsread('PXRF_Facies_final.xlsx',8);

```

```

names=txt(8,:); % names of elements
depths=num_all(:,1); % depths of all measurements [m]
depths_am=num_am(:,1); % depths of ambient mudstone
depths_te=num_te(:,1); % depths of turbidite mudstone
depths_ldt=num_ldt(:,1); % depths of low density turbidites
depths_hdt=num_hdt(:,1); % depths of high density turbidites
depths_db=num_db(:,1); % depths of debrites
depths_sp=num_sp(:,1); % depths of slump deposits
depths_sl=num_sl(:,1); % depths of slide deposits

% remove spikes
spike_depths=[174.9 181.6 193.5 200.4 204.2 239.05 244.9 245.55 250.35...
255.75 262.1 268.3 269.3 278.7 289.1 295.7 302.52 303.1 306.9 309.5
310.7];
[~,idx,~] = intersect(depths,spike_depths); depths(idx)=[];
num_all(idx,:)=[];
[~,idx,~] = intersect(depths_am,spike_depths); depths_am(idx)=[];
num_am(idx,:)=[];
[~,idx,~] = intersect(depths_te,spike_depths); depths_te(idx)=[];
num_te(idx,:)=[];
[~,idx,~] = intersect(depths_ldt,spike_depths); depths_ldt(idx)=[];
num_ldt(idx,:)=[];
[~,idx,~] = intersect(depths_hdt,spike_depths); depths_hdt(idx)=[];
num_hdt(idx,:)=[];
[~,idx,~] = intersect(depths_db,spike_depths); depths_db(idx)=[];
num_db(idx,:)=[];
[~,idx,~] = intersect(depths_sp,spike_depths); depths_sp(idx)=[];
num_sp(idx,:)=[];
[~,idx,~] = intersect(depths_sl,spike_depths); depths_sl(idx)=[];
num_sl(idx,:)=[];

% tops of zones [m] for plotting
zone1_b = 312;
zones_t=[305.5 299 282.5 274 266.4 253 246 239.5 231.9...
202.55 196.9 185.1 176 170.9];
text_d=0.5*([zone1_b zones_t(1:length(zones_t)-1)]+zones_t);

% colour for plotting OCR zones
grey=[0.9 0.9 0.9];

%% plot values
for i_el = 1:length(indexes)
    i_element=xls_column_indexes(i_el); % get column number in excel sheet

    elem=num_all(:,i_element); % all values of element
    elem_am=num_am(:,i_element); % ambient mudstone values
    elem_te=num_te(:,i_element); % turbidite mudstone values
    elem_ldt=num_ldt(:,i_element); % low density turbidite values
    elem_hdt=num_hdt(:,i_element); % high density turbidite values
    elem_db=num_db(:,i_element); % debrite values
    elem_sp=num_sp(:,i_element); % slump values
    elem_sl=num_sl(:,i_element); % slide values

    % plot values
    figure(1), clf

```

```

subplot(1,8,1)
max_elem=max(elem);
hold on
fill([0,max_elem,max_elem,0],[266.4 266.4 253
253],grey,'edgecolor','none')
fill([0,max_elem,max_elem,0],[246 246 239.6
239.6],grey,'edgecolor','none')
for i=1:length(zones_t)
    plot([0 max_elem],[zones_t(i) zones_t(i)],':k')
end
plot(elem,depths,'k')
hold off
set(gca,'ydir','reverse'), xlim([0 max_elem]), ylim([170 312]),
title(names(i_element))
xlabel('%T'), ylabel('depth [m]')

subplot(1,8,2)
max_elem=max(elem_am);
hold on
fill([0,max_elem,max_elem,0],[266.4 266.4 253
253],grey,'edgecolor',grey)
fill([0,max_elem,max_elem,0],[246 246 239.6
239.6],grey,'edgecolor','none')
for i=1:length(zones_t)
    plot([0 max_elem],[zones_t(i) zones_t(i)],':k')
end
plot(elem_am,depths_am,'b.')
hold off
set(gca,'ydir','reverse'), ylim([170 312]), title('AM'), xlabel('%')

subplot(1,8,3)
max_elem=max(elem_te);
hold on
fill([0,max_elem,max_elem,0],[266.4 266.4 253
253],grey,'edgecolor','none')
fill([0,max_elem,max_elem,0],[246 246 239.6
239.6],grey,'edgecolor','none')
for i=1:length(zones_t)
    plot([0 max_elem],[zones_t(i) zones_t(i)],':k')
end
plot(elem_te,depths_te,'b.')
hold off
set(gca,'ydir','reverse'), ylim([170 312]), title('T_e'), xlabel('%')

subplot(1,8,4)
max_elem=max(elem_ldt);
hold on
fill([0,max_elem,max_elem,0],[266.4 266.4 253
253],grey,'edgecolor','none')
fill([0,max_elem,max_elem,0],[246 246 239.6
239.6],grey,'edgecolor','none')
for i=1:length(zones_t)
    plot([0 max_elem],[zones_t(i) zones_t(i)],':k')
end
plot(elem_ldt,depths_ldt,'b.')
hold off
set(gca,'ydir','reverse'), ylim([170 312]), title('LDT'), xlabel('%')
subplot(1,8,5)
max_elem=max(elem_hdt);
hold on

```

```

fill([0,max_elem,max_elem,0],[266.4 266.4 253
253],grey,'edgecolor','none')
fill([0,max_elem,max_elem,0],[246 246 239.6
239.6],grey,'edgecolor','none')
for i=1:length(zones_t)
    plot([0 max_elem],[zones_t(i) zones_t(i)],':k')
end
plot(elem_hdt,depths_hdt,'b.')
hold off
set(gca,'ydir','reverse'), ylim([170 312]), title('HDT'), xlabel('%')

subplot(1,8,6)
max_elem=max(elem_db);
hold on
fill([0,max_elem,max_elem,0],[266.4 266.4 253
253],grey,'edgecolor','none')
fill([0,max_elem,max_elem,0],[246 246 239.6
239.6],grey,'edgecolor','none')
for i=1:length(zones_t)
    plot([0 max_elem],[zones_t(i) zones_t(i)],':k')
end
plot(elem_db,depths_db,'b.')
hold off
set(gca,'ydir','reverse'), ylim([170 312]), title('DB'), xlabel('%')

subplot(1,8,7)
max_elem=max(elem_sp);
hold on
fill([0,max_elem,max_elem,0],[266.4 266.4 253
253],grey,'edgecolor','none')
fill([0,max_elem,max_elem,0],[246 246 239.6
239.6],grey,'edgecolor','none')
for i=1:length(zones_t)
    plot([0 max_elem],[zones_t(i) zones_t(i)],':k')
end
plot(elem_sp,depths_sp,'b.')
hold off
set(gca,'ydir','reverse'), ylim([170 312]), title('SP'), xlabel('%')

subplot(1,8,8)
max_elem=max(elem_sl);
hold on
fill([0,max_elem,max_elem,0],[266.4 266.4 253
253],grey,'edgecolor','none')
fill([0,max_elem,max_elem,0],[246 246 239.6
239.6],grey,'edgecolor','none')
for i=1:length(zones_t)
    plot([0 max_elem],[zones_t(i) zones_t(i)],':k')
    text(1.1*max_elem,text_d(i),num2str(i))
end
plot(elem_sl,depths_sl,'b.')
hold off
set(gca,'ydir','reverse'), ylim([170 312]), title('SL'), xlabel('%')
end

```

Appendix 1.3. Matlab script used to calculate correlation coefficients between elements

```
% Pearson's cross correlation values of all elements for different facies

clear variables

elements={'Nd' 'Pr' 'Ce' 'La' 'Ba' 'Mo' 'Zr' 'Sr' 'Rb' 'Pb' 'Zn' 'Cu'...
          'Ni' 'Fe' 'Mn' 'Ti' 'Ca' 'K' 'Al' 'P' 'Si' 'Cl' 'S' 'Mg'};
indexes=[4 5 6 7 8 13 16 18 20 25 27 28 29 31 32 35 36 37 38 39 40 41 42
         43];

labels={'all values','AM','Te','LDT','HDT','DB','SP','SL'};

spike_depths=[174.9 181.6 193.5 200.4 204.2 239.05 244.9 245.55 250.35...
              255.75 262.1 268.3 269.3 278.7 289.1 295.7 302.52 303.1 306.9 309.5
              310.7];

for i_sheet=1:8
    % read measured values from excel sheet
    [num,~,~] = xlsread('PXRF_Facies_final.xlsx',i_sheet);
    % remove spikes
    depths=num(:,1); % depths of measurements [m]
    [~,idx,~] = intersect(depths,spike_depths); depths(idx)=[];
    num(idx,:)=[];

    % calculate element by element, deleting NaN values where needed
    for i=1:length(indexes)
        for j=1:length(indexes)
            ii=indexes(i);
            jj=indexes(j);
            ix=~any(isnan([num(:,ii),num(:,jj)]),2); % remove values with NaN
            a=corrcoef([num(ix,ii),num(ix,jj)]);
            if (size(a,1)>1&~isnan(a))
                cc(i,j)=a(1,2);
            else
                cc(i,j)=0;
            end
        end
    end
    % write results to excel sheet
    xlswrite('corr_coefs.xlsx',cc,i_sheet,'B2');
    xlswrite('corr_coefs.xlsx',elements,i_sheet,'B1');
    xlswrite('corr_coefs.xlsx',elements,i_sheet,'A2');
    xlswrite('corr_coefs.xlsx',labels(i_sheet),i_sheet,'A1');
end
```

Appendix 1.4. Matlab script used for factor analysis and dendrogram clustering

```
% Plot elemental values, all values and for different facies
% No analysis for slides and slumps because there are too few values
% Elements with few values have not been included

clear variables
```

```

elements={'Nd' 'Pr' 'Ce' 'La' 'Ba' 'Zr' 'Sr' 'Pb' 'Zn'...
          'Ni' 'Fe' 'Ti' 'Ca' 'K' 'Al' 'Si' 'S'};
xls_column_indexes=[4 5 6 7 8 16 18 25 27 29 31 35 36 37 38 40 42];

%% read values from Excel sheets
% pkg load io
[num_all,txt,~] = xlsread('PXRF_Facies_final.xlsx',1);
[num_am,~,~] = xlsread('PXRF_Facies_final.xlsx',2);
[num_te,~,~] = xlsread('PXRF_Facies_final.xlsx',3);
[num_ldt,~,~] = xlsread('PXRF_Facies_final.xlsx',4);
[num_hdt,~,~] = xlsread('PXRF_Facies_final.xlsx',5);
[num_db,~,~] = xlsread('PXRF_Facies_final.xlsx',6);
[num_sp,~,~] = xlsread('PXRF_Facies_final.xlsx',7);
[num_sl,~,~] = xlsread('PXRF_Facies_final.xlsx',8);

names=txt(8,:); % names of elements
depths=num_all(:,1); % depths of all measurements [m]
depths_am=num_am(:,1); % depths of ambient mudstone
depths_te=num_te(:,1); % depths of turbidite mudstone
depths_ldt=num_ldt(:,1); % depths of low density turbidites
depths_hdt=num_hdt(:,1); % depths of high density turbidites
depths_db=num_db(:,1); % depths of debrites
depths_sp=num_sp(:,1); % depths of slump deposits
depths_sl=num_sl(:,1); % depths of slide deposits

% remove spikes
spike_depths=[174.9 181.6 193.5 200.4 204.2 239.05 244.9 245.55 250.35...
              255.75 262.1 268.3 269.3 278.7 289.1 295.7 302.52 303.1 306.9 309.5
              310.7];

[~,idx,~] = intersect(depths,spike_depths); depths(idx)=[];
num_all(idx,:)=[];
[~,idx,~] = intersect(depths_am,spike_depths); depths_am(idx)=[];
num_am(idx,:)=[];
[~,idx,~] = intersect(depths_te,spike_depths); depths_te(idx)=[];
num_te(idx,:)=[];
[~,idx,~] = intersect(depths_ldt,spike_depths); depths_ldt(idx)=[];
num_ldt(idx,:)=[];
[~,idx,~] = intersect(depths_hdt,spike_depths); depths_hdt(idx)=[];
num_hdt(idx,:)=[];
[~,idx,~] = intersect(depths_db,spike_depths); depths_db(idx)=[];
num_db(idx,:)=[];
[~,idx,~] = intersect(depths_sp,spike_depths); depths_sp(idx)=[];
num_sp(idx,:)=[];
[~,idx,~] = intersect(depths_sl,spike_depths); depths_sl(idx)=[];
num_sl(idx,:)=[];

% remove NaN values
num_all=num_all(:,xls_column_indexes);
num_all=num_all(all(~isnan(num_all),2),:);

num_am=num_am(:,xls_column_indexes);
num_am=num_am(all(~isnan(num_am),2),:);

num_te=num_te(:,xls_column_indexes);
num_te=num_te(all(~isnan(num_te),2),:);

num_ldt=num_ldt(:,xls_column_indexes);
num_ldt=num_ldt(all(~isnan(num_ldt),2),:);
num_hdt=num_hdt(:,xls_column_indexes);

```



```

num_hdt=num_hdt(all(~isnan(num_hdt),2),:);

num_db=num_db(:,xls_column_indexes);
num_db=num_db(all(~isnan(num_db),2),:);

% factor analysis
figure(1), clf
subplot(3,2,1)
lambda = factoran(num_all,2,'scores','regression');
biplot(lambda,'varlabels',elements)
title('all measurements')

subplot(3,2,2)
mean_vals=mean(num_am,1);
num_mean=ones(size(num_am));
for i=1:length(num_am(:,1))
    num_mean(i,:)=mean_vals;
end
tree = linkage((num_am./num_mean)');
dendrogram(tree,'labels',elements)
title('AM')

subplot(3,2,3)
mean_vals=mean(num_te,1);
num_mean=ones(size(num_te));
for i=1:length(num_te(:,1))
    num_mean(i,:)=mean_vals;
end
tree = linkage((num_te./num_mean)');
dendrogram(tree,'labels',elements)
title('T_E')

subplot(3,2,4)
mean_vals=mean(num_ldt,1);
num_mean=ones(size(num_ldt));
for i=1:length(num_ldt(:,1))
    num_mean(i,:)=mean_vals;
end
tree = linkage((num_ldt./num_mean)');
dendrogram(tree,'labels',elements)
title('LDT')

```

Appendix 1.5. Matlab script used for crossplotting the studied elements

```

% Crossplots of elements vs Ti and Al for different facies

clear variables

elements={'Nd' 'Pr' 'Ce' 'La' 'Ba' 'Mo' 'Zr' 'Sr' 'Rb' 'Pb' 'Zn' 'Cu'...
         'Ni' 'Fe' 'Mn' 'Ti' 'Ca' 'K' 'Al' 'P' 'Si' 'Cl' 'S' 'Mg'};
indexes=[4 5 6 7 8 13 16 18 20 25 27 28 29 31 32 35 36 37 38 39 40 41 42
         43];

spike_depths=[174.9 181.6 193.5 200.4 204.2 239.05 244.9 245.55 250.35...
              255.75 262.1 268.3 269.3 278.7 289.1 295.7 302.52 303.1 306.9 309.5
              310.7];

% read values from Excel sheets

```

```

%pkg load io
[num_all,txt,~] = xlsread('PXRF_Facies_final.xlsx',1);
[num_am,~,~] = xlsread('PXRF_Facies_final.xlsx',2);
[num_te,~,~] = xlsread('PXRF_Facies_final.xlsx',3);
[num_ldt,~,~] = xlsread('PXRF_Facies_final.xlsx',4);
[num_hdt,~,~] = xlsread('PXRF_Facies_final.xlsx',5);
[num_db,~,~] = xlsread('PXRF_Facies_final.xlsx',6);
[num_sp,~,~] = xlsread('PXRF_Facies_final.xlsx',7);
[num_sl,~,~] = xlsread('PXRF_Facies_final.xlsx',8);

names=txt(8,:); % names of elements
depths=num_all(:,1); % depths of all measurements [m]
depths_am=num_am(:,1); % depths of ambient mudstone
depths_te=num_te(:,1); % depths of turbidite mudstone
depths_ldt=num_ldt(:,1); % depths of low density turbidites
depths_hdt=num_hdt(:,1); % depths of high density turbidites
depths_db=num_db(:,1); % depths of debrites
depths_sp=num_sp(:,1); % depths of slump deposits
depths_sl=num_sl(:,1); % depths of slide deposits

% remove spikes
spike_depths=[174.9 181.6 193.5 200.4 204.2 239.05 244.9 245.55 250.35...
255.75 262.1 268.3 269.3 278.7 289.1 295.7 302.52 303.1 306.9 309.5
310.7];
[~,idx,~] = intersect(depths,spike_depths); depths(idx)=[];
num_all(idx,:)=[];
[~,idx,~] = intersect(depths_am,spike_depths); depths_am(idx)=[];
num_am(idx,:)=[];
[~,idx,~] = intersect(depths_te,spike_depths); depths_te(idx)=[];
num_te(idx,:)=[];
[~,idx,~] = intersect(depths_ldt,spike_depths); depths_ldt(idx)=[];
num_ldt(idx,:)=[];
[~,idx,~] = intersect(depths_hdt,spike_depths); depths_hdt(idx)=[];
num_hdt(idx,:)=[];
[~,idx,~] = intersect(depths_db,spike_depths); depths_db(idx)=[];
num_db(idx,:)=[];
[~,idx,~] = intersect(depths_sp,spike_depths); depths_sp(idx)=[];
num_sp(idx,:)=[];
[~,idx,~] = intersect(depths_sl,spike_depths); depths_sl(idx)=[];
num_sl(idx,:)=[];

% element for correlation (column number in excel sheet)
i_corr=38; %31=Fe, 35=Ti, 38=Al

%for i_el = 1:length(indexes)
for i_el = 23
    i_element=indexes(i_el);
    disp(names(i_element))

    % combined values
    elem=num_all(:,i_element);
    cor_all=num_all(:,i_corr);

    % ambient mud values
    elem_am=num_am(:,i_element);
    cor_am=num_am(:,i_corr);

    % turbidite mud values
    elem_te=num_te(:,i_element);
    cor_te=num_te(:,i_corr);

```

```

% low density turbidite values
elem_ldt=num_ldt(:,i_element);
cor_ldt=num_ldt(:,i_corr);

% high density turbidite values
elem_hdt=num_hdt(:,i_element);
cor_hdt=num_hdt(:,i_corr);

% debrite values
elem_db=num_db(:,i_element);
cor_db=num_db(:,i_corr);

% slump values
elem_sp=num_sp(:,i_element);
cor_sp=num_sp(:,i_corr);

% slide values
elem_sl=num_sl(:,i_element);
cor_sl=num_sl(:,i_corr);

% plot values
figure(1), clf

subplot(2,4,1)
% remove NaN
nan1=find(isnan(cor_all)); nan2=find(isnan(elem));
nan_ind=unique([nan1',nan2']);
cor_all(nan_ind)=[]; elem(nan_ind)=[];
% calculate Pearson's correlation coefficient
r=corrcoef(cor_all,elem, '.')
plot(cor_all,elem, '.')
title(strcat('all, r=', num2str(r(1,2),3)))
xlabel(names(i_corr)), ylabel(elements(i_el))

subplot(2,4,2)
% remove NaN
nan1=find(isnan(cor_am)); nan2=find(isnan(elem_am));
nan_ind=unique([nan1',nan2']);
cor_am(nan_ind)=[]; elem_am(nan_ind)=[];
% calculate Pearson's correlation coefficient
r=corrcoef(cor_am,elem_am, '.')
plot(cor_am,elem_am, '.')
title(strcat('AM, r=', num2str(r(1,2),3)))
xlabel(names(i_corr)), ylabel(elements(i_el))

subplot(2,4,3)
% remove NaN
nan1=find(isnan(cor_te)); nan2=find(isnan(elem_te));
nan_ind=unique([nan1',nan2']);
cor_te(nan_ind)=[]; elem_te(nan_ind)=[];
% calculate Pearson's correlation coefficient
r=corrcoef(cor_te,elem_te, '.')
plot(cor_te,elem_te, '.')
title(strcat('T E, r=', num2str(r(1,2),3)))
xlabel(names(i_corr)), ylabel(elements(i_el))

subplot(2,4,4)
% remove NaN

```

```

nan1=find(isnan(cor_ldt)); nan2=find(isnan(elem_ldt));
nan_ind=unique([nan1',nan2']);
cor_ldt(nan_ind)=[]; elem_ldt(nan_ind)=[];
% calculate Pearson's correlation coefficient
r=corrcoef(cor_ldt,elem_ldt);
plot(cor_ldt,elem_ldt,'.')
title(strcat('LDT, r=',num2str(r(1,2),3)))
xlabel(names(i_corr)), ylabel(elements(i_el))

subplot(2,4,5)
% remove NaN
nan1=find(isnan(cor_hdt)); nan2=find(isnan(elem_hdt));
nan_ind=unique([nan1',nan2']);
cor_hdt(nan_ind)=[]; elem_hdt(nan_ind)=[];
% calculate Pearson's correlation coefficient
r=corrcoef(cor_hdt,elem_hdt);
plot(cor_hdt,elem_hdt,'.')
title(strcat('HDT, r=',num2str(r(1,2),3)))
xlabel(names(i_corr)), ylabel(elements(i_el))

subplot(2,4,6)
% remove NaN
nan1=find(isnan(cor_db)); nan2=find(isnan(elem_db));
nan_ind=unique([nan1',nan2']);
cor_db(nan_ind)=[]; elem_db(nan_ind)=[];
% calculate Pearson's correlation coefficient
r=corrcoef(cor_db,elem_db);
plot(cor_db,elem_db,'.')
title(strcat('DB, r=',num2str(r(1,2),3)))
xlabel(names(i_corr)), ylabel(elements(i_el))

subplot(2,4,7)
% remove NaN
nan1=find(isnan(cor_sp)); nan2=find(isnan(elem_sp));
nan_ind=unique([nan1',nan2']);
cor_sp(nan_ind)=[]; elem_sp(nan_ind)=[];
% calculate Pearson's correlation coefficient
r=corrcoef(cor_sp,elem_sp);
plot(cor_sp,elem_sp,'.')
title(strcat('SP, r=',num2str(r(1,2),3)))
xlabel(names(i_corr)), ylabel(elements(i_el))
subplot(2,4,8)
% remove NaN
nan1=find(isnan(cor_sl)); nan2=find(isnan(elem_sl));
nan_ind=unique([nan1',nan2']);
cor_sl(nan_ind)=[]; elem_sl(nan_ind)=[];
% calculate Pearson's correlation coefficient
r=corrcoef(cor_sl,elem_sl);
plot(cor_sl,elem_sl,'.')
title(strcat('SL, r=',num2str(r(1,2),3)))
xlabel(names(i_corr)), ylabel(elements(i_el))

print(char(elements(i_el)),'-djpeg')
end

```

Appendix 1.6. Matlab script used to study influence of grain size on element distributions

```

% Elements vs. grain sizes

clear variables

```

```

% elements organised in order of link with grain sizes
elements={'Zn' 'Rb' 'Mo' 'K' 'Fe' 'Cu' 'Ni' 'S' 'Al' 'Ti' 'Zr' 'Nd' ...
'Pr' 'Ce' 'La' 'Pb' 'Sr' 'Ca' 'P' 'Mg' 'Mn' 'Si' 'Ba' 'Cl' };
xls_column_indexes=[27 20 13 37 31 28 29 42 38 35 16 4 5 6 7 25 18 36 ...
39 43 32 40 8 41];

% read values from Excel sheets
[num_all,txt,~] = xlsread('PXRF_Facies_final.xlsx',1);

names=txt(8,:); % names of elements
depths=num_all(:,1); % depths of all measurements [m]
grainsize=txt(:,2); grainsize(1:8)=[];

% remove spikes
spike_depths=[174.9 181.6 193.5 200.4 204.2 239.05 244.9 245.55 250.35...
255.75 262.1 268.3 269.3 278.7 289.1 295.7 302.52 303.1 306.9 309.5
310.7];
[~,idx,~] = intersect(depths,spike_depths); depths(idx)=[];
num_all(idx,:)=[];
grainsize(idx,:)=[];

% find indexes of grain size classes
idx_bm=find(strcmp(grainsize,'BM')); % black mud
idx_dm=find(strcmp(grainsize,'DM')); % dark grey mud
idx_s_m=find(strcmp(grainsize,'S_M')); % silty mud
idx_l_sm=find(strcmp(grainsize,'L_SM')); % laminated silty mud
idx_ms=find(strcmp(grainsize,'MS')); % muddy siltstone
idx_l_sbm=find(strcmp(grainsize,'L_SBM')); % laminated fine-sandy mud
idx_ls=find(strcmp(grainsize,'LS')); % laminated fine sandstone
idx_f_s=find(strcmp(grainsize,'F_S')); % fine sand
idx_f_m_s=find(strcmp(grainsize,'F-M_S')); % fine-medium sand
idx_m_s=find(strcmp(grainsize,'M_S')); % medium sand
idx_m_c_s=find(strcmp(grainsize,'M-C_S')); % medium-coarse sand
idx_c_s=find(strcmp(grainsize,'C_S')); % coarse sand
idx_vc_s=find(strcmp(grainsize,'VC_S')); % very coarse sand
idx_cn=find(strcmp(grainsize,'CN')); % conglomeratic sand

% put all mean values in a matrix
num_all=num_all(:,xls_column_indexes);
num_all(isnan(num_all))=0;
mean_per_grain_size=[ mean(num_all(idx_bm,:)); mean(num_all(idx_dm,:));
mean(num_all(idx_s_m,:)); mean(num_all(idx_l_sm,:));
mean(num_all(idx_ms,:)); mean(num_all(idx_l_sbm,:));
mean(num_all(idx_ls,:)); mean(num_all(idx_f_s,:));
mean(num_all(idx_f_m_s,:)); mean(num_all(idx_m_s,:));
mean(num_all(idx_m_c_s,:)); mean(num_all(idx_c_s,:));
mean(num_all(idx_vc_s,:)); mean(num_all(idx_cn,:))];
std_per_grainsize=[ std(num_all(idx_bm,:)); std(num_all(idx_dm,:));
std(num_all(idx_s_m,:)); std(num_all(idx_l_sm,:));
std(num_all(idx_ms,:)); std(num_all(idx_l_sbm,:));
std(num_all(idx_ls,:)); std(num_all(idx_f_s,:));
std(num_all(idx_f_m_s,:)); std(num_all(idx_m_s,:));
std(num_all(idx_m_c_s,:)); std(num_all(idx_c_s,:));
std(num_all(idx_vc_s,:)); std(num_all(idx_cn,:))];
% normalise values
mean_all=ones(size(mean_per_grain_size))*diag(mean(mean_per_grain_size));
std_all=ones(size(mean_per_grain_size))*diag(std(mean_per_grain_size));
num_all_gn=(mean_per_grain_size-mean_all)./std_all;

```

```

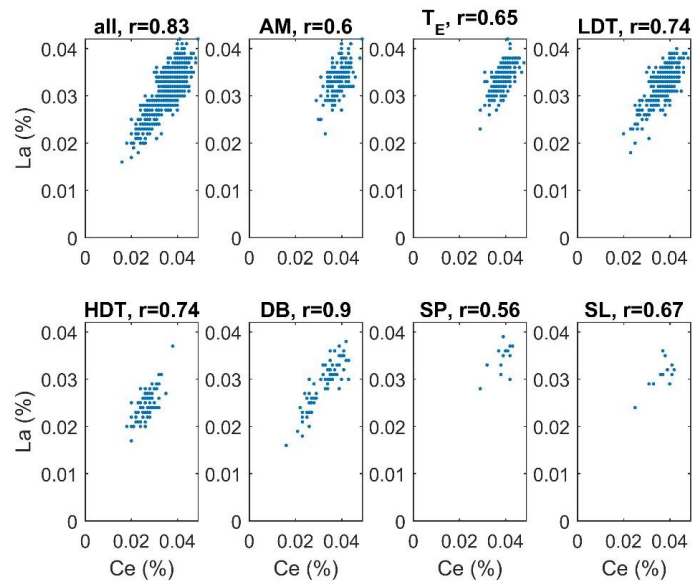
std_all_n=std_per_grainsize./std_all;

figure(1), clf
h=plot(num_all_gn);
xlim([1 14])
legend(h,elements,'location','eastoutside')
labels={'m_b','m_g','m_s','m_ls','ms','m_l','fs_l','fs','f-m','m','m-
c','c','vc','g'};
set(gca,'xtick',(1:14),'xticklabel',labels)

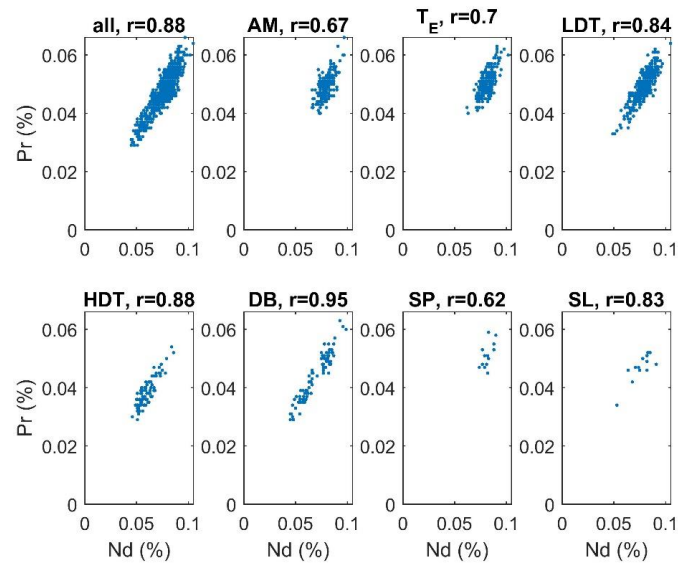
figure(3), clf
ampl=4;
num_all_gn=num_all_gn+ones(size(mean_per_grain_size))*diag((0:23)*ampl);
hold on
for i=1:length(elements)
    plot([1 14],ampl*[i-1 i-1],'k:')
    text(14.2,ampl*(i-1),elements(i))
end
plot(num_all_gn)
hold off
xlim([1 14]), ylim([-2 3+ampl*23]), grid on
xlabel('grain size'), ylabel('(mean(elem for grain size)-
mean(elem))/std(elem)')
labels={'m_b','m_g','m_s','m_ls','ms','m_l','fs_l','fs','f-m','m','m-
c','c','vc','g'};
set(gca,'xtick',(1:14),'xticklabel',labels,'ytick',[])

```

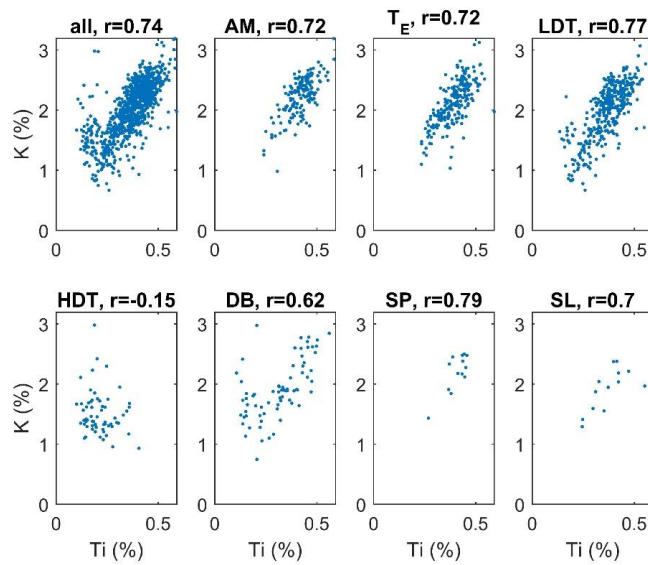
Appendix 2. Crossplots of selected elements



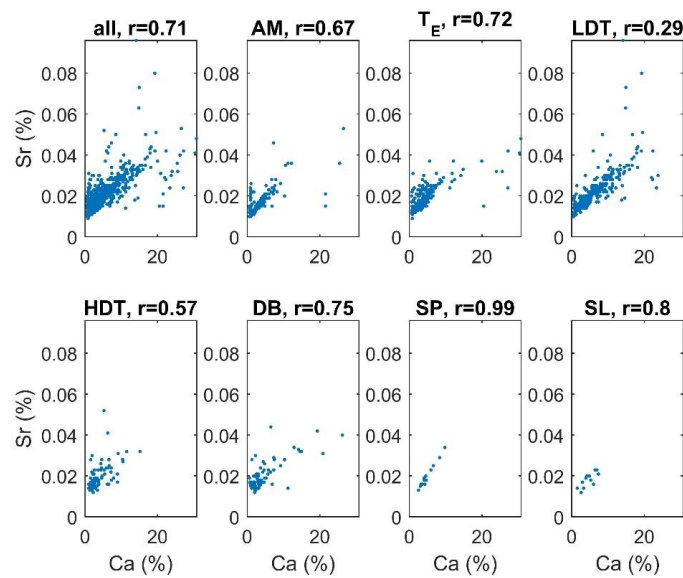
Appendix 2.1. crossplots of La and Ce showing La and Ce correlations across the studied deposit types.



Appendix 2.2. Crossplots of Pr and Nd showing Pr and Nd correlations across the studied deposit types.



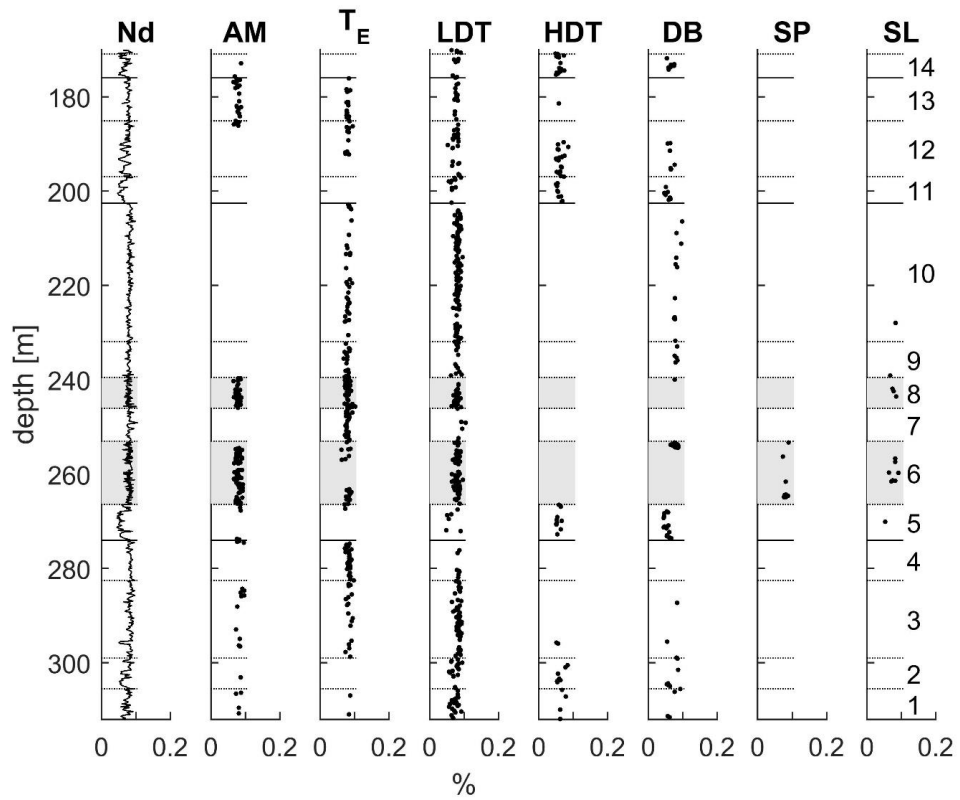
Appendix 2.3. Crossplots of K and Ti showing K and Ti correlations across the studied deposit types.



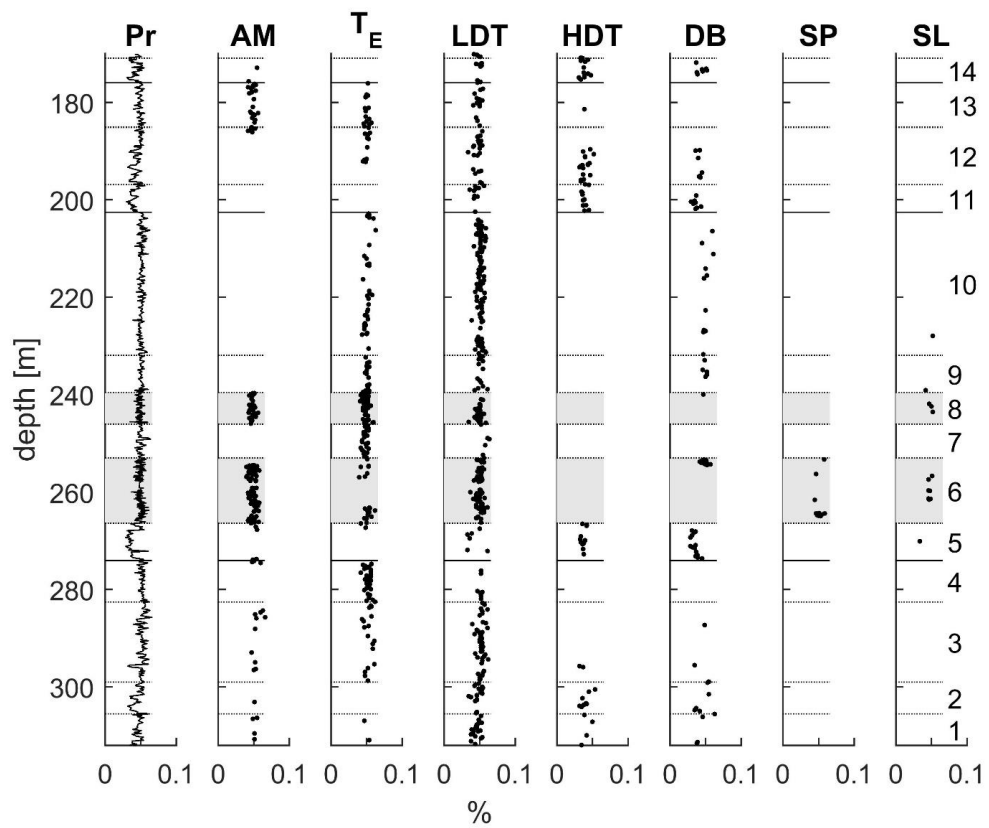
Appendix 2.4. Crossplots of Sr and Ca showing Sr and Ca correlations across the studied deposit types.

Appendix 3. Plots of element distributions across the studied core interval.

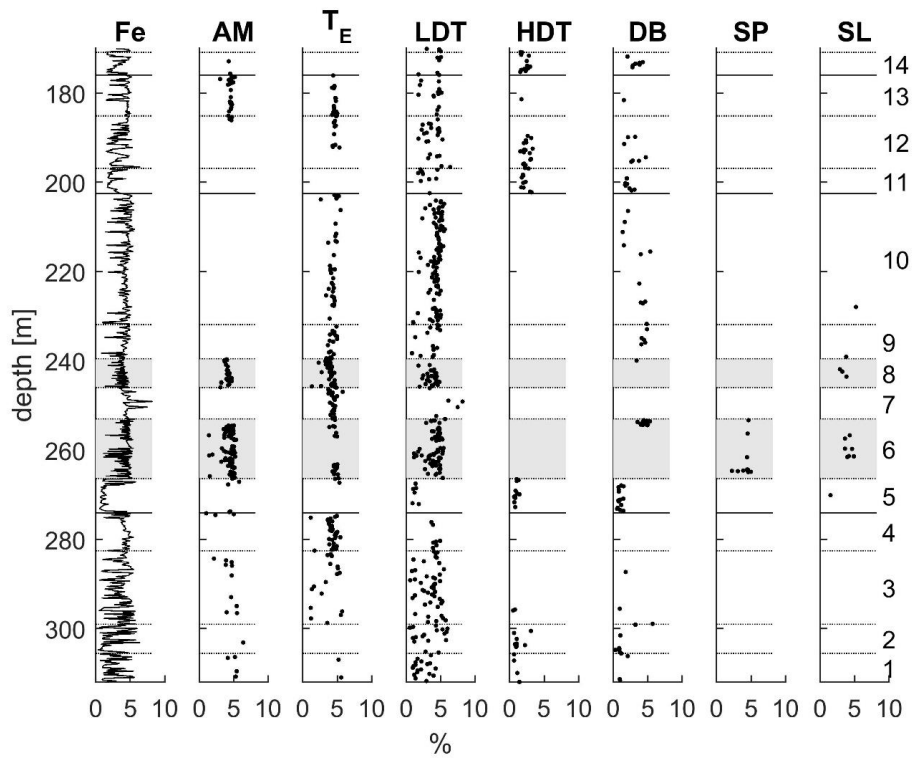
Numbers 1-14 stand for zones/intervals 1-14 respectively indicating vertical variations in deposit types.



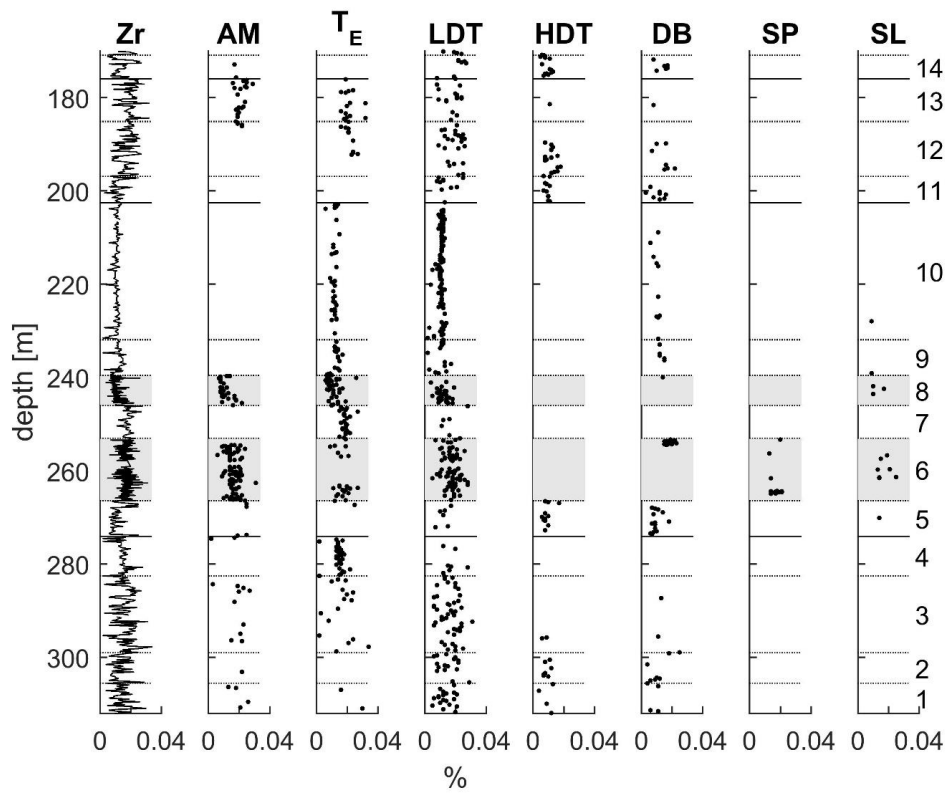
Appendix 3.1. Nd distribution across the whole interval is shown in the leftmost plot. Other plots show Nd distribution across the studied deposit types.



Appendix 3.2. Pr distribution across the whole interval is shown in the first (left) plot. Other plots show Pr distribution across the studied core deposit types.



Appendix 3.3. Fe distribution across the whole scanned core interval (left plot). Other plots show Fe distribution across the studied deposit types.



Appendix 3.4. Zr distribution across the whole interval is shown in the first (leftmost) plot. Other columns show Zr distribution across the studied deposit types.

Appendix 4. Presentation of results in conferences

Poster presentations

1. The Norwegian Sea area Permo-Triassic organic-carbon-rich deposits from seismic

Emily Barnabas Kiswaka¹, Maarten Felix¹, Arve Næss^{1,2}, and Olav Kvamme Leirfall²

¹NTNU Norwegian University of Science and Technology, ²Equinor ASA-Stjørdal

Conference details

Title: EGU General Assembly 2018

Place: Vienna, Austria

Scope: International

Year: 2018

Date from: April 8, 2018

Date To: April 13, 2018

Publication year: 2018

Abstract published online, available at:

<https://meetingorganizer.copernicus.org/EGU2018/EGU2018-14034.pdf>

Accessed on 15th Dec 2019.

2. Use of element proxies to determine palaeodepositional conditions of Permian organic-carbon-rich intervals in the Helgeland Basin

Emily Barnabas Kiswaka¹, Maarten Felix¹, and Arve Næss^{1,2}

¹NTNU Norwegian University of Science and Technology, Trondheim, Norway, ²Equinor ASA-Stjørdal, Norway

Conference details

Place: Bergen, Norway

Scope: International

Year: 2019

Date from: January 7, 2019

Date To: January 9, 2019

Organizer: The Geological Society of Norway

Publication year: 2019

Abstract published online. Available at:

https://www.geologi.no/konferanser/vinterkonferanser/item/download/72_6cdecc52529e2c144ddf98991fba2d8f

Accessed on 15th Dec 2019.

Oral presentation

The Norwegian Sea area Permo-Triassic organic-carbon-rich deposits from seismic

Emily Barnabas Kiswaka¹, Maarten Felix¹, and Arve Næss^{1,2}

¹NTNU Norwegian University of Science and Technology, ²Equinor ASA-Stjørdal

Conference details

Title: Lecture

Place: Dar es salaam, Tanzania

Scope: International

Year: 2018

Date from: October 8, 2018

Date To: October 10, 2018

Organizer: University of Dar es Salaam in collaboration with ESARSWG